ASSEMBLY AND PHYSICO-CHEMICAL PROPERTIES OF POLYELECTROLYTE MULTILAYER FILMS CO-ASSEMBLED WITH GUEST SPECIES

A Dissertation

by

XIAYUN HUANG

Submitted to the Office of Graduate and Professional Studies of
Texas A&M University
in partial fulfillment of the requirements for the degree of

DOCTOR OF PHILOSOPHY

Chair of Committee,	Nicole Zacharia
Co-Chair of Committee,	Andrea Strzelec
Committee Members,	Raymundo Arroyave
	Hong Liang
	Jodie Lutkenhaus
Head of Department,	Andreas Polycarpou

August 2014

Major Subject: Mechanical Engineering

ABSTRACT

Polyelectrolyte multilayer (PEM) films are typically made of two oppositely charged polyelectrolytes held together by electrostatic interactions. PEM films embedded with guest species, that is with foreign small molecules or other chemical moieties, such as surfactants, lubricants, transition metal ions or nanoparticles, have been investigated. The interaction of these various foreign species with the PEM film is of fundamental interest, influencing many properties such as strength or wettability. In one example, when assembled in the film, different types of ions or charged molecules will behave as crosslinkers and make a significant difference in film assembly and related disassembly mechanisms, compared with the more usual case of two polyelectrolytes held together by electrostatic interactions. An amphiphilic surfactant can be co-assembled to fine tune the wettability via modulation of morphology of the hydrophilic head and hydrophobic tail groups of surfactant in the film. A hydrophobic lubricant layer can improve the omniphobicity and slide off properties of a PEM. Incorporation of transition metal ions into the polyelectrolyte multilayer structure gives us a way to modulate both the ionic crosslink density as well as incorporate optical properties unique to those ions (such as color). These doped films show a difference in response to various stimuli such as pH, salt and surfactant, as well as self-healing and swelling properties. Moreover, the transition metal ion incorporated films can be reduced *in situ* to form particle embedded films suitable for various for optical and catalytic applications.

ACKNOWLEDGEMENTS

I would like to acknowledge my advisor and co-advisor, Dr. Nicole Zacharia and Dr. Andrea Strzelec, for their superb mentoring, advice and guidance during my four graduate years at Texas A&M University and my future career. They not only introduced me to a love of science, but also paved the way for me to mature as a scientist and an individual. They have given me the opportunity to work on very interesting and challenging projects, and encouraged me to be the decision maker throughout my research work. They taught me to always question and enjoy the process of discovery. I am truly grateful for having been tutored and trained by them. I would also like to thank my thesis committee members, Dr. Raymundo Arroyave, Dr. Hong Liang, and Dr. Jodie Lutkenhaus for their guidance and support throughout this work.

Moreover, I would like to thank all of my friends and colleagues for all the good times that I have shared with them for the last four years. Without the great help with all the instruments from Dr. Karen Wooley, Dr. Jodie Lutkenhaus, Dr. Mustafa Akbulut, Dr. Sreeram Vaddiraju, Dr. Jaime Grunlan and Dr. Hung-Jue Sue's group and the help of their students, I could not have finished this work so smoothly. I would also like to extend my thanks to Dr. Andreas Holzenberg, Dr. Stan Vitha, Dr. Tom Stephens and Dr. Amanda Young in Microscopy & Imaging Center (MIC) and Material Characterization Facility (MCF) for their technical supports throughout this work.

My deepest appreciation goes to my family and my mentor, Dr. Qing Shen, for always standing beside me over all endeavors. One of the major reasons I decided to pursue a doctor degree in the United States was the encouragement and motivation from Dr. Qing Shen and my parents. Their fully encouragement and support on my enthusiasm of research helps me find out the important things in life.

This thesis is dedicated to all of them.

TABLE OF CONTENTS

Page

ABSTRACT ii

ACKNOWLEDGEMENTS iii

TABLE OF CONTENTS iv

LIST OF FIGURES vii

LIST OF TABLES xvii

CHAPTER I INTRODUCTION AND RESEARCH GOALS 1

CHAPTER II LITERATURE REVIEW 4

2.1. Polyelectrolytes and polyelectrolyte multilayers 4
2.1.1. Polyelectrolyte complexes 4
2.1.2. Polyelectrolyte multilayer: layer-by-layer sequential assembly 5
2.1.3. Mechanism of multilayer buildup 7
2.2. Factors affecting multilayer growth and behavior 8
2.2.1. Salt concentration 8
2.2.2. pH value 11
2.2.3. Molecular weight 12
2.3. Functional LbL film using novel materials 13
2.4. Wettability modulation via surfactant 14
2.4.1. Different types of surfactant 14
2.4.2. Polyelectrolyte-surfactant complex 16
2.4.3. Building surfactant into the polyelectrolyte multilayers 17
2.4.4. Wettability modulation through ion exchange and co-assembly 18
2.5. Omniphobic slippery surfaces-an extreme fluid repellency 19
2.6. Polyelectrolyte-transition metal ion complex films 21
2.6.1. Chelation of polyelectrolyte with transition metal ion 21
2.6.2. Transition metal ion in the polyelectrolyte multilayers 22
2.6.3. Optical properties of polyelectrolyte-metal complex film 24
2.6.4. Catalytic properties of polyelectrolyte-metal complex film 27
2.6.5. Mechanical properties of polyelectrolyte-metal complex film 31

CHAPTER III SURFACTANT CO-ASSEMBLY AND ION EXCHANGE TO MODULATE POLYELECTROLYTE MULTILAYER WETTABILITY 35

3.1. Introduction 35
3.2. Materials and methods 37

3.3. Results and discussions 39
3.3.1. Counterion exchange with fluorinated surfactant 39
3.3.2. Fluorinated surfactant co-assembled with polyelectrolytes 46
3.4. Summary 55

CHAPTER IV OMNIPHOBIC SLIPPERY COATINGS BASED ON LUBRICANT INFUSED POROUS POLYELECTROLYTE MULTILAYERS 57

4.1. Introduction 57
4.2. Materials and methods 59
4.3. Results and discussions 61
4.4. Summary 69

CHAPTER V TUNABLE DISASSEMBLY OF POLYELECTROLYTE-CU^{2+} LAYER-BY-LAYER COMPLEX FILM 71

5.1. Introduction 71
5.2. Materials and methods 73
5.3. Results and discussion 76
5.3.1. The formation of BPEI-Cu^{2+} complex 76
5.3.2. Construction of BPEI-Cu^{2+}/PAA films under different assembly pH 80
5.3.3. Construction of BPEI-Metal ion/PAA film 85
5.3.4. Controllable disassembly and Cu^{2+} release 87
5.4. Summary 94

CHAPTER VI GELATION-ENHANCED FLUORESCENCE EMISSION CHARACTERISTICS OF POLYELECTROLYTE-ION COMPLEX MULTILAYERS 95

6.1. Introduction 95
6.2. Materials and methods 97
6.3.1. Results and discussions 99
6.3.1. Fluorescent (BPEI/PAA)-Ag^{+} complex film 99
6.3.2. Formaldehyde detection via Ag^{+} reduction 105
6.3.3. Formation of Ag nanocluster via thermal reduction 107
6.4. Summary 108

CHAPTER VII SILVER NANOPARTICLE AIDED SELF-HEALING OF POLYELECTROLYTE MULTILAYERS 110

7.1. Introduction 110
7.2. Materials and methods 112
7.3. Results and discussions 115
7.4. Summary 124

CHAPTER VIII CONCLUSIONS AND FUTURE WORK 125

8.1. Thesis summary 125
8.2. Suggestions for future research 126

REFERENCES..... 130

APPENDIX LIST OF ABBREVIATIONS AND FULL NAME OF POLYELECTROLYTES..... 156

LIST OF FIGURES

Page

Figure 2.1. Schematic depiction of the layer-by-layer assembly technique. (a) Simplified depiction of the first two adsorption steps depicting film deposition starting with a positively charged substrate. Polyion conformation and layer interpenetration are an idealization of the surface charge reversal with each adsorption step which is the base of the electrostatically driven multilayer build-up. Counterions are not shown here. (b) Schematic depiction of the film deposition process using flat substrates, such as glass slides and silicon wafer. Steps 1 and 3 represent the adsorption of a polyanion and polycation respectively, while steps 2 and 4 are washing steps. The four steps are the basic building up sequence for the simplest film architecture $(A/B)_n$ and n is the number of deposition cycles. The construction of more complex film architectures is trivial and requires additional beakers and an extended deposition sequence. (c) Instead of bringing the surface into contact with the liquid that contains the adsorbing species by immersion, the liquid is sprayed against the receiving surface onto which the polyelectrolyte multilayer is deposited……...……... 5

Figure 2.2. Basic principles of the layer-by-layer techniques on planar and curved surface.4 (A) The illustration of planar surface alternately immersed in solution of two oppositely charged polyelectrolytes. The template is washed in between the immersion steps in order to remove weakly bounded polyelectrolyte. (B) The illustration of layer-by-layer assembly on curved colloidal templates which is achieved by suspending the templates alternately in solutions of two oppositely charged polyelectrolytes. After each assembly step, the templates are isolated via centrifugation and washed with solvent to remove weakly bounded polyelectrolytes. Dissolution of the colloidal template affords hollow capsule…….. 6

Figure 2.3. The illustration of various types of surfactant according to the composition of their head: nonionic, anionic, cationic and zwitterionic……...…..…….…….. 15

Figure 2.4. The illustration of different types of micellar structures below and above the CMC value in aqueous medium...……...…….. 15

Figure 2.5. Schematic description of possible arrangements in surfactant-polyelectrolyte complexes (SPECs): (a) polyelectrolyte decorated with surfactants; (b) densely packed micelles “glued” together by a polyelectrolyte; (c) pearl-necklace structures; (d) rod-like aggregation of

micelles with a stiff polyelectrolyte; (e) flexible polyelectrolyte attached to a bilayer; and (f) rod-like polyelectrolyte incorporated between bilayers……..... 17

Figure 2.6. Wetting on smooth and structured surfaces. A liquid droplet sitting on (a) a smooth surface with an intrinsic contact angle, (b) a textured surface that is completely wetted by the liquid, known as a Wenzel state droplet, (c) a textured surface with trapped air pockets, known as a Cassie state droplet, and (d) a textured surface that is infused with an immiscible lubricating fluid (or slippery liquid-infused porous surfaces)…… 19

Figure 2.7. Schematic illustration of pH-sensitive fluorescent silver nanocluster. Silver nanocluster is prepared with branched polyethylenimine as capping agent. In the pH from 1 to 12, it shows both the color and fluorescent change……..... 25

Figure 2.8. The fluorescent Ag nanocluster PVPON/PAA films by in situ UV reduction. (A) Loading of Ag^+ into the PVPON/PAA films. (B) Generation of Ag nanoparticles in the film by photo-reduction of Ag^+. The fluorescence intensity can be controlled by particle size. (C) Photographs of a Ag^+-loaded film (right) and a film not loaded with Ag^+ (left) under UV irradiation at various irradiation times as marked in the pictures. The fluorescent intensity of films shows the increase and decrease due the formation and fluorescent quenching due to aggregation……..…..…….…….. 25

Figure 2.9. The illustration of catalytic nanoparticle formation in multilayered polyelectrolyte films. Deposition of a film containing a branched polyethylenimine-metal ion complex followed by reduction of the metal ion yields nanoparticles……..... 27

Figure 2.10. Schematic illustration of Pd nanoparticles embedded in the PEI/PAA shell and it related catalytic properties of hydrogenation reactions..... 28

Figure 2.11. Schematic illustration of fabrication process of Au@Ag core-shell nanoparticles in the polyelectrolyte multilayer films. $NaBH_4$ was used as the in-situ reducer for Au^{3+} reduction, while weak reducer ascorbic acid was chosen to reduce the Ag on the surface of Au particles……..... 29

Figure 2.12. Schematic illustration of fabricate process of hollow Ag@Au nanoparticle by galvanic replacement in the polyelectrolyte multilayer films based on the reactivity series……..... 30

Figure 2.13. (a) Chemical structures of the molecules in the experiments. (b) Schematic illustration of the assembly of the polyelectrolyte multilayer via LbL technique, followed by oxidative crosslinking and pH/reductant induced release process……..... 31

Figure 2.14. Visual observation of $(BPEI_{10.5}/PAA_3)_{30}$ and $(BPEI_{6.5}/PAA_3)_{300}$ coatings with cuts 50 μm wide after different times of immersion in neutral water. (a-f) The $(BPEI_{10.5}/PAA_3)_{30}$ coating immersed in water for 0 s (a, b), 10 s (c,d), and 5 min (e, f). (g, h) The $(BPEI_{6.5}/PAA_3)_{300}$ coating immersed in water for 0 s (g) and 24 h (h)…….. 33

Figure 3.1. Contact angles of 10.5 bilayer PDAC-SPS PEMs before and after APFO exposure. Contact angles significantly increase from less than 60° to as high as 110° after the surfaces are ion exchanged with APFO…… 40

Figure 3.2. Contact angles of 10.5 bilayer PDAC-SPS PEMs assembled with 250 mmol/L NaCl dipped into APFO solutions for different times. The contact angle reaches the plateau (~110°) in a short time (30 s)…… 42

Figure 3.3. f_{APFO} value calculated from contact angles according to Cassie's model for PEMs with surfaces that had been counterion exchanged with APFO. When NaCl concentration in the assembly exceeds 200 mmol/L, the fraction of fluorinated groups on the PEM surface reaches approximately 90%..... 43

Figure 3.4. Thickness of 10.5 bilayer PDAC-SPS PEMs before and after dipping in APFO (5, 25, and 100 mmol/L) solutions for 5 min. The thicknesses increase up to 140% by displacement of SPS and diffusion of APFO surfactant into the PEM structure……..…. 44

Figure 3.5. Thickness (closed symbols) and thickness ratio (open symbols) of 10.5 bilayers PDAC-SPS PEMs before and after APFO (5, 25, and 100 mmol/L) dipping for 5 min. The thicknesses increase up to 140% by displacement and diffusion of APFO surfactant…… 45

Figure 3.6. Thickness and SPS composition of 250 mmol/L NaCl assembled 10.5 bilayers PDAC-SPS PEMs dipping into 5, 25, and 100 mmol/L APFO solutions for different time. Open symbols are the UV absorbance of the film whereas closed symbols are the film thickness. PDAC has a strong tendency to form ionic aggregation with APFO compared with SPS, so that APFO counterion exchange and diffusion are dominated to increase the thickness and removal of SPS occurs quickly……..... 45

Figure 3.7. A monovalent fluorinated surfactant, APFO, was assembled into PEMs of PDAC and combined with NaCl, which was not shown in scheme..... 47

Figure 3.8. Zeta potential as a function of the outmost layer through step-by-step growth of silica-$(PDAC\text{-}APFO\text{-}SPS)_2$. The concentration of APFO was chosen as 5 mmol/L and concentration of PDAC and SPS solutions were chosen to be 20 mmol/L in repeat unit. The charges of PEM surface alternate during each trilayer assembly…… 47

Figure 3.9. Contact angles of APFO assembled PEMs by varying APFO assembly concentrations below CMC, from 0 to 25 mmol/L. NaCl at a

concentration of 250 mmol/L was presented in the polyelectrolyte assembly solutions. Contact angles vary from hydrophilicity (~50°) to hydrophobicity (~140°) at the APFO assembly concentration below CMC value…… 48

Figure 3.10. Thickness (black symbols) of 10.5 trilayer PDAC-SPS PEM co-assembled with APFO and UV-Vis absorbance (red symbols) at 199 nm for varying APFO assembly concentrations below the CMC, from 0 to 25 mmol/L. Both the thickness and the absorbance of SPS go through the same type of two regimes transition as contact angle does…..... 49

Figure 3.11. FTIR spectra of APFO co-assembled PDAC-SPS PEM by varying APFO assembly concentrations. Shoulder peak of APFO can be detected at low concentration as 0.5 mmol/L (blue circle). The decrease in S=O symmetric vibration (red circle) can be observed at higher concentration as 25 mmol/L……. 51

Figure 3.12. Contact angles of APFO co-assembled PEMs with different NaCl concentration in polyelectrolyte solutions and a fixed APFO concentration (5 mmol/L). Contact angle reaches the peak value of ~140°. The first two dots circled do not have the same stability as the value for other NaCl concentration……..... 52

Figure 3.13. Thicknesses ratio of PDAC-SPS PEMs co-assembled with APFO to those PEMs with surface ions exchanged with APFO by a single dipping process across different NaCl concentrations in the polyelectrolyte assembly solutions. Co-assembly process has significant consequences for the coil conformations of polyelectrolyte due to huge thickness increase (~180%)…….. 53

Figure 3.14. (A) UV-Vis spectra of APFO co-assembled PDAC-SPS PEMs varying NaCl concentration in polyelectrolyte solutions and (B) their relative SPS absorption at 199 nm. (C) Thickness of APFO co-assembled 10.5 trilayer PDAC-SPS PEMs with different NaCl Concentration in polyelectrolyte solutions. The concentration of APFO during assembly is fixed as 5 mmol/L. The amount of SPS absorption will increase with increasing the multilayer thickness…….. 54

Figure 3.15. FTIR spectra of APFO co-assembled PDAC-SPS PEMs with different NaCl concentration in polyelectrolyte solutions. The concentration of APFO during assembly is fixed as 5 mmol/L…… 55

Figure 4.1. The pH window over which a BPEI/PAA film is stable when immersed in solutions of varying pH. Optical micrographs of porous structures of 30 bilayers BPEI/PAA film after post-assembly treatment in different pH solutions for 1 hour. Assembly pH of PAA was kept as 4.5, while that of BPEI was 9.5, 7.5 or 6.5 as shown in (A), (C) and (D); (B) Normalized film thicknesses of 30 bilayers of dried BPEI/PAA film with

different assembly pH immersed in varying pH solutions for 1 hour. The window of stability is always in between the assembly pH of BPEI and PAA and becomes narrow when the BPEI assembly pH is decreased to 6.5. The scale bar for all the micrographs is 200 μm…….…… 62

Figure 4.2. SEM images of porous structures of $(BPEI_{6.5}/PAA_{4.5})_{30}$ films that evolve through staged acid etching. The inserts in each image are high magnification SEM images of the porous structures. The scale bars for the low magnification and high magnification images are 100 μm and 20 μm, respectively. The corresponding size and distribution of both the large microscaled pores and the smaller nanoscaled pores are shown in Table 4.1…… 64

Figure 4.3. The design and omniphobicity of SLIPS from polyelectrolyte multilayers. (A) Schematics of the procedure for fabricating SLIPS from $(BPEI_{6.5}/PAA_{4.5})_{30}$ dense film; (B) The set-up used for chemical vapor deposition (CVD) of POTS (the liquid in the vial has been colored to orange for ease of visualization) with a proposed reaction for how POTS adheres to the film; (C) Static contact angles of 5 μL water drop on the film surface before and after lubricant coating; (D) Optical micrograph of the advancing and receding angle of water and decane (5 μL), which are captured at the droplets slide on the polyelectrolyte SLIPS a tilting angle of 3.0°, showing a contact angle hysteresis lower than 2°; (E) Optical micrographs demonstrating the mobility of water and decane droplets (5 μL) sliding on a SLIPS at a low titling angle (α=3.0°)…….. 67

Figure 4.4. Temperature robustness and curved surface coating of polyelectrolyte SLIPS. (A) Dynamic contact angle of water and decane droplets with different temperatures on polyelectrolyte SLIPS. The advancing (black) and receding angle (red) of water (square) and decane (circle) was taken using a drop volume of 5 μL; (B) Water and oil repellant properties of polyelectrolyte SLIPS coated tube compared with a bare glass tube. The upper phase decane colored with red silicone oil, while the lower phase is water dyed with methylene blue; (C) Water and oil repellant properties of polyelectrolyte SLIPS coated tube compared with a bare glass tube. The upper phase is methylene blue dyed water while the lower phase is chloroform. The polyelectrolyte SLIPS coated tube has good repellency to both water and decane (oil), however the bare glass tube does not…..... 69

Figure 5.1. Analysis of the stability of BPEI-Cu^{2+} complex monitored by UV-Vis absorbance at λmax=630 nm for solution pH of 7.5, 8.5 and 9.5. BPEI concentration was fixed at 40 mmol/L with respect to the repeat group. The complex becomes unstable and precipitate forms at a ratio of 0.3 moles of Cu^{2+}/moles of amine group in BPEI. Below that ratio, the complex can be stable over one week at all pH values……..... 77

Figure 5.2. TEM images of BPEI-Cu^{2+} complex after prepared for one week. The low magnification (A) and the high magnification (B) images of the

complex of BPEI and Cu^{2+}; The low magnification (C) and the high magnification (D) images of the complex with same composition reduced by $NaBH_4$. The concentrations of BPEI and PAA were fixed as 40 mmol/L and 20 mmol/L in repeat functional group, while the concentration of Cu^{2+} as 3 mmol/L. pH of complex was fixed as 9.5. The molar ratio of Cu^{2+} to amino groups of BPEI is 0.075…….....…….. 78

Figure 5.3. Degree of Ionization of BPEI and BPEI-Cu^{2+} complex as a function of pH. BPEI concentration was fixed at 40 mmol/L of polymer amine functional groups. Increasing the amount of Cu^{2+} in the complex will decrease the amount of charge groups available for ionic crosslink formation in the polyelectrolyte multilayers…....……..…….. 79

Figure 5.4. Schematic representation of multilayer assembly process, internal structures of BPEI-Me^{n+}/PAA, and Men+ release process. Me^{n+} represents the metal ion, which can be Cu^{2+}, and performs as an ionic crosslinkers between functional groups of both BPEI and PAA. The film would be more realistic to show the interpenetrating networks structures, which is not shown here…… 81

Figure 5.5. Dependence of film thickness of (BPEI-Cu^{2+}/PAA)$_{30}$ PEMs on pH of BPEI-Cu^{2+} complex and/or PAA solution. (A) pH of PAA is fixed as 3.5 and pH of the complex varies; (B) pH of BPEI-Cu^{2+} complex is fixed as 9.5 and pH of PAA varies. The concentration of BPEI and PAA are fixed at 40 mmol/L and 20 mmol/L with respect to the functional group (either carboxylic acid or amine group). The polyelectrolyte charge densities and their conformations influence the overall film thickness..... 82

Figure 5.6. Film thickness values and images of (BPEI-Metal ion/PAA)$_{30}$ PEMs deposited on glass slides under assembly conditions of pH 9.5 and 3.5 for the BPEI-metal ion complex and the PAA solution. The concentrations of BPEI and PAA were fixed as 40 mmol/L and 20 mmol/L in repeat functional group and the concentration of metal ions (Cu^{2+}, Co^{2+}, Fe^{2+}, Ag^{+}, and Zn^{2+}) as 3 mmol/L. Metal ions can be assembled into PEMs through chelation with BPEI and some of these complexes result in strongly absorbing colorful films……... 82

Figure 5.7. TGA graphs of (BPEI/PAA)$_{30}$ and (BPEI-Cu^{2+}/PAA)$_{30}$ PEMs as pH 9.5 for BPEI or BPEI-Cu^{2+} complex and pH 4.5 for PAA assembly solution. The concentrations of BPEI and PAA are fixed as 40 mmol/L and 20 mmol/L in repeat functional group, while the concentration of Cu^{2+} fixed as 3 mmol/L. The free-standing film was built on the polystyrene substrate and release from the substrate once it was dried…….. 83

Figure 5.8. Degree of ionization of PAA in (BPEI-Cu^{2+}/PAA)$_{30}$ PEMs assembled under varying pH values of the of BPEI-Cu^{2+} complex and PAA solutions. (A) pH of PAA is fixed as 3.5 and pH of the BPEI-Cu^{2+} complex varies; (B) pH of BPEI-Cu^{2+} complex is fixed as 9.5 and pH of PAA varies. All the concentration of BPEI and PAA are fixed as 40

mmol/L and 20 mmol/L with respect to the functional group. The majority of the carboxylic acid groups in the PEMs are ionized, consistent with PAA being a minority component in the PEMs……. 84

Figure 5.9. Modulus (black data points) and hardness (red data points) values of $(BPEI\text{-}Cu^{2+}/PAA)_{30}$ PEMs with varying Cu^{2+} concentrations in the BPEI- Cu^{2+} complex solution. The pH values for BPEI-Cu^{2+} complex solution and PAA solution were 9.5 and 4.5, respectively. Both modulus and hardness increase with increasing the Cu^{2+} concentration in the assembly complex solution. The measurement was done at ambient condition with temperature ~25°C and relative humidity ~50%..... 87

Figure 5.10. (A) Cu^{2+} release from $(BPEI\text{-}Cu^{2+}/PAA)_{30}$ PEM in aqueous environment of varying pH. (B) Normalized PEM thickness and (C) degree of ionization of PAA in dried $(BPEI/PAA)_{30}$ and $(BPEI\text{-}Cu^{2+}/PAA)_{30}$ PEM from FTIR spectra after immersion in different pH solutions. (D) Porous structures of $(BPEI/PAA)_{30}$ and $(BPEI\text{-}Cu^{2+}/PAA)_{30}$ PEM immersed in solutions with different pH value for 1 hr. Scale bar is 200 μm. The PEM as deposited on the glass substrate in the assembly pH of 9.5 and 4.5 for BPEI-Cu^{2+} complex and PAA solution. The concentrations of BPEI and PAA were fixed as 40 mmol/L and 20 mmol/L in repeat functional group and the concentration of Cu^{2+} as 3 mmol/L……... 89

Figure 5.11. (A) Cu^{2+} release from $(BPEI\text{-}Cu^{2+}/PAA)_{30}$ PEM in aqueous environment of varying salt type and concentration and (B) normalized film thickness values. The PEM used here is BPEI-Cu^{2+}/PAA assembled under pH 9.5/4.5. The concentrations of BPEI and PAA were fixed as 40 mmol/L and 20 mmol/L with respect to functional group and the concentration of Cu^{2+} as 3 mmol/L. The amount of Cu^{2+} was monitored through the maximum absorbance intensity at 630 nm……..…… 90

Figure 5.12. (A) Cu^{2+} release from $(BPEI\text{-}Cu^{2+}/PAA)_{30}$ PEM in aqueous environment of varying salt and salt concentration and (B) relative normalized thickness. The PEM as deposited on the glass substrate in the assembly pH of 9.5 and 4.5 for BPEI-Cu^{2+} complex and PAA solution. The concentrations of BPEI and PAA were fixed as 40 mmol/L and 20 mmol/L in repeat functional group and the concentration of Cu^{2+} as 3 mmol/L. The amount of Cu^{2+} was monitored through the maximum absorbance intensity at 630 nm…….. 91

Figure 5.13. (A) Cu^{2+} release from $(BPEI\text{-}Cu^{2+}/PAA)_{30}$ PEMs in aqueous environment of varying surfactant and surfactant concentration and (B) related normalized thickness. The PEM was deposited on a glass substrate under assembly conditions of pH 9.5 and 4.5 for BPEI-Cu^{2+} complex and PAA solution. The concentrations of BPEI and PAA were fixed at 40 mmol/L and 20 mmol/L with respect to the functional group and the concentration of Cu^{2+} at 3 mmol/L. The amount of Cu^{2+} was

monitored through the maximum absorbance intensity at 630 nm.…..…….. 91

Figure 5.14. FTIR spectra showing (BPEI-Cu^{2+}/PAA)$_{30}$ PEM interdiffused with different surfactants (A) APFO, (B) SDS, (C) CTAB, (D) TWEEN 20. APFO and SDS exchanged with the components of PEMs in a fast rate, while CTAB and TWEEN®20 exchanged with the components of PEMs in a slow rate……..…... 92

Figure 6.1. (A) UV-Vis and fluorescence spectra of 30 bilayer BPEI-Ag^+/ PAA films. Black color spectrum was the UV-Vis spectrum. Red and blue color spectra were the excitation (with fixed emission wavelength of 615 nm) and emission spectrum (with fixed excitation wavelength of 450 nm), respectively. Concentration of BPEI and PAA were 40 mmol/L and 20 mmol/L with respect to the repeating group. Concentration of Ag^+ in the BPEI-Ag+ complex solution was fixed as 3 mmol/L……..……. 99

Figure 6.2. The growth of BPEI-Ag^+/PAA film. UV-Vis (A), fluorescence spectra (B) and thickness (C) of BPEI-Ag^+/PAA film with different bilayer number. The fluorescence spectra with different bilayers were obtained with excitation wavelength of 450 nm. The photographs of BPEI-Ag^+/PAA film with different bilayer number under visible light (D) and 302 nm UV radiation (E). Films show colorless under visible light, while those under 302 nm UV radiation shows orange emission color and the intensity increase with increasing the bilayer number. Concentration of BPEI and PAA were 40 mmol/L and 20 mmol/L with respect to the repeating group. Concentration of Ag^+ in the BPEI-Ag^+ complex solution was 3 mmol/L……..…… 100

Figure 6.3. UV-Vis (A) and fluorescence spectra (B) of 30 bilayer BPEI-Ag^+/PAA film with different Ag^+ concentration in BPEI-Ag^+ assembly complex solution. The emission spectra were obtained with 450 nm excitation wavelength and the relative intensities increase with Ag^+ concentration from 1 mmol/L to 6 mmol/L. The concentration of BPEI and PAA were 40 mmol/L and 20 mmol/L with respect to the repeating group. The concentration of Ag^+ in the BPEI-Ag^+ complex solution was 1 mmol/L, 3 mmol/L and 6 mmol/L in the BPEI-Ag^+ complex solution for LbL assembly……...……. 101

Figure 6.4. Fluorescence spectra of 30 bilayer (BPEI/PAA)-Ag^+ complex films—BPEI-Ag^+/PAA, BPEI/PAA-Ag^+, and BPEI-Ag^+/PAA-Ag^+ PEM with different molecular weight PAA as assemble solution. The emission spectra were obtained by excited at 450 nm. The concentration of BPEI and PAA were 40 mmol/L and 20 mmol/L with respect to the repeating group. The concentrations of Ag^+ in the BPEI-Ag^+ complex solution or PAA-Ag^+ complex solution were fixed as 1 mmol/L. The fluorescence intensity varies. when change Ag^+ in BPEI and PAA solution and also varies with PAA in different molecular weight…….. 103

Figure 6.5. UV-Vis (A), fluorescence spectra (B) and thickness of 30 bilayer BPEI-Ag^+/PAA film with exposure to formaldehyde gas for different time. The excitation spectra were obtained with 450 nm. The concentration of BPEI and PAA were 40 mmol/L and 20 mmol/L with respect to the repeating group. The concentration of Ag^+ in the BPEI-Ag^+ complex solution was fixed as 3 mmol/L. The fluorescence intensity quenches with elongating the formaldehyde exposure time and the visible absorbance from 400 nm to 700 nm increase in the same time. These changes do not at the cost of the decrease in thickness. (D) Pictures show fluorescence emission color of PEM exposure to formaldehyde from 0 h (left) to 24 h (right) excited by 302 nm UV radiation. (E) The illustration shows the way formaldehyde gas interact with Ag^+ in the PEM and reduce them to Ag nanoparticles (NP) in the existence of moisture…… 106

Figure 6.6. Fluorescence spectra of 10 bilayer BPEI-Ag^+/PAA PEM before (A) and after (B) heating at 200°C for 1 h. The dash line was the excitation spectra with fixed emission peak wavelength and solid line was the emission spectra with fixed excitation peak wavelength, respectively. The fluorescence intensity quenches after thermal treatment but emitting fluorescence at different wavelength. (C) The illustration shows the thermal reduction of Ag^+ to Ag nanoparticle in the film. The concentration of BPEI and PAA were 40 mmol/L and 20 mmol/L with respect to the repeating group. The concentration of Ag^+ in the BPEI-Ag^+ complex solution was fixed as 1 mmol/L, 3 mmol/L and 6 mmol/L……...……... 107

Figure 7.1. The growth curves of polyelectrolyte multilayer films. (a) BPEI/PAA, (b) BPEI-Ag^+/PAA, (c) BPEI-Ag NP/PAA and (d) BPEI-Ag NC/PAA. All PEMs follow the exponential growth initially and rapid linear growth afterwards. Insert pictures show the 30 bilayer PEMs deposited on the white polystyrene films……. 116

Figure 7.2. TEM images of (a) Ag nanoclusters and (b) Ag nanoparticles embedded in the PEMs. Insert images were the respective histogram of 300 silver particles measured in different area. The size of nanocluster was 5.5±1.3 nm, while that of nanoparticles was 54.8±21.1 nm……. 117

Figure 7.3. Time lapse optical micrographs of scratched films immersed in water for as long as 60 min. (a1-a4) 30 bilayers film of BPEI/PAA with a 89 μm scratch (b1-b4) BPEI-Ag^+/PAA film, scratch width 135 μm (c1-c4) BPEI-Ag NC/PAA film, scratch width 60 μm, and (d1-d4) BPEI-Ag NP/PAA film with a 76 μm wide scratch underneath water for 0 min, 10 min, 20 min and 60 min, respectively. The BPEI-Ag NP/PAA film can be completely healed after 10 min, however other films cannot be healed even till 60 min immersed in the water……..……. 118

Figure 7.5. Static water contact angle of polyelectrolyte multilayer films. (a) BPEI/PAA, (b) BPEI-Ag^+/PAA, (c) BPEI-Ag NP/PAA and (d) BPEI-

Ag NC/PAA. Water contact angle decreases from ~75° to ~45° from the introduction of Ag^+ ion or Ag particles to the PEMs……. 119

Figure 7.6. The swelling ratio of 30 bilayers polyelectrolyte multilayer films immersed in the water for different time periods. The water uptake behaviors of BPEI-Ag^+/PAA and BPEI-Ag NC/PAA were similar. However, these behaviors of BPEI/PAA and BPEI-Ag NP/PAA were quite different…… 120

Figure 7.7. Surface Young's modulus E0 determined by the AFM nanoindentation technique for 30 bilayers polyelectrolyte multilayer thin film (a) BPEI/PAA, (b) BPEI-Ag^+/PAA, (c) BPEI-Ag NP/PAA and (d) BPEI-Ag NC/PAA. The thicknesses of these films were ~25 μm……..... 121

Figure 7.8. Illustration of self-healing properties of free standing polyelectrolyte film segments. (a) Dried films of BPEI/PAA, BPEI-Ag^+/PAA, BPEI-Ag NP/PAA and BPEI-Ag NC/PAA (from left to right) were placed on a polystyrene surface slightly overlapping. (b) The dried films were then sprayed with water. (c) The films become tacky and are able to reconfigure into one piece over the course of 2 h while the water evaporates. (d) The resultant "healed" film which contains all of the original PEM segments is peeled off from the polystyrene substrate……. 123

LIST OF TABLES

Page

Table 4.1. Pore sizes and standard deviations of large micrometer size pore and small nanometer size pores created in the various parts of the staged acid etching. Micro-scale pores are formed during the first stage of the etching, then the nanopores are formed during the corresponding second stage of acid etching……..... 64

Table 6.1. Amount of Ag^+ was assembled in 30 bilayer BPEI-Ag^+/PAA film with different Ag^+ concentration in BPEI-Ag^+ assembly complex solution with The concentration of BPEI and PAA were 40 mmol/L and 20 mmol/L with respect to the repeating group. The concentration of Ag^+ in the BPEI-Ag^+ complex solution was 1 mmol/L, 3 mmol/L and 6 mmol/L in the BPEI-Ag^+ complex solution for LbL assembly..... 102

Table 6.2. Amount of Ag^+ was assembled in (BPEI/PAA)-Ag+ complex films—BPEI-Ag^+/PAA, BPEI/PAA-Ag^+, and BPEI-Ag^+/PAA-Ag^+ PEM with different molecular weight PAA as assemble solution. The concentration of BPEI and PAA were 40 mmol/L and 20 mmol/L with respect to the repeating group. The concentrations of Ag^+ in the BPEI-Ag+ complex solution or PAA-Ag^+ complex solution were fixed as 1 mmol/L…… 104

CHAPTER I

INTRODUCTION AND RESEARCH GOALS

Of many nano-fabrication methods, the water-based layer-by-layer (LbL) assembly technique[1] has attracted significant interest due to its simple and highly versatile approach, which has been widely used to fabricate nanostructures materials with tailored properties. Typically, the films are made of two oppositely charged polyelectrolytes bound together through electrostatic interactions, assembled with a sequential dipping process. Additionally, several other interactions, such as covalent bonds,[2] hydrogen bonds,[3] hydrophobic interaction,[4] coordination interactions,[5] and complementary based pairing,[6] have been demonstrated to be suitable for polyelectrolyte multilayer assembly.

The use of various types of advanced materials (i.e. polymers, nanoparticles, metal ions, lipids, proteins, dye molecules, dentrimers and quantum dots) allows for many different functionalities within LbL films. The properties of a LbL film, such as composition, thickness and functionality, can be readily tuned by simply varying the type of species adsorbed, the number of layers deposited, and the conditions employed during the assembly process.

Here, we are interested in the investigation of polyelectrolyte multilayer films embedded with small molecules or other moieties, such as surfactants, lubricants, transition metal ions, or nanoparticles. Although counterions are always present in PEM films to some extent, the intentional introduction into PEMs of other types of ions or small molecules especially is less well studied. It is of fundamental interest to study how these small molecules interact with (diffuse in or diffuse out) the multilayers. When assembled into the film, different types of ionic crosslinkage may be introduced, which results in differences in assembly and related disassembly mechanisms. At the same time, the incorporation of small molecules or ions into the film introduces different

functionalities. The main objective of this thesis is to take advantage of these novel materials (referred to herein as, guest species), including surfactants, lubricants, transition metal ions and nanoparticles, to introduce novel functionalities, such as wettability modulation (chapter III), omniphobicity (chapter IV), fluorescence-based sensing (chapter VI) and modification of mechanical properties (chapter V and Chapter VII).

In chapter III, surface wettability from hydrophilic to hydrophobic was modulated by ion exchange or co-assembly with surfactant during aqueous dipping or LbL assembly. Coatings with controllable wettability are of interest in a number of applications and modulation of surface wettability is often necessary for them. Generally, films made out of commercial water soluble polyelectrolytes limits the range of wettability. 'Doping' the film with surfactant achieves a greater range of surface wettabilities.

In chapter IV, omniphobic and slippery coatings from lubricant-infused, textured surfaces have been shown to have superior properties, such as low contact angle hysteresis and low sliding angles. Even though these coating can reach superhydrophobicity by introducing a specific amount of roughness, in most cases, they still have a high contact angle hysteresis and also cannot be oleophobic at the same time, which are limitations with respect to self-cleaning properties. Both of these, however, can be easily achieved by imbibing a superhydrophobic coating with lubricant (in our case, a perfluorinated oligomer) and the porous polyelectrolyte is the basis for the superhydrophobic coating. These surfaces repel both water and decane with sliding angles as low as 3°.

In Chapter V, VI and VII, a new type of film, made with a polyelectrolyte-metal ion complex, was investigated. A complex between various transition metal ions and branched polyethylenimine is formed in solution and then assembled into multilayer films with poly(acrylic acid). The metal-ligand complex formation results in brightly colored materials that deposit as

thick layers. In Chapter V, Cu^{2+} containing films were chosen as a model system for studying the disassembly of these films in response to various stimuli, including pH, salt, and surfactant. In Chapter VI, the optical properties of Ag^{+} containing films were examined. Then, in Chapter VII, differences in mechanical properties, specifically ability to self-heal, were investigated based on the different species and interactions that existed in the film.

CHAPTER II

LITERATURE REVIEW

2.1. Polyelectrolytes and polyelectrolyte multilayers

Polymers, which have been known since the early 1500's, are large organic molecules with molecular weight high enough to allow for chain entanglements. Polyelectrolytes are a group of polymers which dissociate to form highly charged polymer molecules when dissolved in water or other polar solvent.[1] Well-known examples are DNA, RNA, polysaccharides and proteins. Polyelectrolytes may contain either positively or negatively charged functional groups along the backbone of the polymer chain and are then called polycations and polyanions, respectively.[1] Typically, they are divided into two subgroups by the way they dissociate. When the solvated polyelectrolyte dissociates completely, the polyelectrolyte is termed as a "strong polyelectrolyte" akin to a strong acid or base. The charge density is nearly independent of the solution pH in this case. When only partial ionization occurs it is termed as a "weak polyelectrolyte". The degree of dissociation (α) strongly varies with the pH value.[1]

Application of polyelectrolytes is not limited to the solution state. The polyelectrolyte multilayer buildup technique creates coatings on substrates nearly independent of type and geometry. Polyelectrolyte solutions can literally reach any crevice, pores or cracks on the substrate and coat them without clogging the openings.[1] This is virtually impossible using other types of casting methods with solid-containing or colloidal solutions.

2.1.1. Polyelectrolyte complexes

Mixing two oppositely charged polyelectrolytes results in either an insoluble but swellable complex or a soluble aqueous solution, depending on many factors determined by the nature of the polyelectrolytes and the method of preparation.[1] In most cases, polyelectrolyte

complexes (PECs) and polyelectrolyte multilayers (PEMs) share similar physical and chemical properties in terms of their internal structures, physical structures and morphology.[7,8] Although our research mainly focuses on polyelectrolyte multilayers, it is necessary to give a brief description here about polyelectrolyte complexes.

2.1.2. Polyelectrolyte multilayer: layer-by-layer sequential assembly

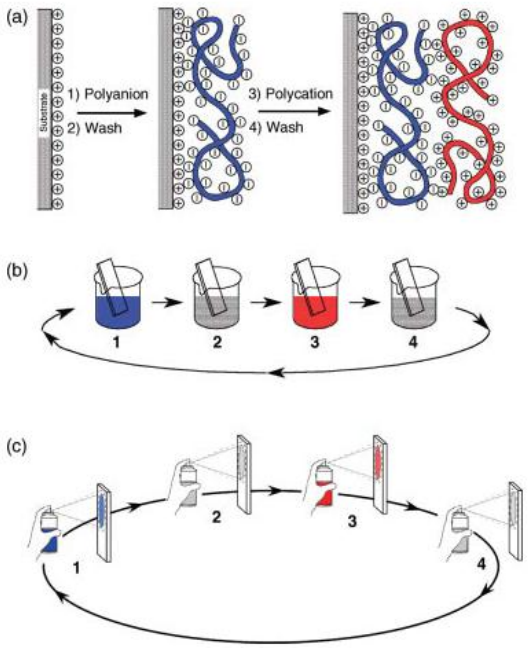

Figure 2.1. Schematic depiction of the layer-by-layer assembly technique. (a) Simplified depiction of the first two adsorption steps depicting film deposition starting with a positively charged substrate. Polyion conformation and layer interpenetration are an idealization of the surface charge reversal with each adsorption step which is the base of the electrostatically driven multilayer build-up. Counterions are not shown here. (b) Schematic depiction of the film deposition process using flat substrates, such as glass slides and silicon wafer. Steps 1 and 3 represent the adsorption of a polyanion and polycation respectively, while steps 2 and 4 are washing steps. The four steps are the basic building up sequence for the simplest film architecture $(A/B)_n$ and n is the number of deposition cycles. The construction of more complex film architectures is trivial and requires additional beakers and an extended deposition sequence. (c) Instead of bringing the surface into contact with the liquid that contains the adsorbing species by immersion, the liquid is sprayed against the receiving surface onto which the polyelectrolyte multilayer is deposited.[1] Reproduced with permission from Wiley Publishing.

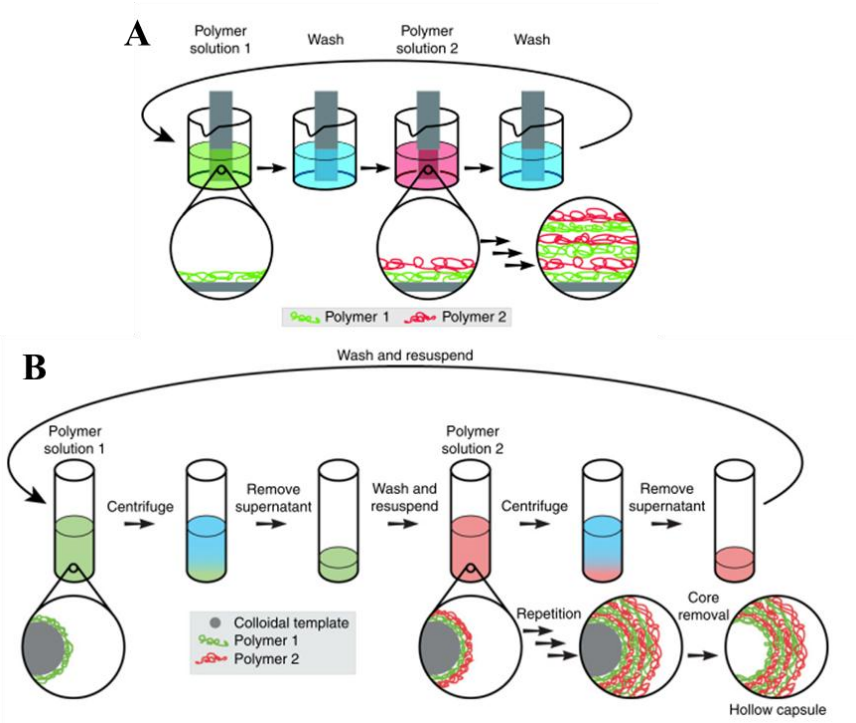

Figure 2.2. Basic principles of the layer-by-layer techniques on planar and curved surface.[9] (A) The illustration of planar surface alternately immersed in solution of two oppositely charged polyelectrolytes. The template is washed in between the immersion steps in order to remove weakly bounded polyelectrolyte. (B) The illustration of layer-by-layer assembly on curved colloidal templates which is achieved by suspending the templates alternately in solutions of two oppositely charged polyelectrolytes. After each assembly step, the templates are isolated via centrifugation and washed with solvent to remove weakly bounded polyelectrolytes. Dissolution of the colloidal template affords hollow capsule. Reproduced with permission from Elsevier Publishing.

The main advantage of this technique is that it allows us to choose from a variety of different components as the constituents of the multilayer films.[1,10,11] Nearly any type of charged material can be considered for a component of a multilayer film so long as it can be dispersed as an aqueous suspension. This large choice of materials allows for the formation of coatings with interesting chemical, biological, optical, electronic, magnetic, adhesive or antibacterial properties, giving rise to a variety of possible applications in different areas.[1,12,13] Moreover, LbL films can coat surfaces with any kind of shape, ranging from flat surfaces for making thin film coatings and

free standing films, to curved surfaces to make core-shell particles, capsules, nanotubes, nanorods, etc.[1,9,11,14] Even with these differences in curvatures and sizes, the first few layers of LbL films have the identical properties.[1] To hasten the multilayer building time, spraying techniques (figure 2.1(c)) were developed recently by Winterton and Schlenoff.[1] "Shaking and centrifuge" technique (figure 2.2(B)) was developed for coating on small scaled surfaces, in which the typical layer-by-layer machine cannot be efficiently used. Besides the typical electrostatic interaction, other interaction possibilities are also available to build up multilayers such as hydrogen bonding, covalent interactions and coordination interactions.[1,3,5,12]

Since this work mainly focuses on the properties of polyelectrolyte multilayers as they relation to their structures, the basic principles behind the mechanism of multilayer buildup as well as factors that affect multilayer assembly will be discussed. A few examples about the use of polyelectrolyte multilayers in wettability modulation and different types of ionic crosslink and related applications will be also presented.

2.1.3. Mechanism of multilayer buildup

The ability of polyelectrolyte absorbed on a charged surface back and forth can be explained by charge reversal and overcompensation.[15-18] Charge reversal was first mentioned by Decher *et al*[1,19] referring to the case of buildup of poly(allylamine hydrochloride)/sodium poly(styrene sulfonate), PAH/SPS, multilayer film. When a polyelectrolyte is deposited on a charged surface, the ionic groups on the chain neutralize the charge by forming an ionic bond (charge compensation), releasing counterions into the solution, making the process entropically favorable. However, at some point during this process the charge on the surface comes to be in excess (overcompensated). The deposited polyelectrolytes not only match the available charge, but also add an excess charge (which depends on several variables, which mentioned in section

2.2), making the surface ready for the next incoming polyelectrolyte deposition step with an opposite charge.[16]

Before an attempt to provide experimental evidence of charge overcompensation and how the process affects multilayer buildup is made, it is worthwhile to ask why it occurs. Consider the polymer chain in solution. It is obviously that the conformation of the chain, depending on the ionic strength of the solution it is in, is usually not completely flat or extended, but contains convoluted segments that tend to make some of the charges inaccessible to the adsorption surface. Consequently when a polyelectrolyte is deposited, the extended segments of the chain aim at neutralizing the surface charge, while the loops extend into solution. Both of these are hydrated by water and neutralized by small counterions.[1]

Therefore, polyelectrolytes in a relatively "salt-free" solution tend to just compensate the surface charge since the conformation of the chain is extended due to Bjerrum length restrictions.[16] In concentrated salt solutions, the polyelectrolyte chains hold a loopier structure and, as a consequence, a higher degree of overcompensation is expected.[16] Thus, the ionic strength of the solution has the tendency of not only regulating the amount of overcompensation, but also the mass of polyelectrolyte deposited. That is the reason that salt can be used to manipulate the multilayer thickness during the assemble process and in the same time salt can be induced to modulate pores openings, which will be discussed in section 2.2.1.

2.2. Factors affecting multilayer growth and behavior

2.2.1. Salt concentration

The effect of ionic strength on polyelectrolyte multilayers can be divided into three sections, including the effect of salt during the polyelectrolyte assembly, polyelectrolyte multilayer rearrangement with post-salt annealing, and the salt ion transportation in the polyelectrolyte multilayer.

When dissolved in solution, a polyelectrolyte is accompanied by an equivalent amount of counterions.[20-24] The charge on the backbone has a controlling effect on the conformation of the chain in solution. A polyelectrolyte that is highly charged, or in a low ionic strength solution, existed in an extended conformation. On the other hand, the polyelectrolyte that it has low charge density or is placed in a high ionic strength solution, its structures is coiled due to charge screening, where counterions shield the charged groups on the backbone and lower the repulsive interaction between same charge groups.[25]

Similar to how the salt effect in the polyelectrolyte complex,[1] both the salt concentration and nature of the ion has a pronounced effect on multilayer buildup. The salt concentration in the assembly solutions matters the conformations for polyelectrolytes and then result in the difference in film thickness and varies of interpenetration. The types of ions, both the anions and cations, can influence the chain conformation in different ways. Moreover, they can be in the film or out of the film after the multilayer assembly due to the assembly process and nature of the ion.

Salt ion, such as sodium and chloride, are also capable of interacting with multilayer post treatment, named as post-salt treatment. To simply put, charged counterions can diffuse across the PEM and break up electrostatic bond formed between the polyelectrolytes, transforming some of the intrinsically compensated segment into extrinsic sites in the PEM, showing the following equilibrium in equation 2.1:[1,26,27]

$$Pol^{+}Pol^{-}_{m} + yNa^{+}_{aq} + yCl^{-}_{aq} \Leftrightarrow yPol^{+}Cl^{-}_{m} + yPol^{-}Na^{+}_{m} + (1-y)Pol^{+}Pol^{-}_{m} \qquad \text{(eqn 2.1)}$$

Where Pol^{+} and Pol^{-} are the positively and negatively polyelectrolyte segment in the multilayers, *m* is the multilayer phase, *aq* refers to the aqueous phase, and *y* is the fraction of extrinsic sites caused by the presence of polyelectrolyte ionic groups that are neutralized by small counterions. The extrinsic site fraction is proportional to the concentration of salt, NaCl in this case, in solution. Over a certain concentration, called as critical concentrations, PEM starts

decomposition by changing conformation and rearranging the polyelectrolyte and release out the chain with less charge out of the PEM. Salt-induced decomposition works for both the strong and weak polyelectrolyte system. The relative critical decomposition concentration is depending on the polyelectrolyte system and how is the way they are assembled. For example, PDAC/SPS multilayers are reported to be able to withstand the NaCl concentration of 2 mol/L before any decomposition is observed.[27] On the other hand, PDAC/PAA multilayers are more sensitive to salt and start decomposition from 0.3 mol/L NaCl.[27]

The way ions move through the multilayers is another interesting topic to discuss. The study of ion permeation through PEMs has been ongoing for some time.[28] In the first study, Krasemann *et al*[29] found that the permeation rate for NaCl in PAH/SPS multilayer was 15 times higher than that for $MgCl_2$. Other studies have reported that the separation factor for Na^+/Mg^{2+} and Cl^-/SO_4^{2-} was 112.5 and 45, respectively.[30] Both the separation factor and the permeation rates were influenced by the number of adsorbed layer, the charge density of the polyelectrolyte, pH value and NaCl concentration in the polyelectrolyte solution when assembling the PAH/SPS multilayer. Numerous subsequent work has been reported on different cation and anion transport through a variety of polyelectrolyte multilayer systems, such as PAH/SPS, PVAm/PVS, PDAC/SPS, and PAH/PAA.[28]

Other than alkali and alkaline earth metal cation, Toutianoush and Tieke[31] have studied the transport of transition metal salt, like $CuCl_2$, $LaCl_3$, $BaCl_2$, and $K_4[Fe(CN_6)]$ though PVAm/PVS multilayers. Cu^{2+} was incorporated into the multilayer by the complex formation between copper and amino groups of PVAm. Balachandra *et al*[32] incorporates Cu^{2+} into the polyelectrolyte multilayers. The first method involves partial complexation of carboxylic acid group with Cu^{2+} ions during the PAH/PAA multilayer assembly and remove Cu^{2+} to result in the additional $–COO^-$ sites. The Cu^{2+} template PAH/PAA multilayers showed a 4-fold increase in Cl^-

/SO_4^{2-} transport selectivity compared with the one without Cu^{2+}. Toutianoush *et al*[33,34] presented the first studies of ion transport across the multilayer of *p*-sulfonato-calix[*n*]arenes and polyelectrolyte. The multilayers were prepared via LbL assemblies of anionic calixarenes, such as tetra-*p*-sulfonato-calix[4]arene (calix4), hexa-*p*-sulfonato-calix[6]arene (calix6), and octa-*p*-sulfonato-calix[8]arene (calix8), and cationic PVAm onto porous PAN supports. The permeation rate of monovalent alkali-metal chlorides (L, Na, K, Cs), divalent transition-metal chlorides (Ni, Cu, Zn), trivalent lanthanide chloride (La, Ce, Pr, Sm) across the calix4/PVA, calix6/PVA, and calix8/PVA multilayer were studied. The permeation rate follows monovalent alkali-meal chlorides>divalent transition-metal chloride>trivalent lanthanide chloride.

2.2.2. pH value

The effect of pH on polyelectrolyte multilayers becomes noticeable when the weak polyelectrolytes are used in the multilayer system. As mentioned, the charge density of the weak polyelectrolytes can be modulated by pH of the assemble solutions.[35,36] Varying the pH will modulate the charge density along the polymer backbone and therefore the coil conformation. It matters the flexibility of these during LbL assembly,[35] interpenetration and composition of deposited polyelectrolytes in the multilayers[33] and post-responsibility.[35,37] For instance, employing a strong polyelectrolyte and a weak polyelectrolyte with a reduced ionization below 70%-90%, charged units was also shown to have a dramatic effect on bilayer thickness.[38]

Post-pH treatment after multilayer build-up can cause the reversible or irreversible transformation of the porous morphology. Rubner *et al*[39] reported the irreversible porous transformation of PAH/PAA system. The PAH/PAA multilayer, built at a pH 7.5 for PAH and pH 3.5 for PAA assemble solutions, creates the microporous structures by immersion in acidic solution (i.e. pH 2.4) after multilayer assembly.[39] A sequent immersion in a combined acidic solution gives the possibility to form the honeycomb-like structure with both micro- and nano-

porosity.[40] This irreversible porous transition is due to the charge density induced phase separation (a spinodal-type decomposition) modulated by environmental pH and then the rearrangement of the polyelectrolyte in the PEM occurs.[39] Therefore, it will make sense that this kind of porosity transition happens for most of the weak polyelectrolyte system, like PAH/PAA,[39,40] LPEI/PAA,[41] and BPEI/PAA.[42] However, reversible porous transition has also been observed in short immersion time and used to develop porous zones.[43-45] Since the porous transition from a dried polyelectrolyte multilayer will undergo few steps—diffusion, swell and decomposition. By nicely controlling the immersion time and conditions (stop before decomposition starts) let it possible has the reversible porous transition back and forth.[43] This reversible pH-gated porosity transition, effective opening and closing the pores, is driven by changes in the degree of ionization of the carboxylic acid groups of PAA and the concomitant change in degree of electrostatic repulsion.[45]

During pH-induced rearrangement the polymer chains undergo diffusion, swelling and decomposition, another interesting effect will be the permeability switch through a simple pH stimuli. Multilayers composed of PDAC-co-PAA and SPS were reported to be able to control the direction and magnitude of the electro-osmotic flow in the microfluidic system through charge rearrangement by pH modulation.[46]

2.2.3. Molecular weight

Multilayer assembly is governed by the chain length via molecular weight of polyelectrolytes and similar phenomenon was observed by polyelectrolyte complexes.[1] The high molecular weight polyelectrolyte provides a stable growth of multilayer with an anticipated increase in thickness.[47,48] However, short chains inhibit multilayer buildup. One explanation is that the incoming long chain has the tendency to strip the shorter chain form the surface and form a soluble polyelectrolyte complex in the solution. Short chains, however, cannot strip longer chains that are already on the surface due to the interpenetration formed.

The nature of the polyelectrolyte is always another consideration that regulates the extent of this chain length effect. Rubner *et al*[48] has recently reported both polyelectrolyte complex and multilayer growth based on the hydrogen bonding multilayer systems—PVA/PAA and PVA/PMAA system. Both the degree of hydrolysis and molecular weight of PVA were investigated in terms of their influence on growth complex phase behavior. The extent of PVA hydrolysis becomes a significant issue only when weak hydrogen bonding pairs, like PVA and PAA, were used. In comparison, the more strongly interacting pairs, PVA and PMAA, did not show this significantly sensitivity on molecular weight and degree of PVA hydrolysis.

2.3. Functional LbL film using novel materials

Of many nano-fabrication methods, the water-based layer-by-layer (LbL) assembly technique has attracted significant interest due to its simple and highly versatile approach, which has been widely used to fabricate nanostructures materials with tailored properties.[49]

Exploring the functionalities of LbL film based on the use of novel materials maintains the high activities in this area. The versatility of the LbL approach has allowed a broad range of materials[49-51] (i.e. polymer, nanoparticles, metal ion, lipids, proteins, dye molecules dentrimer and quantum dots) to be assembled on various substrates, on the basis of not only electrostatic interaction,[49] but also hydrogen bonding,[49] hydrophobic interactions,[50] coordination interaction,[5,52] covalent bonding,[48] and complementary based pairing.[50,51] The properties of LbL film, such as composition, thickness and functionality, can be readily tuned by simply varying the type of species adsorbed, the number of layers deposited, and the conditions employed during the assembly process.

Because LbL assembly can be applied to various kinds of materials, fields of application for LbL assemblies have great diversity, involving physics, chemistry, biology, and biomedical applications.[51] Great advances have been made in the fields of drug delivery,[9] antimicrobial

coating,[53] self-healing coating,[54] anticorrosion coating,[55] flame-retardant coating,[51] superhydrophobic coating,[40] light-emitting diodes,[49] electronically conductive polymer,[49] electrochemically reversible capsules,[49] electrolytes,[49] proton exchange membranes and direct methanol fuel cells,[49] lithium-ion batteries,[51] organic field effect transistor,[51] electrochemical capacitors,[51] photovoltaic and biosensors.[49]

Here, we take advantage of this novel materials (called as guest species), including surfactant, lubricant, transition metal ion and nanoparticles, to introduce the functionalities, such as wettability modulation (chapter III), omniphobicity (chapter IV), fluorescence sensing (chapter VI) and mechanical properties (chapter V and Chapter VII).

2.4. Wettability modulation via surfactant

Similar to the interactions between oppositely charged polyelectrolytes, complexes between polyelectrolytes and surfactants can also be formed. In solution, they can self-assemble into multiple types of structures controlled by the ratio of components, pH, salt, etc. When assembled into polyelectrolyte multilayers, it is impossible, in most cases, to achieve these perfect self-assembled structures like they did in solution. However, the properties of the surfactant, such as hydrophobicity, can be introduced into the multilayer thin film. Moreover, the thickness and post-treatment features can be different because of the competitive absorption of surfactant with charged polyelectrolyte.[56]

2.4.1. Different types of surfactant

Surfactants are compounds that lower the surface tension of a liquid, their interfacial tension between two liquids, or that between a liquid and a solid. Generally, surfactants encompass two groups of opposite polarity or solubility. The polar portion is known as the hydrophilic (head, water loving) group, while the nonpolar portion is known as the hydrophobic (tail, water fearing)

group.[57] Depending on variations in polar head groups, surfactants can be classified as nonionic, anionic, cationic and zwitterionic ,[57] as shown in figure 2.3.

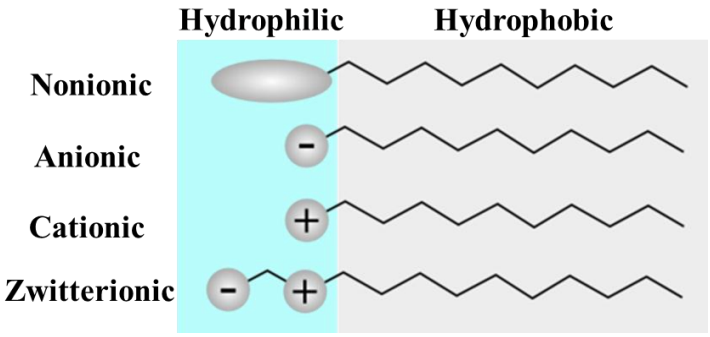

Figure 2.3. The illustration of various types of surfactant according to the composition of their head: nonionic, anionic, cationic and zwitterionic.[57] Reproduced with permission from Elsevier Publishing.

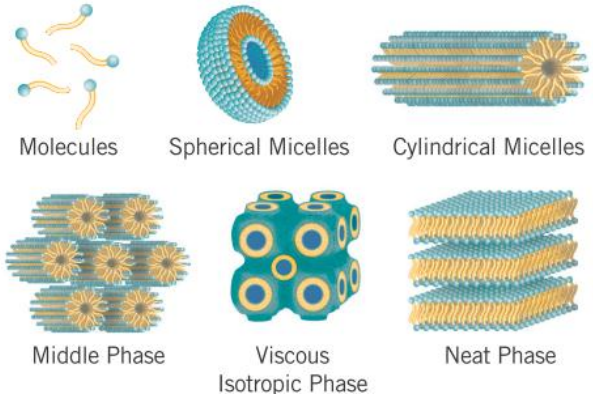

Figure 2.4. The illustration of different types of micellar structures below and above the CMC value in aqueous medium.[57] Reproduced with permission from Elsevier Publishing.

In the aqueous medium, both head and tail of the surfactant has their respective assembly preferences due to of a balance between entropy and enthalpy. The hydrophobic effect is the

driving force for micelle formation, despite the fact that assembling surfactant molecules together reduces their entropy. At concentrations below CMC (critical micelle concentration), the individual surfactant molecules are presented. As the concentration reaches a point at which the unfavorable entropic considerations due to hydrophobic tail becomes dominant, the tails gather together to get out of water and form micelles. At the same time, the enthalpic portion due to the electrostatic interaction must also be taken into account. Beyond the most common spherical micelle formation shown in figure 2.4, various mesophases can be formed in the presence of suitable additives.[57]

2.4.2. Polyelectrolyte-surfactant complex

When polyelectrolyte and surfactant meet each other in the aqueous medium, complexes were formed through electrostatic or secondary interaction. Phase diagram of these complexes is complicated and depending on total concentration, mixing ratio, molecular weight and distribution of polyelectrolyte, the stiffness of the polyelectrolyte chain, the charge density along the polyelectrolyte chain and so on.[58,59]

Some possible structures of the complexes are shown in figure 2.5.[58] For polyelectrolyte rich case, one may either have the situation where single surfactant molecules are attached to the polyelectrolyte chain (figure 2.5 (a)) or form micelle aggregation (figure 2.5 (b) and (c)). This aggregation will take place well below CMC. It is induced by the locally enhanced surfactant concentration and the hydrophobic effect as the driving force. When the polyelectrolyte is more rigid with the rather high persistence length, one may then observe the arrangements of the micelles locally along one axis, and thereby forming tube-like complex (figure 2.5 (d)). For the opposite case that surfactant structure is flat, such as bilayer membranes, one may require the stiff polyelectrolyte and results in the lamellar structures (figure 2.5 (f)). When the polyelectrolyte is less stiff, it will come up with the bilayer decorated by the polyelectrolyte (figure 2.5 (e)).

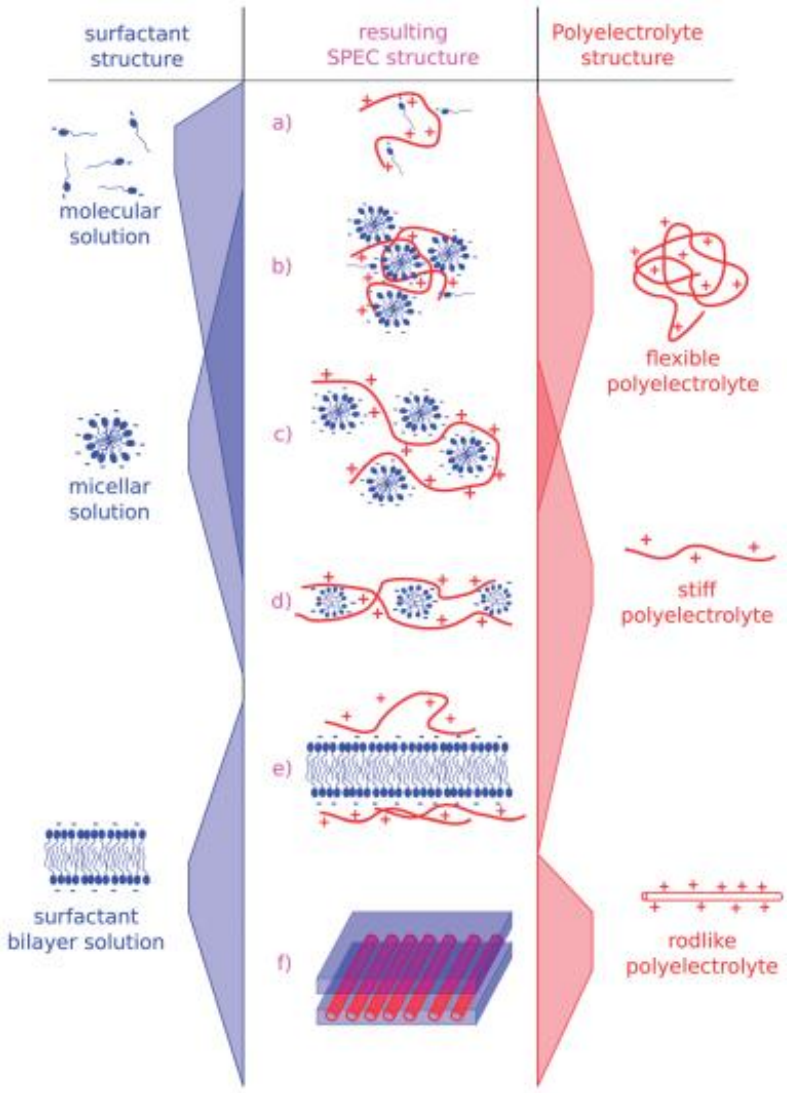

Figure 2.5. Schematic description of possible arrangements in surfactant-polyelectrolyte complexes (SPECs):[58] (a) polyelectrolyte decorated with surfactants; (b) densely packed micelles "glued" together by a polyelectrolyte; (c) pearl-necklace structures; (d) rod-like aggregation of micelles with a stiff polyelectrolyte; (e) flexible polyelectrolyte attached to a bilayer; and (f) rod-like polyelectrolyte incorporated between bilayers. Reproduced with permission from RSC Publishing.

2.4.3. Building surfactant into the polyelectrolyte multilayers

The polyelectrolyte-surfactant complex has been studied for a long time and the increased availability of water soluble synthetic polyelectrolyte led to a great number of studies on their

complexation at aqueous interface.[59] Coming from the ideas of polyelectrolyte complex and polyelectrolyte multilayer assembly, the interesting behavior of the polyelectrolyte-surfactant complex was hoped to be built into the polyelectrolyte multilayers via layer-by-layer electrostatic self-assembly method. Incorporate amphiphilic surfactant into multilayered polyelectrolyte architectures have not only provided fundamental insight of polyelectrolyte-surfactant complexation, but also introduce the functionalities based on the specific polyelectrolyte-surfactant system.

Another importance of studying the polyelectrolyte-surfactant interaction, especially the behavior when assembled into the polyelectrolyte multilayer is from the fact that most of the inorganic materials were made or modified with the charged surfactant as a protective agent during synthesis or stabilizer afterwards. When assembled into the polyelectrolyte multilayer, these surfactants-capped inorganic materials will always interacted with other species, polyelectrolyte in most of the case, in the multilayer and matters the distribution of these inorganic materials and multilayer growth.

Similar to the inter-diffusion of other small molecules, the surfactant is also possible to diffuse and swell the polyelectrolyte multilayer. The charged surfactant exchanges with small counterions and gives the extra chemistry in the film, while the charged surfactant exchanges with charged polyelectrolyte and come up with the decomposition of the films.[52,60] In some systems, surfactants have been used to partially dissolve PEMs just as salts are able to[52,60-64] and result in the roughly porous film.[52,62,64]

2.4.4. Wettability modulation through ion exchange and co-assembly

The surface wettability of polyelectrolyte multilayer is determined mainly by the chemistries of the few layers near the surface.[65] There are some reports of using counterion exchange from small counterions to larger surfactant molecules on the top surface of a

polyelectrolyte multilayer surface in order to modify the wettability.[35,56,66-68] Several examples exist of using chemistry to modulate the wettability properties of PEM surfaces. Rubner, *et al*[35] has modulated the wettability by varying the pH value of the absorbing polyelectrolyte. Johal *et al*[66] show the adsorption of an anionic surfactant, sodium dodecyl sulphate (SDS), onto the outer layer can be used to fine-tune the wettability. Su *et al*[67,68] fabricate an erasable-rewritable wettability gradient between superhydrophobicity to superhydrophilicity via counterion exchange of the polyelectrolyte multilayer film. With fluorinated surfactant co-assembly, a gradient of wettability from hydrophilic to hydrophobic can be achieved and modulated through simply changing the surfactant concentration of assemble solutions.[69]

2.5. Omniphobic slippery surfaces-an extreme fluid repellency

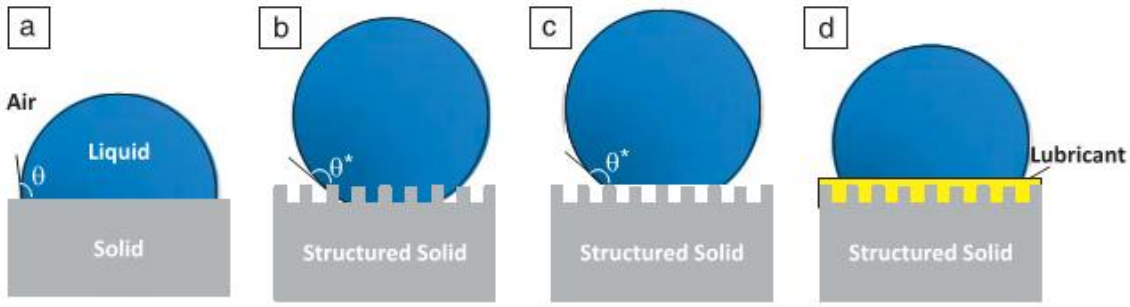

Figure 2.6. Wetting on smooth and structured surfaces. A liquid droplet sitting on (a) a smooth surface with an intrinsic contact angle, (b) a textured surface that is completely wetted by the liquid, known as a Wenzel state droplet, (c) a textured surface with trapped air pockets, know as a Cassie state droplet, and (d) a textured surface that is infused with an immiscible lubricating fluid (or slippery liquid-infused porous surfaces).[70] Reproduced with permission from Cambridge University Press.

Surfaces that display liquid contact angle greater than 150^{o} along with low contact angle hysteresis (<5^{o}) for liquids with both high (water) and low (oil) surface tension values are known as super-omniphobic surface.[71] The ability of surface to repel various liquids (called as

omniphobicity) has broad practical applications in self-cleaning surface, nonfouling surfaces, stain-free clothing, spill-resistant protective wear, refinery processes, and fuel transportation.[70-72]

The very famous example of superhydrophobicity will be the lotus effect, where micro/nano-structures are carefully designed to maintain an air pocket so that form a stable interface between surface and the applied liquid—Cassie state (figure 2.6 (c)).[68,69] However, this superhydrophobic surface starts become unstable for low-surface-tension liquids (i.e. oil) due to their enhanced the ability to wet the surface.[70-75] Moreover, since surface tension decreases with increasing temperature, which further destabilized the liquid-air interface, it is very challenging to design surfaces that can repel a wide range of liquids at high temperature.[72,74]

Carefully engineering surface texture, it is possible to create the omniphobic surface. One strategy is created by producing coven topography—re-entrant curvature, instead of aiming at low surface energy material.[71,76] The droplet pins at the edges of the micro/nano structures to prevent the penetration. Using lithography and electrospinning, Cohen *et al*[76] show us the importance of the geometry and the spacing, the critical parameter in their design, and the practical way to get to that surface. More recently, a conceptually different approach was developed to creating omniphobic surface--repellent material—inspired by the slippery Nepenthes pitcher plants. The surface consists of a continuous film of lubricant locked in place by a micro/nano-structured substrate (figure 2.6 (d)), which is termed as slippery liquid-infused porous surfaces (SLIPS).[77,78] The SLIPS outperforms its natural counterparts and most of the synthetic surfaces in its ability of liquid repellency. It repels water, organic solvent, oil, blood, etc with the low contact angle hysteresis (<2.5°).[77] Moreover, lots of potential properties can be incorporated into one coating. That includes rapidly restoring liquid repellency after physical damage (within 1 s),[77] functioning at high pressure (up to 6.85×10^7 Pa)[77] and high temperature (~200°C),[72] resisting bacterial bio-

fouling[79] and ice adhesion,[80] enhancing condensation,[81] and switching wettability in response to mechanical stimuli.[82]

2.6. Polyelectrolyte-transition metal ion complex films

LbL films are made of the oppositely charged polycations and polyanions. Clearly, with charged functional groups there must also be small counterions present, and a good deal of work has been done to determine what role these counterions and any other added ions play during LbL assembly.[5] Although the use of alkali and alkaline earth metal ions which are well represented,[1] the assembly of PEMs with transition metal ions is less well studied. Most of case, the transition metal ions were incorporated to polyelectrolyte multilayer via salt solution immersion after the film was assembled.[5,83] The transition metal ion can either stably existed in the film[5] or reduced chemically or physically to obtain hybrid nanoparticle film.[83]

Incorporating transition metal ion directly during LbL assembly will be the efficient way and be able to achieve high capacity metal ion concentration at the same time. However, most of the polyelectrolyte system can not form the stable complex with high amount of transition metal. The stability of the polyelectrolyte/transition metal ion complex as a solution and in the film will be interesting to be investigated in the very beginning. The special properties evoked from this chelation existed in the film — such as fluorescence, catalytic and mechanical properties will be another research field to look at. It includes not only the colorimetric shift for different transition metal ion capture and hybrid nanoparticle film after reduction, but also the optical and mechanical properties.

2.6.1. Chelation of polyelectrolyte with transition metal ion

Transition metal ions interact with the polymer through the formation of metal-ligand coordination bond as well as electrostatic interaction with oppositely charged moieties. Taking advantage of the partially-filled *d* orbitals, it will chelate with ligands to split into two groups

without rising overall energy. The energy gap due to the energy splitting results in the color what we noticed. Different types of ligands give the large or small energy splitting and have the complex color differently.[84]

The molecular geometry of oligomeric and low molecular weight amine-containing macromolecules has a large influence on their ability to form coordination complexes with metal ions and the stability of the resulting complexes. Although bunches of polyelectrolyte-transition metal chelation have been reported,[85] we are more focus on this branched polyelectrolyte-branched polyethylene imide (BPEI). First, the association constant for Cu^{2+} and amines (K_f of $[Cu(NH_3)_4]^{2+}$ as 1.1×10^{13}) is higher than for amines with most other metal ions (i.e. K_f of $[Co(NH_3)_6]^{2+}$, $[Ag(NH_3)_2]^{+}$, and $[Zn(NH_3)_4]^{2+}$ as 5.0×10^{4}, 1.6×10^{7}, and 7.8×10^{8}, respectively), meaning that it is very easy for this complex to form.[85] Moreover, the branch structure of BPEI contains primary, secondary and tertiary amine groups in the ratio of 25%, 50%, and 25%, respectively.[86] This makes the BPEI-Cu^{2+} complex an ideal model system for transition metal ion complexes within polyelectrolyte multilayers. Due to its highly branched and dense structure, BPEI does not change conformation in aqueous solution very easily[86] and will therefore form complexes with Cu^{2+} in a square planar geometric arrangement.[87] Recently, we found this kind of stable coordination can also be presented in BPEI with most of transition metal ion, such as Cu^{2+}, Co^{2+}, Ag^{+}, Au^{3+}, Zn^{2+}, etc.[52]

2.6.2. Transition metal ion in the polyelectrolyte multilayers

Polyelectrolyte-transition metal ion complex can existed stably due to the formation of metal-ligand coordination bond as well as electrostatic interactions with oppositely charged moieties in the complex. It will be interesting to incorporate these interactions into the buck materials. Utilizing LbL technique, Kurth *et al*[88] reported a metallo-supramolecular coordination polyelectrolyte by reaction of Co^{2+} with a novel bisterpyridine ligand to build electrochromically

active multilayers. Taking advantage of the coordination bond between transition metal ion and pyrinde, Zhang *et al*[89] report multilayers of PSS-Cu^{2+}/PVP and Ji *et al*[90] assembled similar film with Co^{2+}. They can either reduce the ion to make a nanoparticle-polymer hybrid film or keep the ions stable in the film used for ion-depended unique separation properties. Based on these unique coordination pairs, these films ligand containing films can also be used for transition metal ion capture. Kurth *et al*[91] designed a film containing polyelectrolyte with bipyrindine ligands to behave as a metal ion receptor using the ability to bind through metal ion coordination. Tieke *et al*[30,33,34,92-94] built PEMs with macrocycles, such as calyx[n]arene and crown ethers, as ligands for multiple sequential captures of transition metal ions for ion-selective membrane for water softening and seawater desalination.

Specifically for the BPEI/PAA multilayer system we are interested in, there are only a few reports of the possibility of incorporating transition metal ions (e.g. Cu^{2+}) into the films during the LbL process. In other multilayer systems using PAA, Cu^{2+} has been incorporated into the $(PAH/PAA)_n$ film as observed by both Bruening[32] and Caruso[95], either by the addition of ions in the deposition solution that then complex with a fraction of the carboxylic acid groups of PAA or by dipping the substrates in Cu^{2+} solution after being immersed in PAA solution. Hammond *et al*[96] doped transition metal ions (Cu^{2+}, Fe^{2+}, and Ag^{+}) into a similar film during the LbL process through interaction with the carboxylic acid groups of PAA as metal-ligand complexation to get optimized capture of ions in the film. However, PAA-metal ion complexes have only been demonstrated to trap small amounts of ions into the film by just dipping methods. In the case of BPEI/PAA, a roughened surface pattern is formed after immersing the film in Cu^{2+} or Zn^{2+} solution.[95] Transition metal ions, like Cu^{2+} and Zn^{2+}, coordinate strongly with carboxylic acid group of PAA. At the same time, they can also bind with the amine groups of BPEI through electron transfer. Sukhishvili *et al*[5] show that BPEI/PAA films do have the capacities to absorb the transition metal ions (Cu^{2+}

and Co^{2+}) through forming chelation complexes with amine and carboxylic acid groups in the film. Although post-assembly absorption method are the good way to achieve high capacity metal ion concentration in PEMs,[73] it do not the efficient way to obtain these high capacity.[5,85]

2.6.3. Optical properties of polyelectrolyte-metal complex film

Taking advantage of the partially-filled *d* orbitals, it will chelate with ligands to split into two groups without rising overall energy. The energy gap due to the energy splitting results in the color what we noticed. Different types of ligands give the large or small energy splitting and have the complex color differently.[84]

Coordinative assembly allows organic-inorganic coordination polymer,[1] metal ion,[5,52] and metallopolymers[98] to built up as the supramolecular functional assemblies. Most of case, they are conjugated polymer and resulting film have color change or emitting light (from UV to near IR) when met with metal ion.[1,99,100] The polyelectrolyte, made by conjugated polymer with ionic moieties such as caboxylates, sulfonates and quaternary ammonium salts, quenches in luminescence when met with metal ion. This can be simply explained by self-quenching and intermolecular energy transfer caused by the aggregation of chromophores in the aqueous solution.[99,100]

The luminescence of polyelectrolyte film can also from metal particles in the film. When the size of metal particle is reduced to few nanometer—call as nanocluster), the band structure becomes discontinuous and it broken down into discrete levels, somewhat similar as the energy levels of molecules.[101] Nonetheless, it can still interact with light via electronic transitions between energy levels and result in intense light absorption and emission, like fluorescence.[102-104]

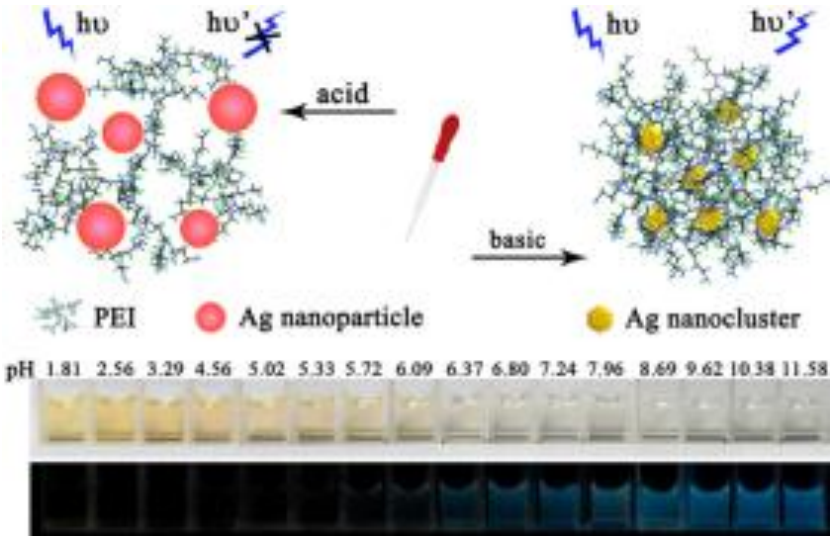

Figure 2.7. Schematic illustration of pH-sensitive fluorescent silver nanocluster. Silver nanocluster is prepared with branched polyethylenimine as capping agent. In the pH from 1 to 12, it shows both the color and fluorescent change.[102] Reproduced with permission from ACS Publishing.

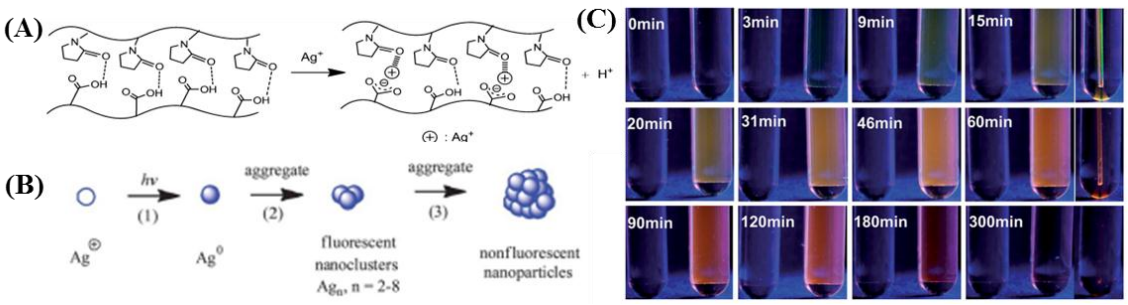

Figure 2.8. The fluorescent Ag nanocluster PVPON/PAA films by in situ UV reduction. (A) Loading of Ag^+ into the PVPON/PAA films. (B) Generation of Ag nanoparticles in the film by photo-reduction of Ag^+. The fluorescence intensity can be controlled by particle size. (C) Photographs of a Ag^+-loaded film (right) and a film not loaded with Ag^+ (left) under UV irradiation at various irradiation times as marked in the pictures. The fluorescent intensity of films shows the increase and decrease due the formation and fluorescent quenching due to aggregation.[106] Reproduced with permission from RSC Publishing.

Using polyelectrolytes as stabilizer, Luo *et al*[102,103] have reported the Ag nanocluster capped by BPEI, which responds rapidly to pH fluctuations by both the color and fluorescence

intensity (figure 2.7). They also find out this silver nanocluster shows the selective recognition of halide ions (i.e. Cl^-, Br^-, and I^-) due to a strong fluorescence quenching.[104] Although Ag nanocluster in the solution is robust and convenient, they still have tendency to aggregation in longer time. Considering the long-term stability of the nanocluster, nanocluster was embedded in the form of solid thin films.[105]

Zhu *et al*[106] reported the *in-situ* photochemical reduction of Ag nanocluster in the polyelectrolyte multilayer film. Here, LbL technique provides a simple way to distribute ion well dispersed in the matrix and therefore get the well dispersed nanoparticles afterwards. Based on nanoreactor chemistry, the Ag^+ can be capture into the PVPON/PAA film with a simple immersion. After UV reduction, Ag nanocluster was formed and showed the fluorescent color from greenlish yellow to red, as shown in figure 2.8. The florescence will be quenched with elongate the UV exposure time over 100 min. This is due to the aggregation of Ag nanoclusters to larger particles.

However, in most of case, *in-situ* reduction can not produce particles small enough to be an nanocluster.[85] That is the reason why fluorescent properties and the further application of Ag particles embedded in the polyelectrolyte multilayer films are not well studied, even though it is a simple and producible method.

Here, we concentrate on the preparation of this fluorescence polyelectrolyte multilayer film and further application. It has been successfully embedded in the film with controllable concentration without aggregation even with post-assembled process, which is less investigated. Moreover, we notice that the existence of Ag^+ in the polyelectrolyte film have already shown the fluorescence without further reduction to nanoclusters. This interesting phenomenon is explained to be that Ag^+ make the complex with both BPEI and PAA in some way and were split to highest occupied molecular orbital (HOMO) and lowest unoccupied molecular orbital (LUMO) in some

way and the energy difference is fit to that photoluminescence emission. In most of case, they occurs in metal-organic ligands.[107] However, it also possible for the metal ion-polyelectrolyte pairs as reported when the HOMO and LUMO was go closer and into a certain energy difference.[99] However, this will be more complicated when it happens to the metal ion/polycation/polyanion system. It will be really interesting to study this complicated system since they can be assembled as a solid matrix instead of solution, the advantage of which have been discussed before ahead.

2.6.4. Catalytic properties of polyelectrolyte-metal complex film

Rubner and Möhwald[83,85] have introduced the nanoreactor concept to fabricate the polyelectrolyte/nanoparticle hybrid film. The multilayer films capture metal ions during salt dipping process[108-109] (or called post-absorbing treatment[83]). During the reduction procedure, the existence of the polyelectrolytes in the film prevents aggregation of nanoparticles, and then achieves the small particle size (~3 nm).[108]

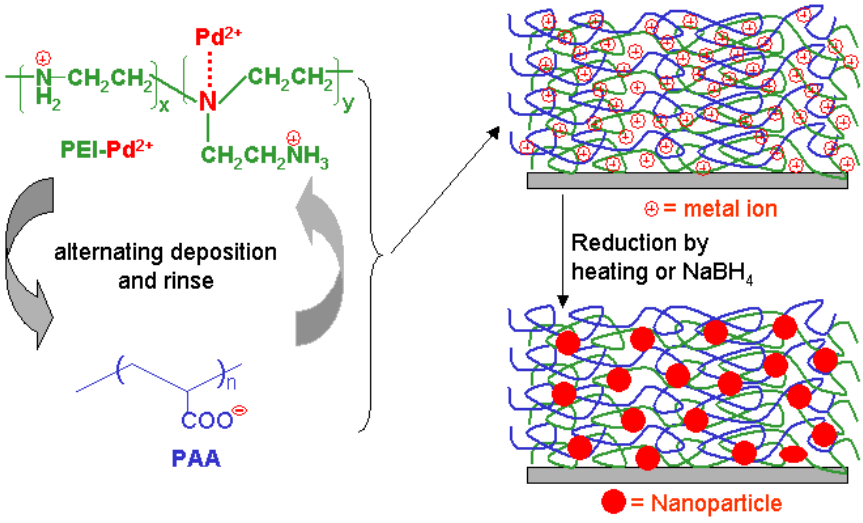

Figure 2.9. The illustration of catalytic nanoparticle formation in multilayered polyelectrolyte films. Deposition of a film containing a branched polyethylenimine-metal ion complex followed by reduction of the metal ion yields nanoparticles.[108,109] Reproduced with permission from ACS Publishing.

Rubner *et al*[83] have also employed the polyelectrolyte multilayer as nanoreactors through PAH/PAA film. They immersed a preformed PAH/PAA film into a solution containing Ag^+ to trap the metal ion in the film though ion exchange, and subsequent reduction of Ag^+ with H_2 resulted in Ag nanoparticles. Bruening *et al*[108-112] created metal nanoparticle catalysts in the multilayers through alternating adsorption of BPEI-metal ion (Ag^+, Au^{3+} or Pd^{2+}) complexes and PAA and followed by reduction of metal ion with $NaBH_4$, as shown in figure 2.9. This affords a convenient method for controlling the amount of metal ion in the film, which in turn allows the control of the particle size during reduction. The use of different ratio of PAA to Pd^{2+} in deposition solutions gives a series of films with Pd nanoparticles whose average diameter from 2.2 to 3.4 nm, and the catalytic selectivity of these nanoparticles varys dramatically with their size.[110] Ratios of turn over frequencies for hydrogenation of allyl alcohol and β-methallyl alcohol are as high as 240 with the smallest nanoparticles (figure 2.10), whereas larger nanoparticles show selectivity only 3. The selectivity of 1/2 and 1/3 with the smallest nanoparticles are especially notable because Wilkinson's catalyst—the prototypical homogeneous catalyst for selective hydrogenation—shows essentially not selectivity in the hydrogenation of mono– and distributed double bonds.

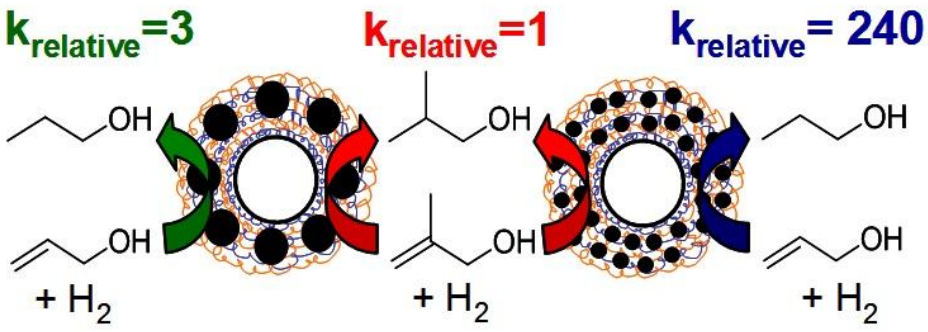

Figure 2.10. Schematic illustration of Pd nanoparticles embedded in the PEI/PAA shell and it related catalytic properties of hydrogenation reactions.[109] Reproduced with permission from ACS Publishing.

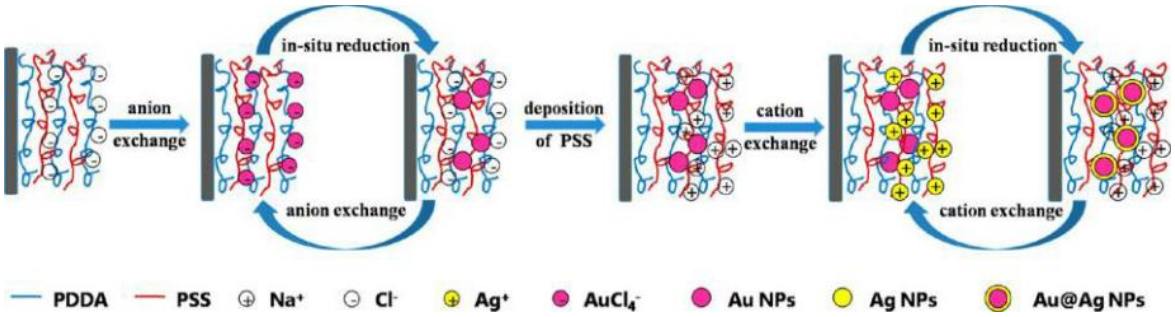

Figure 2.11. Schematic illustration of fabrication process of Au@Ag core-shell nanoparticles in the polyelectrolyte multilayer films.[117] $NaBH_4$ was used as the *in-situ* reducer for Au^{3+} reduction, while weak reducer ascorbic acid was chosen to reduce the Ag on the surface of Au particles. Reproduced with permission from ACS Publishing.

A broad range of monometallic nanoparticles (like, Au, Ag, Pd, Pt) have been synthesized in the polyelectrolyte multilayer films[83,108-111,113] based on nanoreactor concept. More recently, fabrication of Au@Ag bimetallic nanoparticles was reported to be synthesized in the polyelectrolyte multilayer films.[114-118] In the field of catalysis, bimetallic nanoparticles are of great importance because they often show better catalytic performance than their corresponding monometallic counterparts.[119] Dong *et al*[114] load the $AuCl_4^-$ and Ag^+ in to the film assembled from two weak polyelectrolytes, BPEI and PAA. The subsequent thermal reduction would give rise to the formation of Au@Ag bimetallic nanoparticles. A similar approach was adopted by Choi *et al*[115] to fabricate Au@Ag bimetallic nanoparticles in much thicker and freestanding films assembled from polyelectrolyte complex. Xie *et al*[116] directly assembled a PEI-Ag^+ complex with $AuCl_4^-$ ion and obtained a composite film by chemical reduction of incorporated ions by $NaBH_4$. Su *et al*[117,118] develop a new synthetic strategy to develop the Au@Ag bimetallic core-shell nanoparticles using the polyelectrolyte multilayers films. As shown in figure 2.11, polyelectrolyte multilayer film was assembled from PDAC and SPS. The film terminated with polycation is loaded with $AuCl_4^-$ ion via ion exchange, which are reduced by $NaBH_4$ to generate Au particles, and then a layer of SPS is deposited to covert the cap layer into the polyanion so that Ag^+ ions can be

introduced into the film by counteraction exchange. Then the Ag^+ ion are reduced with a weak reducing agent, ascorbic acid, with Au particles as seeds to yield Au@Ag core-shell nanoparticles. The thickness of Au core and Ag shell can be controlled independently by the number of ion-exchange/reduction cycles. This bimetallic particles show much higher catalytic activity than the corresponding monometallic particles, even the sum of these two.[118]

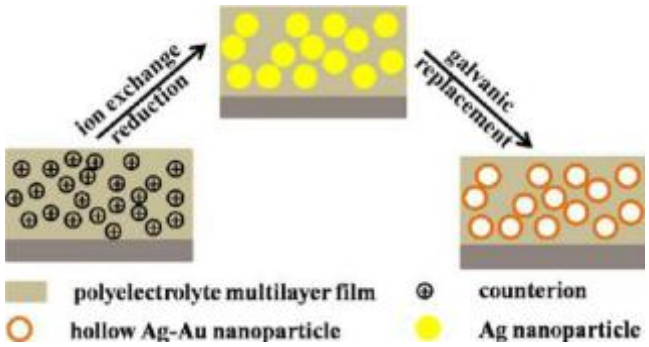

Figure 2.12. Schematic illustration of fabricate process of hollow Ag@Au nanoparticle by galvanic replacement in the polyelectrolyte multilayer films based on the reactivity series.[120] Reproduced with permission from ACS Publishing.

Take advantage of metal reactivity series and galvanic replacement reaction, Su *et al*[120] fabricate the hollow Ag@Au bimetallic nanoparticles using the similar polyelectrolyte multilayers film as nanoreactors without adding further templates. The first step of Ag seed particles reduction (figure 2.12) is similar to mentioned ahead using strong redactor $NaBH_4$. The seed regrowth step then needs ascorbic acid to let the individual seed grow larger. Ag particles here were used as sacrificial template to synthesize the hollow Ag-Au particles by simple immersion in $AuCl_4^-$ solution. We can imagine that this kind of hollow core shelled structures can give us the special catalytic and optical properties.

Moreover, this post-absorbing method can also be used to construct metal sulfide, such as semiconductor (PbS) nanocomposite, by absorbing the metal ions and subsequentially treating the film with H_2S.[121]

2.6.5. Mechanical properties of polyelectrolyte-metal complex film

The crosslink is a bond that links one polymer chain to another. It can be covalent bonds or ionic bonds. When polymer chains are linked together by crosslinks, they lose some of their ability to move as individual polymer chains and be turn into a "gel" or "solid".

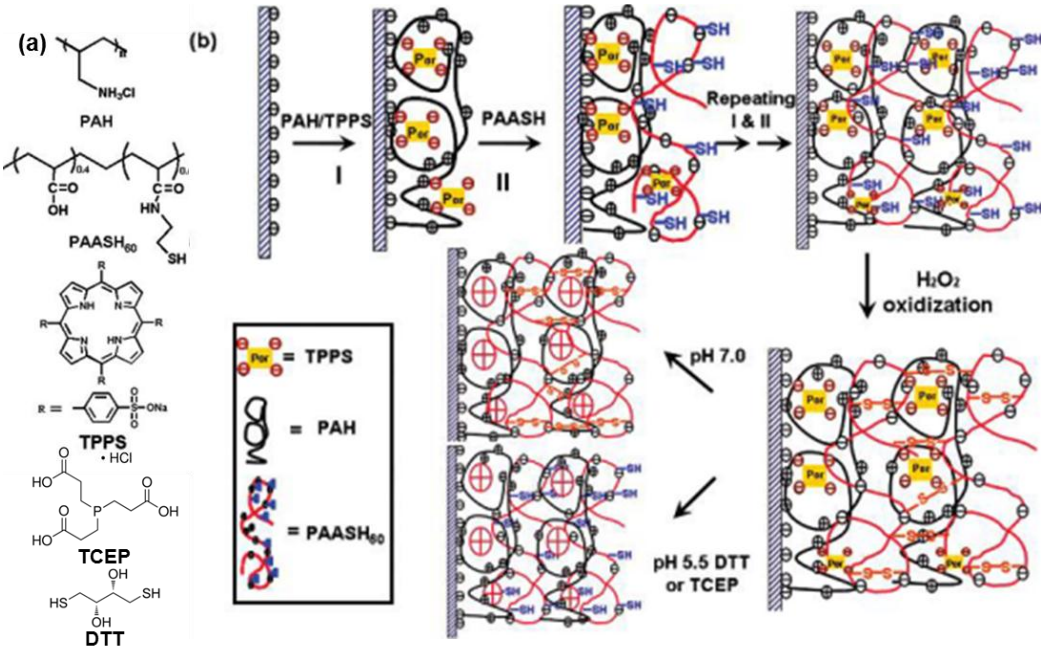

Figure 2.13. (a) Chemical structures of the molecules in the experiments. (b) Schematic illustration of the assembly of the polyelectrolyte multilayer via LbL technique, followed by oxidative crosslinking and pH/reductant induced release process.[127] Reproduced with permission from ACS Publishing.

The covalent crosslinking reaction can be promoted via thermal-[122,123], photo-[122] or chemical-[124] crosslinking. After crosslinking, the films show different properties—enhanced

stabilities against pH-induced decomposition[3,122] and changed ion permeability,[3] increased mechanical modulus.[3,125] Most typical covalent crosslink reported was irreversible. As an example, glutaraldehyde (GA) has been used in the first successful attempt to synthesize cationic single component LbL hydrogel films and capsules by selective crosslinking of chitosan with chitosan/PAA multilayers.[124] The crosslink reaction can be done in neutral pH and degree of crosslinking can be modulated with changing the GA concentration and treatment time.[3] In another example, GA was used to selectively crosslink PAH within PAH/SPS capsules via formation of a Schiff base between aldehyde and amine group in PAH.[126]

However, the covalent crosslink can be reversible, such as disulfide bond crosslink, which is reversible and responsive to the external redox environment. Zhang *et al*[127] introduce the thiol groups to PAA and obtain the PAA-SH (figure 2.13), which was served as the crosslinker to building up this reversible disulfide bond. The corresponding multilayer can used as dually controllable release by breaking the reversible disulfide crosslinking and destabilizing the charge binding sites in the pH-responsive weak polyelectrolyte multilayers films.

The ionic crosslinked films are not very stable under various pH environments. However, it gives much more versatile rearrangement of polymer chain and gives other interesting behavior, such as porous structures and self-healing properties. It has been mentioned section 2.2.2 that the post-pH treatment rearranges both the charge densities and the polyelectrolytes in the multilayer and forms either the irreversible or reversible porous structures. The charge densities of polyelectrolytes mentioned can be directly related to the ionic crosslinking in the films. Our studies on the film stabilities against pH[52] and the porous formation[42] have pointed out that both the assemble pH and post treated pH will matters the porous size and decomposition speed of the film. The degree of ionic crosslink can be modulated initially by building the film, especially for the

weak polyelectrolyte pairs. The post treatment changed the charge density of the initial ionic crosslinked film in some degree, but it is hard to rebuild the films.

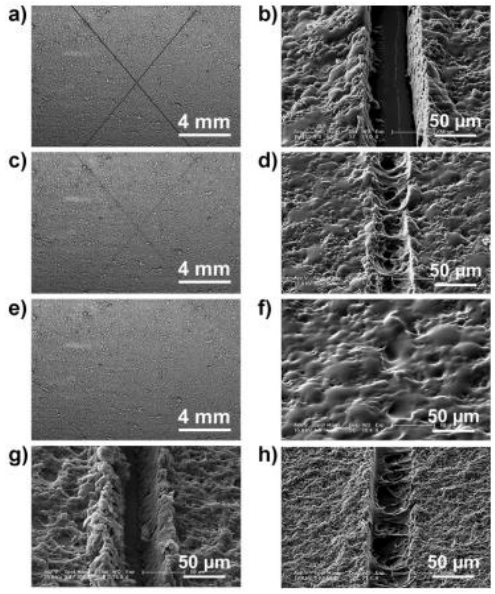

Figure 2.14. Visual observation of $(BPEI_{10.5}/PAA_3)_{30}$ and $(BPEI_{6.5}/PAA_3)_{300}$ coatings with cuts 50 µm wide after different times of immersion in neutral water. (a-f) The $(BPEI_{10.5}/PAA_3)_{30}$ coating immersed in water for 0 s (a, b), 10 s (c,d), and 5 min (e, f). (g, h) The $(BPEI_{6.5}/PAA_3)_{300}$ coating immersed in water for 0 s (g) and 24 h (h).[54] Reproduced with permission from Wiley Publishing.

Sun *et al*[54] have also shown the self-healing properties of PEM made from weak polyelectrolyte pairs (BPEI and PAA). Due to BPEI is highly protonated in acidic solution, $BPEI_{6.5}/PAA_3$ films have a higher ionic crosslinking density than $BPEI_{10.5}/PAA_3$ films have. Due to the less crosslinking of $BPEI_{10.5}/PAA_3$ film, cuts can be healed in few minutes which does not occur for $BPEI_{6.5}/PAA_3$(figure 2.14). It is originated from the high flow-ability of the coatings and their inter-diffusion of polyelectrolytes at the fractured surface in the present of water.

The ionic crosslink can also be combined with other elements, such as chelation and nanoparticles. It has been shown that films assembled with different pH have the difference in Ag^+

capture ability due to the ionization degree of PAA in the film. It will be interesting to study a new type of ionic crosslink—coordination bond. The exited transition metal ion in the film will chelate with functional group of polyelectrolytes and in the same time they will have the electrostatic interaction. Moreover, the existence of nanoparticles will be another type of ionic crosslink. *In-situ* reduction of nanoparticles gives some kinds of interaction between particles and nearby polyelectrolytes. They can be covalent-bond or ionic bond due to the reduction methods and polyelectrolyte system. Here, we will focus on investigating the mechanical performance, especially the modulus and self-healing property.

CHAPTER III

SURFACTANT CO-ASSEMBLY AND ION EXCHANGE TO MODULATE POLYELECTROLYTE MULTILAYER WETTABILITY*

3.1. Introduction

Materials based on blends of polyelectrolytes, such as complexes and multilayers, have shown a great deal of promise for a range of applications from functional devices (electronic, biomedical) to coatings to responsive materials for release of active compounds.[7,128] One of the advantages of the layer-by-layer (LbL) fabrication method to make these thin films and coatings is that there are a number of commercially available polyelectrolytes that can be used, but at the same time this does somewhat limit the possible chemical properties of the resultant materials. Property modification based on charge screening with salt and varying charge density of weak polyelectrolytes by pH are common, need references but modification with surfactant is less well studied. We present here counter ion exchange of polyelectrolyte multilayers (PEMs) with a perfluorinated surfactant, as well as the co-assembly of polyelectrolytes with the surfactant. This second method has only rarely been reported in the literature, and for purposes different than our own, and we believe that surfactant co-assembly may become a significant way to modify the chemical properties of polyelectrolyte multilayers and complexes while using commercially available materials.

One active area of research is to modulate the wettability of these materials for self-cleaning materials (coatings for clothing, car windshields, or the insides of pipes), or possibly for

*Part of the data reported in this chapter is reprinted with permission from "Surfactant co-assembly and ion exchange to modulate polyelectrolyte multilayer wettability" by Xiayun Huang and Nicole S. Zacharia, 2013, *Soft Matter*, 9, 7735-7742, http://pubs.rsc.org/en/content/articlehtml/2013/sm/c3sm50782c, Copyright 2013 by Royal Society of Chemistry.

the separation of water from organic materials.[129] A high static water contact angle is generally required for these types of surfaces. A number of superhydrophobic (as defined by a water contact angle of 150° or greater) or superoleophobic surfaces have been created using polyelectrolyte multilayers (PEMs).[130] These are generally realized by creating morphologies with multiple length scales of features; microscaled features on which there are nanoscale features, mimicking the lotus leaf structure. One way to achieve this type of morphology is by adding inorganic nanoparticles to the polymer surface.[40,130]

While geometry is clearly necessary to achieve certain extreme conditions of hydrophobicity or hydrophilicity of a surface, the underlying chemistry or surface energy of the material is also critical. Using commercially available polyelectrolytes, there is a limited range of wettability that can be engineered into flat surfaces. The work shown here represents a new way to achieve higher contact angle values for PEM surfaces that have not been further texturized with any kind of post-assembly processes, as high as 140°, using commercially available non-fluorinated polyelectrolytes.

There are some reports of using counterions exchange from small counterions to larger surfactant molecules on the top surface of a polyelectrolyte multilayer surface in order to modify contact angle.[35,66-68] Incorporation of small molecule surfactants may be a simple way to change the chemistries and expand functionality of PEMs made from the standard library of commercially made materials. Several examples exist of using chemistry to modulate the wettability properties of PEM surfaces. Rubner *et al*[35] has modulated the wettability by varying the pH value of the absorbing polyelectrolyte. Johal *et al*[66] show the adsorption of an anionic surfactant, sodium dodecyl sulfate (SDS), onto the outer layer can be used to fine-tune the wettability. Su *et al*[67,68] fabricate an erasable-rewritable wettability gradient between superhydrophobicity to superhydrophilicity via counterion exchange in a polyelectrolyte multilayer. Understanding the

interaction between surfactant and polymer chains is a key in order to develop this ability. In some systems surfactants have been used to partially dissolve PEMs, just as salts are able to.[61] Understanding what parameters affect the stability of the polyelectrolyte-surfactant complex is necessary for this.

We report here both the co-assembly of polyelectrolytes with a fluorinated surfactant and the exposure of pre-assembled PEMs to the same surfactant in order to modulate their surface wettability. Surfactant co-assembly shows a significant increase in contact angle compared to surfaces that are only counter ion exchanged after assembly, implying that the two resultant structures are distinct. There are fewer reports of surfactant aided polyelectrolyte assembly[53,56,131-133] as compared to post-assembly treatment with surfactants, and as mentioned above salts and pH variation are even more typically employed to modify polyelectrolyte chain conformation in solution.[56,134] One exception would be the use of surfactants to modulate surface charge interactions for nanoparticles dispersed in polar/nonpolar media.[133,135] In our case the fluorinated molecule is adsorbed during a separate step onto the growing multilayer surface, binding to some sites of opposite charge. The system we report here is novel and opens new possibilities in using surfactants and other small, charged molecules to modify the properties of polyelectrolyte multilayers.

3.2. Materials and methods

Poly(diallyl dimethyl ammonium chloride) (PDAC, MW=100,000-200,000 g/mol), sodium poly (4-styrene sulfonate) (SPS, MW=70,000 g/mol), and ammonium perfluorooctanoate (APFO, >98.0%) were purchased from Sigma-Aldrich. Sodium Chloride (>99.5%), sulfuric acid (98%), hydrogen peroxide (48%), and tetraethyl orthosilicate were purchased from EMD Chemicals. All chemicals were used as received. Distilled water (18.2 MΩ • cm) was purified with a Millipore system and used for all experiments.

Static water contact angles were measured using VCA optima (AST products. Inc) at room temperature with DI water (18.2 MΩ • cm) as a probe fluid (1.25 μL). PEMs were stored in the test environment with a relative humidity of ~40% for over 24 h before the tests. Each contact angle reported was the average value of at least five independent measurements and the standard deviations were found to be below 3° in each case. The film thickness and surface roughness was measured by stylus profilometer (KLA-Tencor Instruments P-6) after the surface was scratched. The values reported represent average of at least 5 separate measurements on each film, and at least 2 films are used for each data point on the plots presented. The chemical structures of films were examined by Fourier transformed infrared attenuated total reflection spectroscopy (FTIR-ATR) method using a multiple reflection mode with an Alpha (Bruker Corporation, Germany). UV-Vis spectra were recorded by growing the PEMs on the quartz glass and taken between 190 and 250 nm on 6705 UV-Vis spectrophotometer (JENWAY, UK). Zeta potential measurements were performed on the Zeta Plus/PALS analyzer (Brookhaven, USA). For zeta potential measurements 588 nm silica nanoparticles were chosen as substrates since they have similar charge properties as the glass slides or native silica layer on the silicon wafers that were used as substrates in this work. The silica spheres were synthesized via a Stöber method.[138] The polyelectrolyte and surfactant solutions (pH, concentration) are the same as the APFO co-assembled film and the APFO concentration as chosen as 5 mmol/L. The concentration of the silica particles was 5 mg/mL. The particles were exposed to either polyelectrolyte or surfactant for 20 minutes while being shaken. After each assembly step the particles were centrifuged at 3000 rpm for 1 minute. The supernatant was removed and the particles were rinsed 3 times with DI water before exposure to the next step. The particles were lightly sonicated in order to re-disperse them each time a new polyelectrolyte or surfactant solution is added to them.

All the substrates (glass, silicon, and quartz glass) were immersed in the piranha solution (H_2SO_4/H_2O_2, 7:3 mixture) for 1 h and then rinsed with a large amount of water. PEMs were assembled by sequential dipping of a substrate in PDAC (20 mmol/L with respect to the repeat unit, with NaCl present at various concentrations) and SPS (20 mmol/L with respect to the repeat unit, with matching NaCl concentrations as that in the PDAC solution) aqueous solutions for 20 min each until 10.5 bilayers were obtained with a three minute agitation in DI water in between each deposition step. The counterion exchange was carried out by immersing the PEMs into APFO aqueous solution followed by rinsing with water and drying with N_2. APFO assembled PDAC-SPS PEMs were assembled by sequential dipping the substrates in PDAC (20 mmol/L in repeat unit, with NaCl present at various concentrations), APFO (concentration: 0-50 mmol/L), and SPS (20 mmol/L in repeat unit, with NaCl present at various concentrations) aqueous solutions for 20 min repeatedly. The substrate was rinsed by water before immersing into other solutions. The process was repeated until $(PDAC\text{-}APFO\text{-}SPS)_{10}$ PDAC-APFO PEMs were fabricated. Immediately after assembly is completed, the films are dried under a stream of compressed, dried, and filtered air, then stored at room temperature and humidity for at least 24 hours before further characterization is performed. Over the course of the experiments the atmospheric humidity was typically ~40%.

3.3. Results and discussions

3.3.1. Counterion exchange with fluorinated surfactant

The first type of surfactant modification performed was exposure of preformed PEMs to aqueous solution of APFO in order to exchange the counterions on the PEM surface for the surfactant. A number of literature reports show that the surface wettability of PEMs is determined primarily by the outmost layer.[35] 10.5 bilayers of PDAC-SPS PEMs were firstly assembled in NaCl solutions with concentrations varying from 50 mmol/L to 1000 mmol/L. Addition of salt

creates a more coiled polyelectrolyte conformation in solution due to charge screening as opposed to the extended strong polyelectrolyte conformations that would be encountered in low ionic strength conditions.[137] Increasing salt concentration in the dipping solutions can be seen to slightly increase contact angles due to these changes in conformation, as shown in figure 3.1.

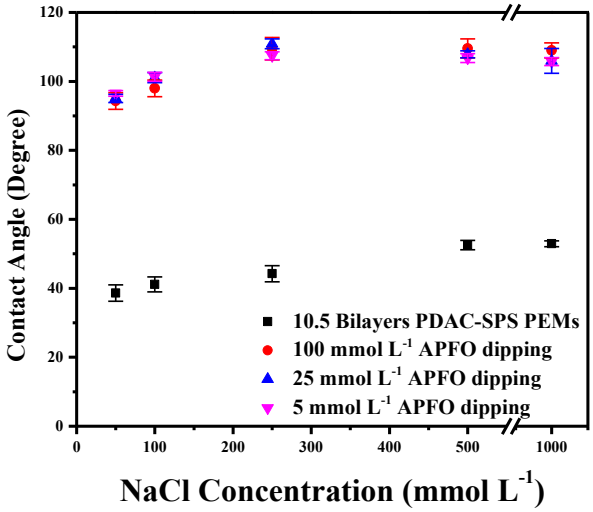

Figure 3.1. Contact angles of 10.5 bilayer PDAC-SPS PEMs before and after APFO exposure. Contact angles significantly increase from less than 60° to as high as 110° after the surfaces are ion exchanged with APFO.

After exposure to 5, 25, and 100 mmol/L APFO solutions for 5 min, the contact angles increase from hydrophilic to hydrophobic (Figure 3.1), indicating that APFO surfactant molecules have replaced some counterions even at very low APFO concentrations below the critical micelle concentration (CMC, ~27 mmol/L),[138] and with the hydrophilic head embedded into the PEMs and the hydrophobic tail extend outwards.[66-67] Low NaCl assembly concentration (50 mmol/L) gives a dense PEM with relative low counterion density on the surface. The ion exchange process in these cases does not result in a complete exchange of all the counterions in the PEM and therefore yields a relatively low contact angle. As the NaCl concentration during film assembly is increased from

50 to 250 mmol/L, the surface counterion density of the film reaches a saturation level. This translates to a greater degree of fluorinated surfactant on the film surface as a result of the ion exchange process. The contact angle also rises to a plateau value following the salt concentration, which indicates most of PEM surface covered with APFO molecules instead of polyelectrolyte chains or sodium or chloride counterions. Further increasing the NaCl assembly concentration to 1000 mmol/L slightly decreases the contact angle. In this case, the PEM as assembled has a lower ionic crosslink density due to the high degree of charge screening. This allows APFO to diffuse into the multilayer film more easily during the ion exchange process as the segments between ionic crosslinks are longer in this case. Performing the ion exchange with APFO concentrations lower than the CMC value results in similar contact angle values as compared to when the APFO concentration is over the CMC level. Based on these data, it seems that the structure is not an assembly of APFO micelles or a bilayer on the top surface of the PEM, but rather fluorinated tails pointing away from the multilayer film. If there were a self-assembled structure the water contact angle would be lower as charged head groups would present themselves to the water drop. The fact that there is a high static contact angle that remains so over time and multiple tests also indicates that the ionic interaction between APFO and PDAC is strong enough to prevent the rearrangement of the APFO molecules when exposed to water.

The ion exchange occurs at a rapid pace. As shown in figure 3.2, the contact angle value reaches its plateau in a short time (30 s). With prolonged ion exchange, the contact angles do not change appreciably.

$$\cos\theta_A^C = f_1 \cos\theta_1 + f_2 \cos\theta_2 \qquad \text{(eqn 3.1)}$$

where θ_A^C is the apparent contact angle, f_1 and f_2 are the area fractions of materials 1 and 2 ($f_1 + f_2 = 1$), and θ_1 and θ_2 are the contact angle on pure materials 1 and 2, respectively.

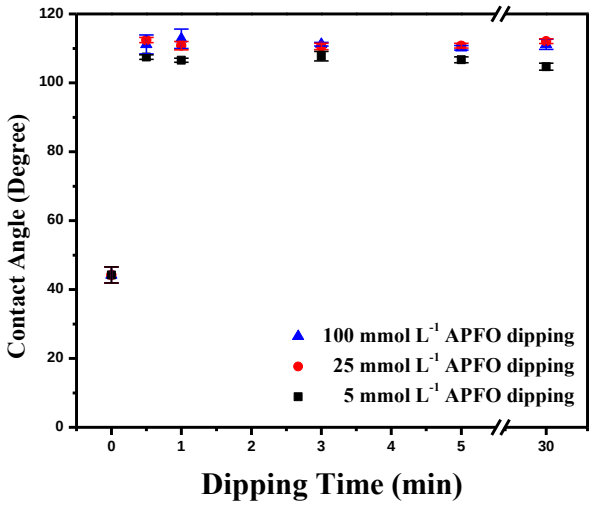

Figure 3.2. Contact angles of 10.5 bilayer PDAC-SPS PEMs assembled with 250 mmol/L NaCl dipped into APFO solutions for different times. The contact angle reaches the plateau (~110^{o}) in a short time (30 s).

Cassie's model[139,140] was chosen to calculate the fraction of APFO molecules (f_{APFO}) on the PEM surface, as shown in equation 3.1. Cassie's model presumes that overall contact angle of a surface with two types of chemical functional groups can be considered a weighted average of the fraction of surface sites covered with either of those surface functional groups. Based on this model, the saturation fraction f_{APFO} values are nearly 0.9, which indicate 90% of the PEM surface is covered with APFO molecules by ion exchange (Figure 3.3).

Due to the displacement of small counterions, the association between polyelectrolyte and ionic surfactant is both entropically and electrostatically driven.[56] The thickness of the PEM films significantly increase during exposure to APFO solution, as shown in figure 3.4. This change in thickness is much greater than for PEMs immersed in small molecule salt solutions such as NaCl,[134,141] indicating that the APFO creates more significant changes in chain conformation and the film overall as compared to small ions. Presumably APFO will diffuse into the PEM along the

concentration gradient where both electrostatic and hydrophobic interactions will cause changes in the PEM structure. The thickness ratio (defined as final film thickness/initial film thickness) of the PEMs before and after APFO dipping can be as high as 140% (figure 3.5) when they are dipped into APFO solution with higher concentrations such as 100 mmol/L. For low APFO concentrations like 5 or 25 mmol/L the thickness still increases, but to a lesser degree.

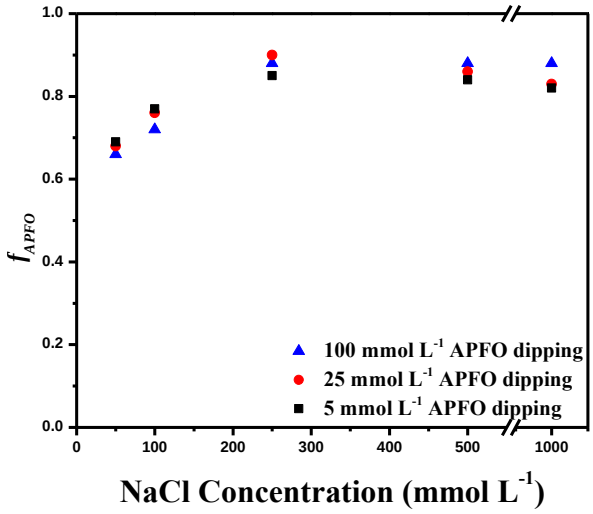

Figure 3.3. f_{APFO} value calculated from contact angles according to Cassie's model for PEMs with surfaces that had been counterion exchanged with APFO. When NaCl concentration in the assembly exceeds 200 mmol/L, the fraction of fluorinated groups on the PEM surface reaches approximately 90%.

The interaction of APFO with the PEM was investigated by dipping 250 mmol/L NaCl assembled PDAC-SPS PEMs into 5, 25, and 100 mmol/L APFO solutions for different times, shown in figure 3.6. UV-Vis absorbance peaks at approximately 199 nm and 225 nm correspond to π-π* transition of the phenol side groups of SPS.[62] Tracking the absorption at 199 nm and based on the Lambert-Beer Law, the amount of SPS in the film seems to decrease sharply at first and then reach a plateau value with time (figure 3.6). The release of SPS from the film also increases

with increasing APFO concentration in the ion exchange solutions. Assuming a linear absorption for SPS even in a solid thin film, for the 25 mmol/L and 100 mmol/L ion exchange cases as little as 40% of the initial SPS remains after 30 minutes. Interestingly, the thickness (figure 3.6) of the PEMs increases following the same trend as the loss of SPS — a step increase and then quickly reaching saturation. The thickness values increase with the concentrations of APFO dipping solutions and is much higher for high APFO dipping concentrations (25 and 100 mmol/L) compared with the PEMs that were ion exchanged with low APFO dipping concentration. This can also be shown by the decrease in the asymmetric and symmetric vibrations bands of SO_3^- groups at 1208 and 1035 cm^{-1} [142] and the increase in the C-F stretching vibration at 1206 and 1149 cm^{-1}. [144] However, for the low APFO ion exchange concentration case the changes in the intensities of SO_3^- groups are not obvious and the C-F peak at 1149 cm^{-1} only show as weak shoulder peaks.

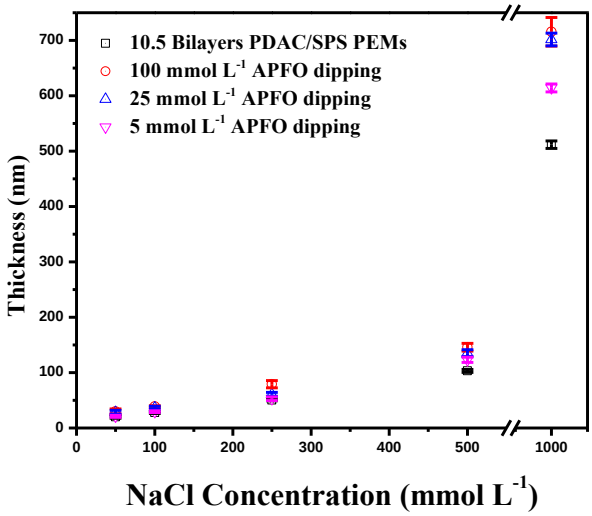

Figure 3.4. Thickness of 10.5 bilayer PDAC-SPS PEMs before and after dipping in APFO (5, 25, and 100 mmol/L) solutions for 5 min. The thicknesses increase up to 140% by displacement of SPS and diffusion of APFO surfactant into the PEM structure.

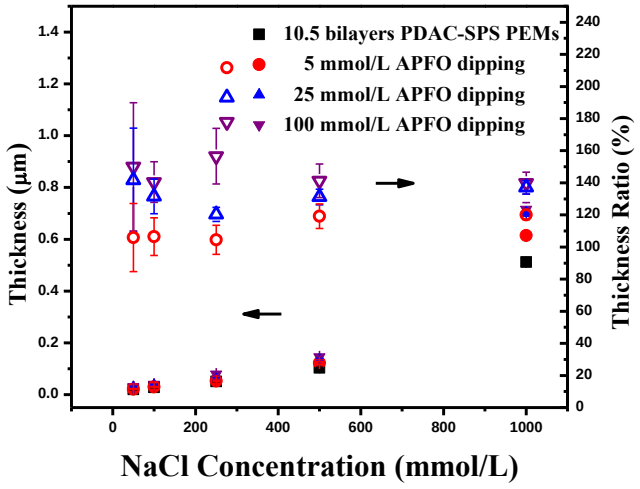

Figure 3.5. Thickness (closed symbols) and thickness ratio (open symbols) of 10.5 bilayers PDAC-SPS PEMs before and after APFO (5, 25, and 100 mmol/L) dipping for 5 min. The thicknesses increase up to 140% by displacement and diffusion of APFO surfactant.

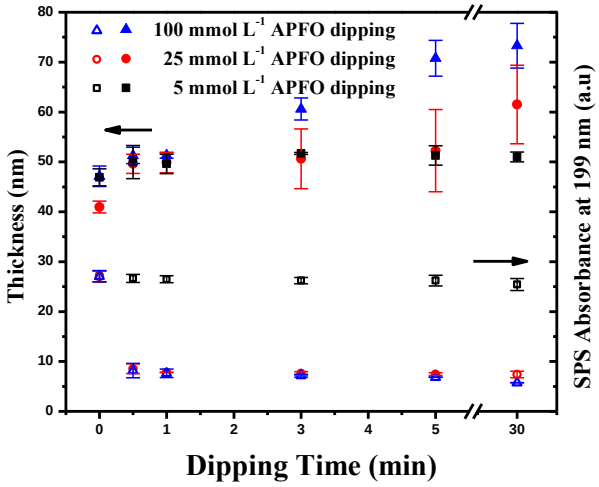

Figure 3.6. Thickness and SPS composition of 250 mmol/L NaCl assembled 10.5 bilayers PDAC-SPS PEMs dipping into 5, 25, and 100 mmol/L APFO solutions for different time. Open symbols are the UV absorbance of the film whereas closed symbols are the film thickness. PDAC has a strong tendency to form ionic aggregation with APFO compared with SPS, so that APFO counterion exchange and diffusion are dominated to increase the thickness and removal of SPS occurs quickly.

It seems that the presence of surfactant can strongly influence the chain conformations, even for polymer chains that are already part of the PEM assembly. Since APFO is able to displace SPS, the weakening of the ionic crosslinks in the film allow for more ready chain rearrangement. The fluorinated tails interact with the hydrophobic polymer backbones, causing a more coiled chain conformation. Multiple processes are occurring during the ion exchange. One is the surfactant exchanging with the surfaces counterions, a second is the diffusion of APFO into the PEMs, and a third is the displacement of SPS by APFO. All of these processes are controlled by the different interactions between APFO and the two different polyelectrolytes.[61] The loss of SPS from the film suggests that PDAC interacts more strongly with APFO than it does with PDAC. Similar phenomena are observed when using mixed polyelectrolytes in assembly solutions and preferential deposition of one polyelectrolyte over the other is observed.[144] Both the increase of contact angle and removal of SPS occur quickly.

3.3.2. Fluorinated surfactant co-assembled with polyelectrolytes

As a second strategy towards modifying the surface wettability of these multilayers, fluorinated surfactant was co-assembled with the polyelectrolytes as shown in figure 3.7. Instead of alternating exposure of the substrate from polycation to polyanion, the assembly sequence is now polycation, surfactant, polyanion. The PEM has a surface layer of PDAC when exposed to the APFO solution. The negative charges of APFO can bind to the PDAC surface, but the overall surface charge remains positive, even for longer exposure times to the surfactant solution. Figure 3.8 shows zeta potential of the multilayer surface as the film grows, showing that the surface charge remains positive after APFO adsorption. This is true for the range of relatively dilute concentrations of APFO that were chosen for this study.

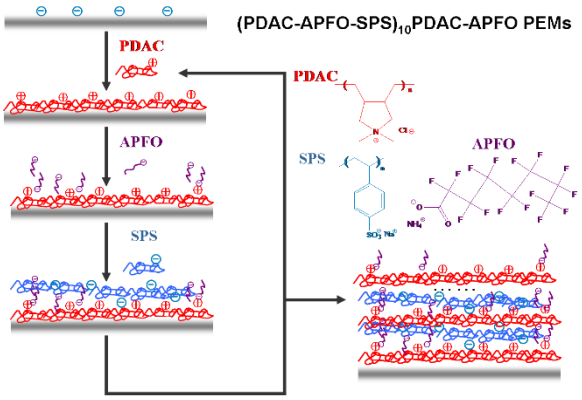

Figure 3.7. A monovalent fluorinated surfactant, APFO, was assembled into PEMs of PDAC and combined with NaCl, which was not shown in scheme.

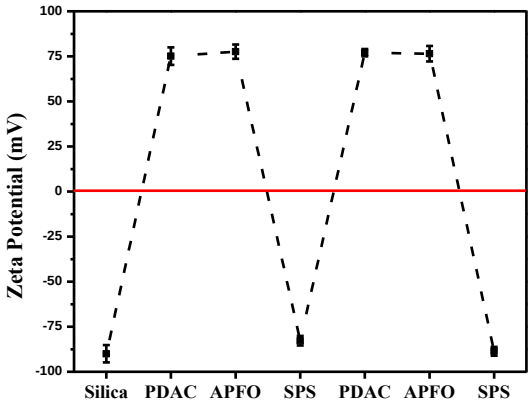

Figure 3.8. Zeta potential as a function of the outmost layer through step-by-step growth of silica-$(PDAC\text{-}APFO\text{-}SPS)_2$. The concentration of APFO was chosen as 5 mmol/L and concentration of PDAC and SPS solutions were chosen to be 20 mmol/L in repeat unit. The charges of PEM surface alternate during each trilayer assembly.

The effective formation of multilayers requires available binding sites on the outermost layer. Typically, each adsorption step of polyelectrolyte is accompanied by a reversal in surface charge. Therefore, the surfactant concentration should have an impact on multilayer growth, as the monovalent surfactant molecules bind some of the charge sites available for polyelectrolyte adsorption. The adsorption of a stoichiometric amount of APFO on a PDAC terminal layer would

result in a lack of available cationic sites of PDAC for further adsorption of SPS.[56] Different APFO assembly concentrations below the CMC (from 0 mmol/L to 25 mmol/L) were chosen to control the amount of APFO being adsorbed onto binding sites of that terminal PEM layer.

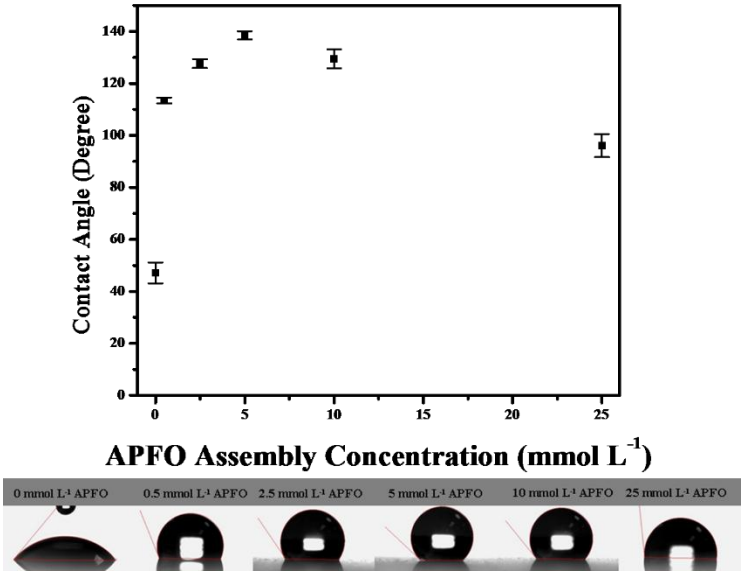

Figure 3.9. Contact angles of APFO assembled PEMs by varying APFO assembly concentrations below CMC, from 0 to 25 mmol/L. NaCl at a concentration of 250 mmol/L was presented in the polyelectrolyte assembly solutions. Contact angles vary from hydrophilicity (~50°) to hydrophobicity (~140°) at the APFO assembly concentration below CMC value.

To achieve stable film growth, $(PDAC\text{-}APFO\text{-}SPS)_{10}$-PDAC-APFO PEMs were prepared with varying APFO concentrations. After the films are dried with N_2, the fluorinated tails of the surfactant molecules on the surface of the PEMs will extend outwards, resulting in a hydrophobic surface. Figure 3.9 shows the contact angles of PDAC-SPS PEMs co-assembled with APFO under different APFO assembly concentrations. With the combination of APFO surfactant co-assembled with the polyelectrolytes and on the surface of PEMs, wettability will increase from the hydrophilicity (~50°) of a PDAC-SPS surface to hydrophobicity (~140°) even at APFO concentrations much lower than the CMC value. The contact angle values for the co-assembly

case are much higher than those of the films which have APFO only on the surface (~110°). The films formed by the co-assembly process have a higher surface roughness and we hypothesize that this helps to increase the hydrophobicity. When APFO is co-assembled with the polyelectrolytes, presumably the surfactant is embedded throughout the PDAC-SPS PEMs.

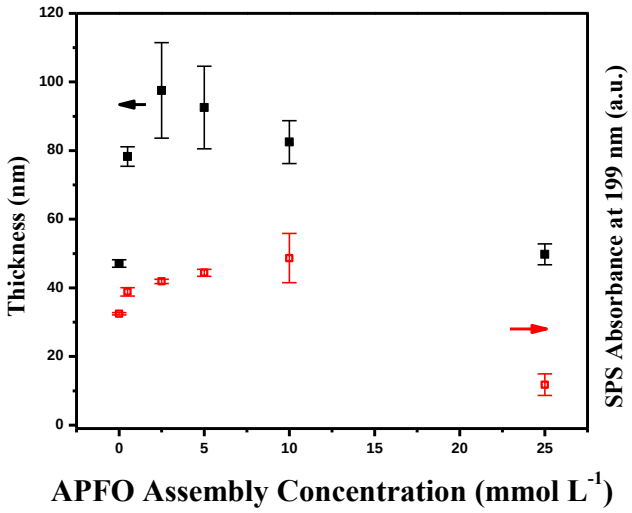

Figure 3.10. Thickness (black symbols) of 10.5 trilayer PDAC-SPS PEM co-assembled with APFO and UV-Vis absorbance (red symbols) at 199 nm for varying APFO assembly concentrations below the CMC, from 0 to 25 mmol/L. Both the thickness and the absorbance of SPS go through the same type of two regimes transition as contact angle does.

In the case of ion exchange, APFO will be presented just on the outermost surface and perhaps be able to diffuse into the outermost bilayers of the PEM at the concentration below CMC value. At the low concentrations being used, the concentration gradient and therefore driving force for diffusion from the solution into the bulk of the film during ion exchange will be low, and it is not expected that the surfactant should diffuse into the entire bulk film. The interaction between the surfactant molecules and the polyelectrolytes may influence the polyelectrolyte coil conformation, increasing the surface roughness of the multilayers. In accordance with the Wenzel

model[146] this additional roughness causes the contact angles be higher than the contact angle of a closed packed APFO monolayer (~119°).

The contact angle is observed to increase with APFO assembly concentration from 0 to 5 mmol/L. However, further increase of the APFO assembly concentration from 5 to 25 mmol/L results in a slight decrease of contact angle. This decrease in contact angle after initial increase is somewhat counterintuitive. The morphology and ratio of the components in the films are different in these two regimes, which may explain the change in wettability. The ion exchange experiments demonstrate that APFO seems to preferentially bind to PDAC over SPS binding with PDAC, but the decrease in contact angle is not due to increased presentation of PDAC at the surface. For PDAC/SPS multilayers, surfaces terminated in PDAC have been shown to have a more hydrophobic character than SPS terminated surfaces.[147] Therefore, we propose that at assembly solution concentrations higher than 5 mmol/L, the concentration of APFO is sufficiently high that the surfactant molecules can aggregate in such a way to 'hide' the fluorinated tails from the hydrophilic environment, thereby reducing the overall contact angle of the thin film.

Figure 3.10 shows that the amount of SPS in the PEMs also goes through this same type of transition in these two regimes, first increase with APFO concentration and then decrease. The absorbance of the multilayer film at 199 nm is a gauge for the amount of SPS in the PEM, as this is the wavelength of maximum absorbance for SPS (corresponding to a π-π^* transition of benzene group[62]).

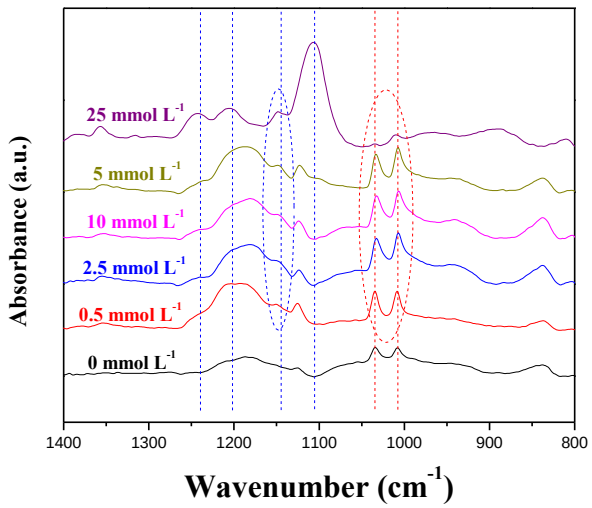

Figure 3.11. FTIR spectra of APFO co-assembled PDAC-SPS PEM by varying APFO assembly concentrations. Shoulder peak of APFO can be detected at low concentration as 0.5 mmol/L (blue circle). The decrease in S=O symmetric vibration (red circle) can be observed at higher concentration as 25 mmol/L.

The amount of SPS increases when increasing APFO concentration at the region from 0 to 5 mmol/L. When further increasing APFO assembly concentration to 25 mmol/L, the amount of SPS in the PEMs decreases. Similar results can be seen for the thickness of the PEMs. In the low concentration regime, a slight increase in APFO concentration results in thicker film growth, possible from coil rearrangements as a result of the presence of APFO. The chains may become more coiled in order to expose hydrophobic backbones to the hydrophobic tails of the APFO molecules. However, with a further increase of APFO concentration above 5 mmol/L, absorption of SPS and overall film thickness decrease significantly. One possible explanation is that as more significant amounts of APFO are adsorbed onto the growing multilayer a large fraction of surface charge sites are bound and this process inhibits further absorption of SPS and PDAC.

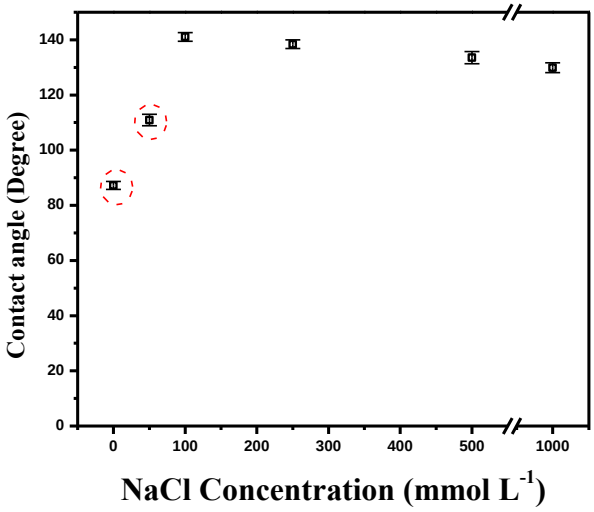

Figure 3.12. Contact angles of APFO co-assembled PEMs with different NaCl concentration in polyelectrolyte solutions and a fixed APFO concentration (5 mmol/L). Contact angle reaches the peak value of ~140°. The first two dots circled do not have the same stability as the value for other NaCl concentration.

Even at extremely low adsorption concentrations (below 5 mmol/L), APFO is present in the film and the resulting PEM is hydrophobic. FTIR spectra (figure 3.11) clearly show the C-F stretching vibration at 1149 cm^{-1} as a shoulder peak. This shoulder peak increases with increasing APFO co-assembly concentration. The amount of APFO in the PEM is enough to have a significant impact on film properties even at low APFO assembly concentration. In addition to electrostatic interactions, APFO may interact with the multilayer via hydrophobic interactions.

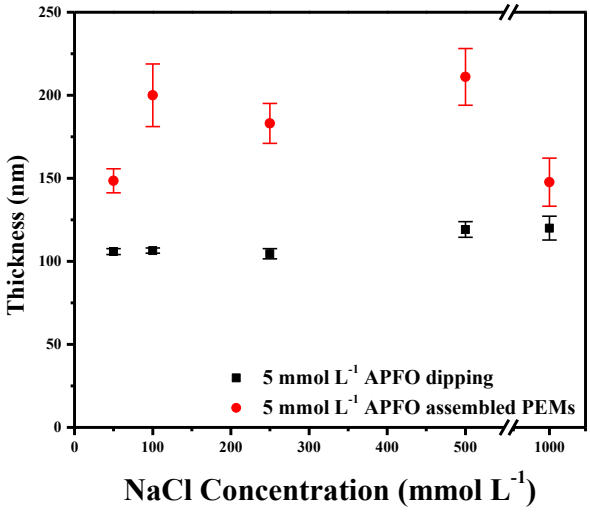

Figure 3.13. Thicknesses ratio of PDAC-SPS PEMs co-assembled with APFO to those PEMs with surface ions exchanged with APFO by a single dipping process across different NaCl concentrations in the polyelectrolyte assembly solutions. Co-assembly process has significant consequences for the coil conformations of polyelectrolyte due to huge thickness increase (~180%).

Modulating the ionic strength of the polyelectrolyte solutions during assembly is one way to control the morphology of the polymer chains within the polyelectrolyte layers. NaCl was added to the polyelectrolyte solutions during the assembly process with surfactant, and a range of NaCl concentrations were examined. With increasing ionic strength, charges are shielded and the polyelectrolyte conformations go from extended chains to something more akin to random coils.[138] For this experiment, a constant concentration of 5 mmol/L APFO was chosen for the assembly of the $(PDAC\text{-}APFO\text{-}SPS)_{10}PDAC\text{-}APFO$ PEMs with varying NaCl concentrations in the PDAC and SPS solutions. The resulting surface wettability can be seen in figure 3.12.

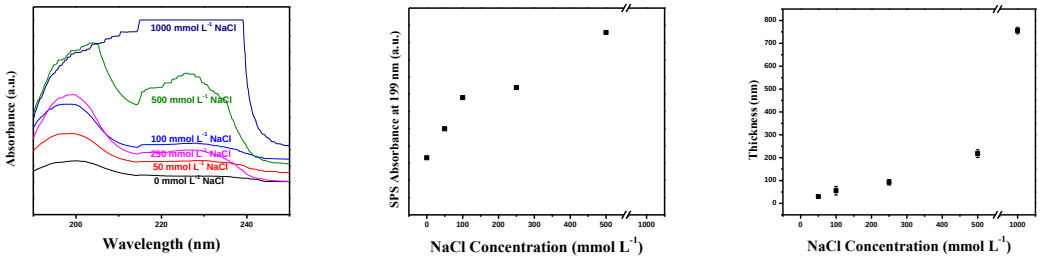

(A) (B) (C)

Figure 3.14. (A) UV-Vis spectra of APFO co-assembled PDAC-SPS PEMs varying NaCl concentration in polyelectrolyte solutions and (B) their relative SPS absorption at 199 nm. (C) Thickness of APFO co-assembled 10.5 trilayer PDAC-SPS PEMs with different NaCl Concentration in polyelectrolyte solutions. The concentration of APFO during assembly is fixed as 5 mmol/L. The amount of SPS absorption will increase with increasing the multilayer thickness.

The contact angle reaches a peak value of ~140° with increasing NaCl assembly concentrations. The contact angle values for the films assembled with either no salt or only 50 mmol/L NaCl in the polyelectrolyte solutions, marked with a red circle in figure 3.12, do not have the same stability as the values for other salt concentrations. For these two cases, the droplet holds the angle marked for a few seconds before being absorbed into the film. This does not happen for other PEMs co-assembled with APFO nor for the PDAC-SPS multilayers assembled with 0 mmol/L and 50 mmol/L NaCl without APFO. The thickness of the films also significantly increases (~180% as a ratio of thickness of the film co-assembled with APFO to the film with surface ion exchange with APFO) compared with PEMs ion exchanged with 5 mmol/L APFO, as illustrated in figure 3.13. Clearly, the co-assembly process has significant consequences for the coil conformations of the polyelectrolytes within the multilayers.

Due to the mediation of electrostatic interactions caused by the addition of NaCl to the assembly solutions, in these films we observed an increase in the amount of SPS with increasing NaCl assembly concentrations, as shown by UV-Vis (figure 3.14). In fact, for the case of 1 mol/L NaCl the amount of SPS had increased to such a degree that the absorbance peak actually

saturated the detector. Moreover, the amount of APFO in the film also increases when raising the NaCl assembly concentrations with increasing the intensity of shoulder peak at 1149 cm^{-1}, as shown in figure 3.15. The amount of APFO and SPS both increase to yield extremely thick PEMs.

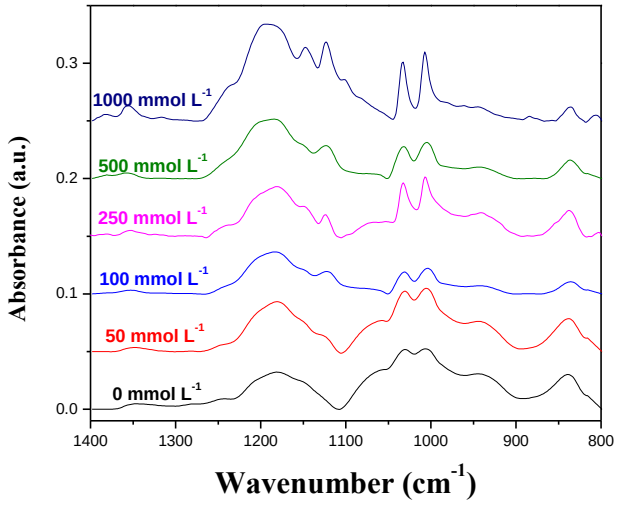

Figure 3.15. FTIR spectra of APFO co-assembled PDAC-SPS PEMs with different NaCl concentration in polyelectrolyte solutions. The concentration of APFO during assembly is fixed as 5 mmol/L.

3.4. Summary

We have demonstrated the modification of surface tension of a strong polyelectrolyte multilayer (made of PDAC-SPS) using a perfluorinated surfactant. This modification is made in two ways: first by counterion exchange on the surface of the as-assembled multilayer and secondly by co-assembly of the polyelectrolyte multilayer with the surfactant. Counter ion exchange with surfactant modifies the entire film as well as the surface, and creates a selective dissolution of the anionic component in our films. Exposure to surfactant may prove to be a way to selective etch PEM films or otherwise modify them. Co-assembly with surfactant is achieved by simply adding

a dipping step of surfactant solution into the layer-by-layer process. Surfactant molecules do not bind with all of the available charge sites, as shown from zeta potential data, which allows for subsequent adsorption of other polyelectrolyte chains. We demonstrate that both methods result in appreciable changes in surface properties, but that surfactant co-assembly can modify the surface static contact angle to a greater degree (from 60° to 140°) than merely counter ion exchange after assembly (from 60° to 110°). We believe that surfactant co-assembly will prove to be a general method of modifying polyelectrolyte multilayer properties without changing the chemistry of the constitutive polyelectrolytes.

CHAPTER IV

OMNIPHOBIC SLIPPERY COATINGS BASED ON LUBRICANT INFUSED POROUS POLYELECTROLYTE MULTILAYERS*

4.1. Introduction

Omniphobic and non-fouling coatings have many different potential uses, ranging as widely as energy savings from suppression of frost formation or improved aerodynamics to increased product lifetimes by the resistance of biofouling or staining.[38,39,52,54,86,148] While the lotus leaf structure (a rough surface with a combination of micro and nanoscaled features) has been the inspiration for many superhydrophobic coatings, these surfaces have some limitations due to the fact that they rely on trapped air pockets.[7] Because of this reliance on air pockets it has been found that humidity, temperature, and pressure can all damage these lotus leaf structures.[149-152] Also, they are not necessarily able to repel low surface energy liquids.[150] More recently, a class of lubricant infused surfaces based on the structure of the pitcher plant has shown to have superior properties for repelling all types of liquids.[38,39,52,54,86,148,153,154] These surfaces have been named slippery liquid infused porous surface (or SLIPS), and their properties include very low sliding angles and low contact angle hysteresis.[86] Simply put, the requirements for making a SLIPS surface is to start with a textured surface that will wick the lubricant into it, that this surface preferentially wet the lubricant compared to the liquids to be repelled, and that the liquids to be repelled be immiscible with the lubricant.[86] The lubricant film will necessarily be perfectly smooth and defect free and enhances the slipperiness of the overall surface, reducing the sliding angle. Many types of porous

*Part of the data reported in this chapter is reprinted with permission from "Omniphobic slippery coatings based on lubricant-infused porous polyelectrolyte multilayers" by Xiayun Huang, James D. Chrisman, and Nicole S. Zacharia, 2013, *ACS Macro Lett.*, 2, 826-829, http://pubs.acs.org/doi/pdf/10.1021/mz400387w, Copyright 2013 by American Chemical Society.

or textured protect against ice formation on a surface as well as be a superior material for dropwise condensation.[39,154]

We present here a new approach to the fabrication of these omniphobic slippery surfaces by the use of polyelectrolyte multilayers (PEMs) assembled by the layer-by-layer (LbL) technique. LbL is a sequential assembly technique that directs the complexation of oppositely charged polyelectrolytes onto a surface by exposing that surface to solutions of polyelectrolytes and rinse baths.[77] The method has a strong track record of being a robust and versatile platform for fabrication of films with a wide range of functionality[155], including superhydophobic[156] and oleophobic surfaces.[157] PEMs are generally assembled from aqueous solvent using commercially available polyelectrolytes. They can be assembled by dipping, spraying, spin coating, or other methods; they can be patterned, and they can coat substrates of arbitrary complexity or geometry.[79] For other SLIPS or lubricant infused polymer surfaces, the textured surfaces are defined by lithographic means,[86,151] deposited electrochemically which requires a conductive substrate,[6] or require an adhesion layer.[148,153] Many commercially available textured substrates cannot be applied to curved surfaces. Polyelectrolyte multilayers provide advantages in these respects; they take advantage of a bottom up assembly process and the charge groups of the polymer chains (especially for amine containing polymers) act as their own adhesion layer.

In this work, water soluble weak polyelectrolytes, branched polyethylenimine (BPEI) and poly(acrylic acid) (PAA), were used as the basis for the polyelectrolyte multilayer structure. These weak polyelectrolytes have a variable charge density based on changes in protonation that accompany variations in the pH of the surrounding environment. Lower charge density polymer chains take conformations approaching a random coil and highly charged polyelectrolytes take on extended conformations. Manipulating the pH of polyelectrolyte solutions influences the properties of the resultant LbL film, such as film thickness. Exposing these films to changes in pH

after assembly can create the formation of pores[80] through breakage and reforming of ionic crosslinks as well as changes in coil conformation that accompany changes in chain protonation. The resultant porous structure is dependent on both the pH the films are exposed to after assembly as well as on the initial assembly pH. Honeycomb-like microporous structures can be achieved through staged acid etching. A semifluorinated silane treatment creates superhydrophobicity from an otherwise hydrophilic polyelectrolyte multilayer. Infusing the surface with lubricant gives a perfect film with omniphobic slippery properties. These surfaces repel water and decane with sliding angles as low as 3° and with contact angle hysteresis lower than 2°. An advantage of using polyelectrolyte multilayer is the ease with which they can coat curved surfaces and those with more complex geometries without the need for additional adhesion layers.

4.2. Materials and methods

Branched polyethylenimine (BPEI, MW=25,000 g/mol) was obtained from Sigma-Aldrich and poly(acrylic acid) (PAA, MW=50, 000 g/mol, 25 wt% solution) was purchased from Polysciences Inc. Silica (20 nm and 4 nm) colloidal dispersions were purchased from Alfa Aesar. 1*H,* 1*H,* 2*H,* 2*H*-Perfluorooctyltriethoxysilane (POTS) was purchased from Sigma-Aldrich. The perfluoropolyether lubricant (Dupont Krytox PFPE GPL 100) was obtained from Miller-Stephenson and decane from TCI. De-ionized (DI) water with 18.2 MΩ • cm resistivity from a Milli-Q filtration system was used for all experiments. All materials were used as received without further purification.

Film thickness was measured using a stylus profilometer (KLA Tencor Instruments P6), and values reported represent an average of 5 different position of the film. Scanning electron microscopy (SEM) images were acquired using an FEI Quanta 600 field emission scanning electron microscope with an accelerating voltage of 10 kV. FTIR spectra were obtained using an IR Prestige 21 system (Shimadzu Corp., Japan) and analyzed by IRsolution V.1.40 software. Films

coated on the silicon wafer were measured via attenuated total reflection (ATR) mode. Both the contact angle and photograph of droplets sliding on the surfaces were taken using VCA optima (AST products) equipped with tilting stage and the video camera.

PEMs were assembled onto glass slides, silicon wafers and a glass tube. Before use, the silicon wafer and glass substrates were treated in a freshly prepared piranha solution (mixture of H_2SO_4 (98%) and H_2O_2 (30%) with the volume ration v/v=7/3) at room temperature for 4 h and rinsed with DI water until neutralized. The substrates were then dried by nitrogen steam before being used for layer-by-layer assembly.

BPEI/PAA multilayer films were assembled using concentrations of 40 mmol/L BPEI and 20 mmol/L PAA with respect to the functional group (either amine groups or carboxylic acid). The pH of these solutions was adjusted with 1 mol/L NaOH or 1 mol/L HCl solution as needed. All the multilayer assembly was carried out at room temperature using a Zeiss HMS series programmable slide stainer. The cleaned and dried substrates were first exposed to BPEI solution for 10 min followed by three separate DI water rinse baths. Then, the substrates are exposed to PAA solution for 10 min and then again to three DI water rinse baths. This cycle was repeated until 30 bilayers were reached. The multilayer films are dried at room temperature for 24 hours before any testing.

The films assembled on glass slides with 30 bilayers of BPEI/PAA were exposure to post-assembly acidic treatments. The DI water was adjusted to the desired pH using 1 mol/L NaOH or 1 mol/L HCl. PEM samples of defined dimension (1.25 cm×5 cm) and 14 ml of solutions were placed in a centrifuge tube for 1 hour. The staged acid etching was performed in a similar method. The 30 bilayer BPEI/PAA PEMs were immersed in pH 2.7 and then pH 2.3 for defined time intervals. After the film was air dried, it was crosslinked at 180^{o}C for 2 hours.

Three bilayers of BPEI/silica particles (0.06 wt% mixing dispersion of 20 nm and 4 nm silica particles in 1:1 ratio) were deposited on to the crosslinked porous multilayer film with the pH values of both the BPEI solution and the silica particle dispersion fixed at pH 6.5. The silane treatment was carried out by chemical vapor deposition of POTS in a close-capped weighting bottle. 100 μL of POTS in a 2 mL vial and the crosslinked film were put into the close-capped weighting bottle. The silanization reaction was performed at 120°C for 3 hours. After the CVD step the film was placed under vacuum for 1 h in order to ensure that all unbound silane was removed from the film. 100 μL of PFPE lubricant was impregnated into the nano-textured porous film through spin coating at 2000 rpm for 1 min.

4.3. Results and discussions

We have previously found that multilayers assembled from branched polyethylenimine (BPEI) and poly(acrylic acid) (PAA) with the BPEI assembly solution at pH 9.5 and the PAA assembly solution at pH of 4.5 formed porous structures with the pore size from very large to submicron size.[82] Post-assembly acid treatment in this case creates pores much smaller than post-base treatment.[82] Recently, we have studied the possible pore sizes and pH region of stability and how they are influenced by both the pH value of post-assembly treatment solution and also the pH values of the assembly solutions.

BPEI has a branched structure containing primary, secondary and tertiary amine groups in a ratio of 25%, 50% and 25%, respectively.[158] The p*K*a values for the different amine groups of branched PEI are 4.5 for primary, 6.7 for secondary and 11.6 for tertiary amine groups.[159] Moreover, highly branched structures mean denser coils as compared to linear polymers. For PAA, the p*K*a is roughly 5.5-6.5.[160] At a pH value such as 4.5 (lower than p*K*a) PAA is only partially charged, but there is still sufficient charge to grow polyelectrolyte multilayers. For the BPEI and PAA system, film growth can easily be in the micrometer range in thickness and has been reported

to follow exponential deposition during the initial 15 bilayers and then a rapid linear growth afterwards to quickly form thick films in the micrometer range.[161] BPEI/PAA films with 30 bilayers (assembly pH 9.5, 7.5 and 6.5 for BPEI and assemble pH 4.5 for PAA) as assembled here are all in the micrometer range (>2.5 μm), shown in chapter 5.

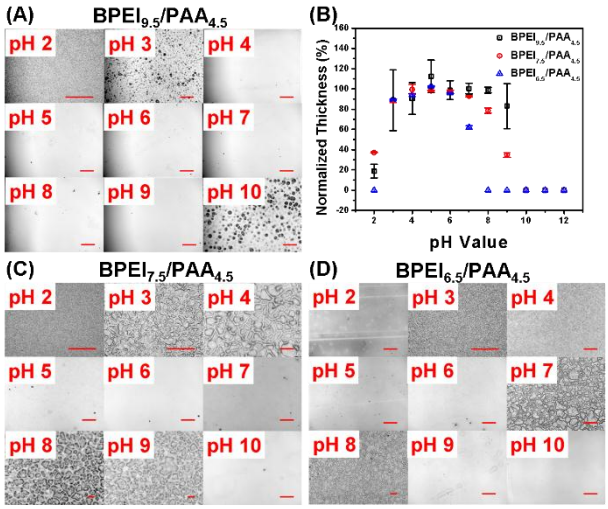

Figure 4.1. The pH window over which a BPEI/PAA film is stable when immersed in solutions of varying pH. Optical micrographs of porous structures of 30 bilayers BPEI/PAA film after post-assembly treatment in different pH solutions for 1 hour. Assembly pH of PAA was kept as 4.5, while that of BPEI was 9.5, 7.5 or 6.5 as shown in (A), (C) and (D); (B) Normalized film thicknesses of 30 bilayers of dried BPEI/PAA film with different assembly pH immersed in varying pH solutions for 1 hour. The window of stability is always in between the assembly pH of BPEI and PAA and becomes narrow when the BPEI assembly pH is decreased to 6.5. The scale bar for all the micrographs is 200 μm.

When immersed into post-treatment solutions of varying pH values for 1 hour, porous features are seen for both the acid and base ranges due to the decomposition and rearrangement of the charged polyelectrolyte chains and the release of some polyelectrolyte chains from the film.[80,162,163] We have shown that under exposure to solutions with pH in between the values of the original assembly solutions the film is stable, showing a smooth surface and retaining nearly 100% of original film thickness. Figure 4.1 shows that the stable range for $BPEI_{9.5}/PAA_{4.5}$ films is from

pH 4 to pH 9, which is similar to the pH values of the assembly solution (pH 9.5 for BPEI and pH 4.5 for PAA). A noticeable decrease in the size of the pH stability window to pH 5-pH 6 is seen when the assembly pH of BPEI is decreased from 9.5 to 6.5. Although optical micrographs after the post-assembly treatment at pH 9 still shows a smooth surface, film thickness decreases to nearly 0%, meaning that most of the film has decomposed and been dissolved into the exposure solution. The pH stability window becomes narrow when pH values of the assembly solutions are close to each other, as in the pH 6.5/BPEI and pH 4.5/PAA case. This kind of film with a narrow stability window can be decomposed much more easily and quickly compared to those films with a broad window of stability. When the pH of the BPEI is as high as 9.5 the charge density of the polymer is relatively low (shown in chapter 5), and the polymer chains become more coiled. The resultant multilayer structure has less PAA and those PAA chains have a higher charge density as compared to solution. Such a film deposits in thick layers due to the BPEI conformation, and the multilayer has many loops and unbound functional groups.[160] A higher BPEI charge density (low assembly pH), however, results in a more extended conformation and thinner layers. Post-assembly treatments will change the polyelectrolyte charge densities within the films, causing morphological rearrangements. We hypothesize that when BPEI is deposited in a more extended conformation (higher charge density) the resultant film is more readily dissolved with changes in external environment due to lower levels of diffusion and entanglement between the film components.

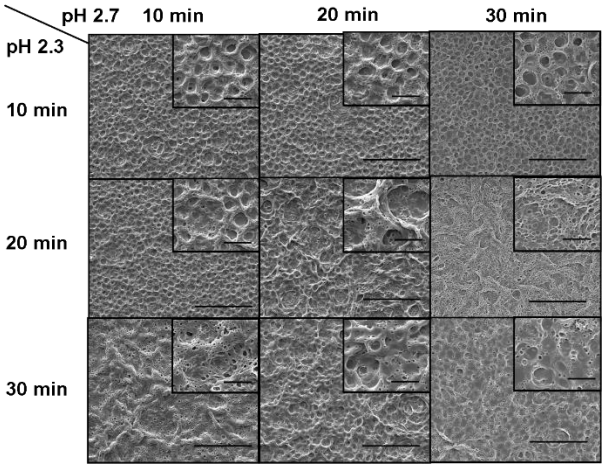

Figure 4.2. SEM images of porous structures of $(BPEI_{6.5}/PAA_{4.5})_{30}$ films that evolve through staged acid etching. The inserts in each image are high magnification SEM images of the porous structures. The scale bars for the low magnification and high magnification images are 100 μm and 20 μm, respectively. The corresponding size and distribution of both the large microscaled pores and the smaller nanoscaled pores are shown in Table 4.1.

Table 4.1. Pore sizes and standard deviations of large micrometer size pore and small nanometer size pores created in the various parts of the staged acid etching. Micro-scale pores are formed during the first stage of the etching, then the nanopores are formed during the corresponding second stage of acid etching.

pH 2.7 immersion (min)	pH 2.3 immersion (min)	Micronsized pores (μm)	Nanosized pores (μm)
10	10	9.17±2.35	0.73±0.35
	20	8.74±2.16	0.75±0.35
	30		1.21±0.62
20	10	8.17±1.43	0.85±0.33
	20	7.73±3.00	1.22±0.52
	30	7.88±3.02	3.02±0.41
30	10	24.90±4.44	0.42±0.17
	20		9.81±4.10
	30	8.35±2.60	0.69±0.34

The different assembly conditions combined with different post-assembly processes is found to result in different types of porous structures being formed. In this work, we particularly focus on the micro-scale and submicron sized pores created by post-assembly acid treatment, giving us the optimal microstructure for our application here. Optical micrographs from figure 4.1 show the range of structures possible. BPEI/PAA films with assembly pH value for BPEI at 6.5 result in the finest pore features. Here we have chosen $BPEI_{6.5}/PAA_{4.5}$ films as the optimal multilayer system to manipulate the pore size and features by staged acid etching.

Rubner *et al*[1,156] have studied microporous formation of PAH/PAA films and report that PAH/PAA films can be induced to form pores on the order of 10 microns with honeycomb-like structures and submicron pores on the surface by using an appropriate combination of post-acid treatments. $BPEI_{6.5}/PAA_{4.5}$ films behave similarly and can form both the micron and submicron pore sizes through a combination of post-assembly acid treatments of pH 2.7 and pH 2.3, a process called staged acid etching. First, the as-prepared dried BPEI/PAA film is immersed in to pH 2.7 solution for a fixed time. Without rinsing with neutral water, the wet film is directly immersed into pH 2.3 solution for another amount of time. The film is then dried without neutral water immersion. Figure 4.2 shows the SEM images of porous $BPEI_{6.5}/PAA_{4.5}$ film through staged acid etching at pH 2.7 and pH 2.3. The first acid solution at pH 2.7 etches the film and forms pore sizes about 10 microns. These honeycomb-like structures can be formed at short immersion times, such as 10 min. For PAH/PAA films, on the other hand, a few hours is required to achieve these honeycomb-like porous structures.[1] In the BPEI/PAA case the pores become deeper when the pH 2.7 solution etching time is increased to 30 min. Further etching with a more acidic solution of pH 2.3 bites into the submicron pores at the boundaries of the honeycomb-like structures created with the pH 2.7 etching. By increasing the exposure time in the pH 2.3 solution, the honeycomb-like structures will eventually be destroyed (Figure 4.2, pH 2.7/10 min-pH 2.3/30 min; pH 2.7/30 min-

pH 2.3/20 min) and in some cases when exposure in the lower pH solution is sufficiently long the structure is restored to a smoothened surface (Figure 4.2, pH 2.7/30 min-pH 2.3/30 min).

Here, we have chosen staged acid etching conditions (pH 2.7 for 30 min and pH 2.3 for 10 min) for polyelectrolyte SLIPS fabrication. The porous $BPEI_{6.5}/PAA_{4.5}$ film based on these staged acid etching condition gives both the micro-scaled and submicron porous features, which will is the optimal structure for purpose of a slippery and omniphobic surface, as shown in figure 4.3(A). The porous film was thermally crosslinked at 180°C for 2 h to fix the porous structures for the further dipping and reaction procedures.[1, 156] Nanoscale roughness was introduced through a further 3 bilayer dip coating of BPEI and silica nanoparticles (a mixture of 20 nm and 4 nm particle dispersion).[164] Porous structures with micro- and nanoscale roughness features are achieved by this step. Although there are reports that nanoscaled roughness as opposed to a hierarchically structured material is adequate to create a SLIPS surface,[148] we have found that the hierarchical surface optimizes our coating's properties. This may be due to the increased surface area for deposition of the nanoparticles that is made available by using a porous polyelectrolyte multilayer instead of a flat one.

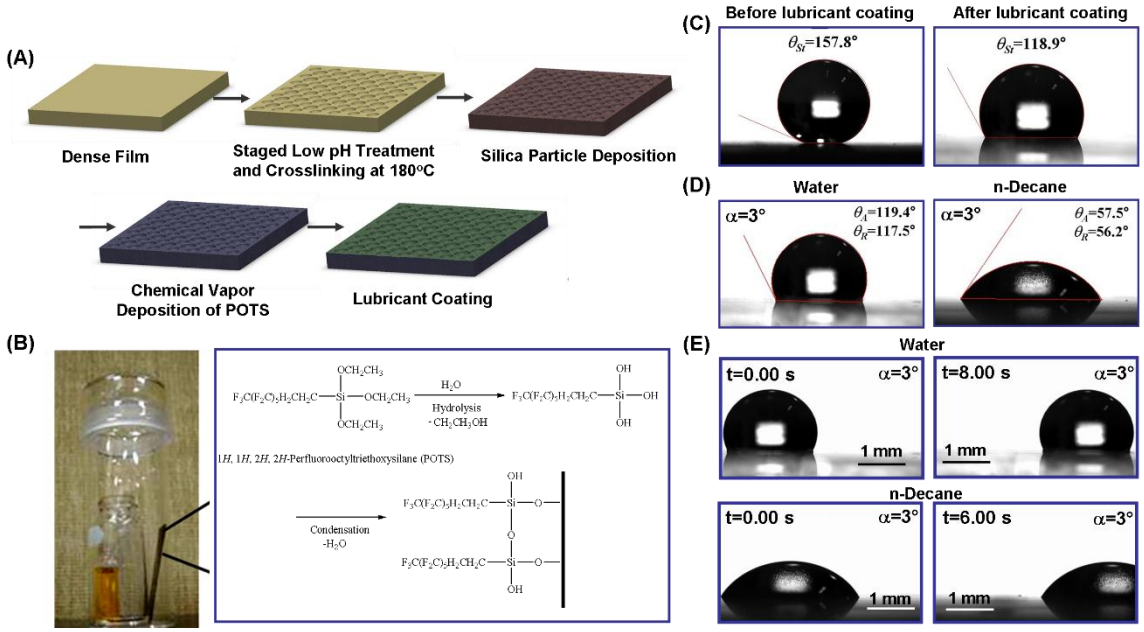

Figure 4.3. The design and omniphobicity of SLIPS from polyelectrolyte multilayers. (A) Schematics of the procedure for fabricating SLIPS from $(BPEI_{6.5}/PAA_{4.5})_{30}$ dense film; (B) The set-up used for chemical vapor deposition (CVD) of POTS (the liquid in the vial has been colored to orange for ease of visualization) with a proposed reaction for how POTS adheres to the film; (C) Static contact angles of 5 µL water drop on the film surface before and after lubricant coating; (D) Optical micrograph of the advancing and receding angle of water and decane (5 µL), which are captured at the droplets slide on the polyelectrolyte SLIPS a tilting angle of 3.0°, showing a contact angle hysteresis lower than 2°; (E) Optical micrographs demonstrating the mobility of water and decane droplets (5 µL) sliding on a SLIPS at a low titling angle (α=3.0°).

The rough film surface is then made to be superhydrophobic through a chemical vapor deposition (CVD) of POTS at 120°C for 3 h.[12] The reaction was performed in a closed-capped weighing bottle as shown in figure 4.3(B) and POTS reacted with hydroxyl groups of the porous film to form the hydrophobic molecular thin layer. The unreacted POTS was removed from the film by holding it under vacuum at room temperature for 1 hour. The CVD step transforms the hydrophilic porous film to a superhydrophobic one with a water contact angle at 157.8°, illustrated in figure 4.3(C). This film is further coated with a low surface energy lubricant that actually reduces the water contact angle (118.9°). However, this lubrication gives the porous film an excellent liquid repellency to both water and oil. Figure 4.3(D) shows the advancing and receding

angles of both water and decane droplets when the droplet is sliding at a 3° tilting angle. SLIPS film here, repels both the polar (water) and nonpolar liquid (decane). The contact angle hysteresis for both polar and nonpolar liquids is also very low (<2°) for drop volume as small as 5 μL. They start sliding at a very low tilting angle (~3°) and move off the screen which is 5 mm in width within a few seconds as shown in figure 4.3(E).

The robustness of the polyelectrolyte SLIPS films regarding temperature was also investigated. Similar to the lotus leaf, the porous polyelectrolyte multilayer system used here is hydrophilic itself but the addition of a thin hydrophobic layer can be used to obtain superhydrophobicity. It has been reported[164] that 55°C hot water can wash off the hierarchical roughness and wax surface layer (with its melting point around 40-50°C) of the lotus leaf and ruin its hydrophobicity. Most artificial lotus leaf structures with either hydrophilic or hydrophobic bulk properties exhibit worse performance regarding water contact angle at water temperature over 55°C, as the surface tension of water is reduced at higher temperature.[164] SLIPS systems have been reported to retain their high water contact angle and slippery property when touched with high temperature water.[158] Although the polyelectrolyte multilayer system chosen here has hydrophilic properties before our processing,[163] it can repel water and oil after having been coated with a thin layer of a low surface energy lubricant. These slippery properties of the polyelectrolyte based SLIPS can be kept maintained for both water and oil from room at temperature from 25°C to 95°C, as shown in figure 4.4(A). The advancing and receding angles are not significantly different from one another for both cases, and contact angle hysteresis remains small (~2°) over this temperature range. Each droplet of specific temperature was transferred to the surface for 30 s before the test, and all of the test points were taken within a 2 cm square sample of the same film. Properties with water remain similar when tried the multilayer itself is chilled to -10°C.

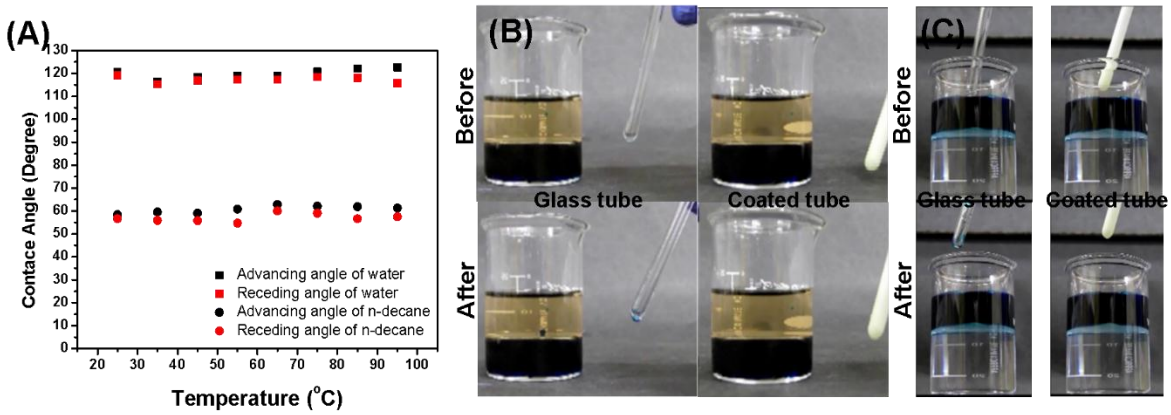

Figure 4.4. Temperature robustness and curved surface coating of polyelectrolyte SLIPS. (A) Dynamic contact angle of water and decane droplets with different temperatures on polyelectrolyte SLIPS. The advancing (black) and receding angle (red) of water (square) and decane (circle) was taken using a drop volume of 5 µL; (B) Water and oil repellant properties of polyelectrolyte SLIPS coated tube compared with a bare glass tube. The upper phase decane colored with red silicone oil, while the lower phase is water dyed with methylene blue; (C) Water and oil repellant properties of polyelectrolyte SLIPS coated tube compared with a bare glass tube. The upper phase is methylene blue dyed water while the lower phase is chloroform. The polyelectrolyte SLIPS coated tube has good repellency to both water and decane (oil), however the bare glass tube does not.

Another advantage of working with polyelectrolyte multilayers is the ease with which they can coat curved surfaces with molecular level adhesion layer (no other type of adhesion layer required). The curved surface shown here, a glass tube as shown in Figure 4.4(B and C), can be coated with the same procedures described above. Figure 4.4(B) shows water dyed with methylene blue (the lower phase) and a mixture of decane with silicone oil (the oil added for color) as the upper phase in the beaker. Figure 4.4(C) has oil and water phases inverted, and the heavy oil phase used is chloroform. The polyelectrolyte SLIPS on the glass tube can repel water, decane and chloroform without any droplets adhering to the tube's surface, while the bare glass tube itself will become coated with an adhesion layer, especially the blue dyed water.

4.4. Summary

We have demonstrated a new method for fabrication of a slippery, omniphobic coatings based on a textured polyelectrolyte multilayer. The weak polyelectrolyte multilayer is made porous

by a staged acid etching, then coated with silica nanoparticles, a hydrophobic silane to enhance wetting with the lubricant, and then imbibed with a perfluorinated lubricant. Our materials are repellant to both oil and water with sliding angles of 3° and extremely low contact angle hysteresis of 2°. These films work over a range of temperatures and are still slippery in an environment where water has condensed on the film. The low sliding angles make these surfaces truly self-cleaning. Polyelectrolyte multilayers are inherently simple to coat on curved surfaces regardless of radius of curvature, and the polyelectrolyte SLIPS coating is demonstrated on a glass tube.

CHAPTER V

TUNABLE DISASSEMBLY OF POLYELECTROLYTE-CU^{2+} LAYER-BY-LAYER COMPLEX FILM*

5.1. Introduction

The Layer-by-Layer (LbL) technique has garnered a great deal of attention due to the ease with which thin films of controllable thickness can be fabricated. Generally, LbL films are made of the oppositely charged polycations and polyanions. Clearly, with charged functional groups there must also be small counterions present, and a good deal of work has been done to determine what role these counterions and any other added ions play in LbL assemblies.[165] We are interested in examining the role of intentionally introduced small ions in LbL assemblies, particularly multivalent metal ions. LbL networks are different than traditional rubbers, in that their linkages (electrostatic or hydrogen bonds) are weaker than covalent bonds and potentially reformable after being damaged.[166] LbL assemblies are already formed with these reversible types of bonds, and the further introduction of multivalent metal ions creates linkages of different strengths, potentially leading to new properties.

Although the use of alkali and alkaline earth metal ions which is well represented in the literature,[1] the assembly of PEMs with transition metal ions is less well studied. Transition metal ions interact with the polymer through the formation of metal-ligand coordination bonds as well as electrostatic interactions with oppositely charged moieties. Kurth *et al*[167] reported a metallo-supramolecular coordination polyelectrolyte by reaction of Co^{2+} with a novel bisterpyridine ligand

*Part of the data reported in this chapter is reprinted with permission from "Formation and tunable disassembly of polyelelctrolyte-Cu^{2+} layer-by-layer complex film" by Xiayun Huang, Amanda B. Schubert, James D. Chrisman, and Nicole S. Zacharia, 2013, *Langmuir*, 29, 12959-12968, http://pubs.acs.org/doi/pdf/10.1021/la402349r, Copyright 2013 by American Chemical Society.

between transition metal ion and pyrinde, Zhang *et al*[89] report multilayers of PSS-Cu^{2+}/PVP and Ji *et al*[168] assembled similar film with Co^{2+}. They can either reduce the ion to make a nanoparticle-polymer hybrid film or keep the ions stable in the film used for ion-depended unique separation properties. Based on these unique coordination pairs, these films ligand containing films can also be used for transition metal ion capture. Kurth *et al*[91] designed a film containing polyelectrolyte with bipyrindine ligands to behave as a metal ion receptor using the ability to bind through metal ion coordination. Tieke *et al*[30,32,34,93,94,169] built PEMs with macrocycles, such as calix[n]arene and crown ethers, as ligands for multiple sequential captures of transition metal ions for ion-selective membrane for water softening and seawater desalination.

Specifically for the BPEI/PAA multilayer system, there are only a few reports of the possibility of incorporating transition metal ions (e.g. Cu^{2+}) into the films during the LbL process. In other multilayer systems using PAA, Cu^{2+} has been incorporated into the $(PAH/PAA)_n$ film as observed by both Bruening[32] and Caruso[96], either by the addition of ions in the deposition solution that then complex with a fraction of the carboxylic acid groups of PAA or by dipping the substrates in Cu^{2+} solution after being immersed in PAA solution. Hammond *et al*[170] doped transition metal ions (Cu^{2+}, Fe^{2+}, and Ag^{+}) into a similar film during the LbL process through interaction with the carboxylic acid groups of PAA as metal-ligand complexation to get optimized capture of ions in the film. However, PAA-metal ion complexes have only been demonstrated to trap small amounts of ions into the film by the dipping deposition. Although Rubner *et al*[83] have reported the high amount of Ag nanoparticles reduction in the PAH/PAA film by post Ag salt absorbing and reduction, each cycles takes a long time and it is hard to use to the dipping deposition due to low stable complexation ratio of metal ion to PAA. In the case of BPEI/PAA, a roughened surface pattern is formed after immersing the film in Cu^{2+} or Zn^{2+} solution.[98] Transition metal ions, like Cu^{2+} and Zn^{2+}, coordinate strongly with carboxylic acid group of PAA. At the same time, they can

also bind with the amine groups of BPEI through electron transfer. Sukhishvili *et al*[165] show that BPEI/PAA films do have the capacities to absorb the transition metal ions (Cu^{2+} and Co^{2+}) through forming chelation complexes with amine and carboxylic acid groups in the film. However, post-assembly absorption methods are not the best way to achieve high capacity metal ion concentration in PEMs in a short time.

Here, we report a system (BPEI-metal ion/PAA) with the ability to capture higher amounts of transition metal ions into the film's structure through both chelations with the amine groups of BPEI and carboxylic acid groups of PAA. For some transition metal ions, the chelation with BPEI creates a strongly colored material, like royal blue for Cu^{2+}, brick red for Co^{2+}, and bright yellow for Fe^{2+}. Moreover, this is a universal method that works for most transition metal ions. While it is not surprising that this works for divalent ions, this also works for the incorporation of monovalent ions, such as Ag^{+}.

Higher amounts of metal ion incorporated in the PEMs make it possible to then tune film properties such as release of the transition metal ions-polyelectrolyte complex. Because of the strong chelation with BPEI and PAA, the PEMs are very stable within certain parameters of ionic strength and pH. In this paper, we choose BPEI/PAA films with Cu^{2+} as a model system to demonstrate the release of Cu^{2+} triggered by pH, salt, and surfactants.

5.2. Materials and methods

Poly(acrylic acid) (PAA, MW=50,000 g/mol, 25wt% solution) was purchased from Polysciences Inc and branched polyethylenimine (BPEI, MW=25,000 g/mol) was obtained from Sigma-Aldrich. Copper nitrate, cobalt chloride, and zinc acetate were purchased from Alfa Aesar. Ferric chloride and silver nitrate were from EMD. Sodium dodecyl sulfate (SDS), pentadecafluorooctanoic acid ammonium salt (APFO), and Tween® 20 was purchased from Sigma-Aldrich and cetyl trimethyl ammonium bromide (CTAB) from AMRESCO. De-ionized

(DI) water with 18.2 MΩ • cm resistivity was obtained from a Milli-Q filtration system and used for all the experiment. All materials were used as received without further purification.

The BPEI-Cu^{2+} complex was characterized using a USB2000-UV-Vis spectrometer (Ocean Optics, Dunedin, FL). Titration and pH adjustment of the BPEI-Cu (II) complex was performed with pH meter (VWR, USA). Transmission electron microscopy (TEM) images were taken using a JEOL (1200-EX) transmission electron microscope operated at 100 kV as accelerating voltage. The same volume of BPEI-Cu^{2+} complex and BPEI-Cu^{2+} complex reduced by $NaBH_4$ was casted on the carbon supported copper grid. The grids were fully dried in vacuum before the TEM imaging. Thermogravimetric analysis (TGA) was performed with a Q500 TGA (TA instruments, West Sussex, UK). Samples were held at 100°C for 20 min to remove unbound water in the film and equilibrate the system and then ramped to 800°C at 5°C/min with air flow. The Cu^{2+} release was tracked by a UV-2250 system (Shimadzu Corp., Japan). FTIR spectra were obtained using an IR Prestige 21 system (Shimadzu Corp., Japan) and analyzed by IRsolution V.1.40 software. Free-standing films were used for transmission mode FTIR measurements by peeling PEM films off of polystyrene substrates. Films on glass substrates were measured using attenuated total reflection (ATR) mode. The thickness of the PEMs were measured using a stylus profilometer (KLA Tencor Instruments P6), and values reported represent an average of 5 different positions on the film. Nanomechanical testing was carried out using the Triboindener (Hysitron Inc., USA) with a load-control and displacement-sensing device. The measurement was done at ambient condition with temperature ~25°C and relative humidity ~50%.

PEMs were assembled onto glass slides and silicon wafers, or polystyrene substrates in order to make freestanding films. Before use, the silicon and glass substrates were treated in a freshly prepared piranha solution (mixture of H_2SO_4 (98%) and H_2O_2 (30%) with the volume ration v/v=7/3) at room temperature for 4 h and rinsed with water until neutralized, while polystyrene

substrates are rinsed with soapy water and then DI water. The substrates were then dried by nitrogen steam before being used for layer-by-layer assembly. The polycation BPEI solution (40 mmol/L with respect to the repeat unit) was mixed with $Cu(NO_3)_2$ to form a stable complex. This complex is then used for building up a multilayer film with negative weak polyelectrolyte, PAA, at the concentration of 20 mmol/L with respect to the polymer repeat unit. The pH of these solutions was adjusted with 1 mol/L NaOH or 1 mol/L HCl solution as needed. For BPEI-Ag^+/PAA PEM, 1 mol/L HNO_3 was chosen to adjust pH instead of HCl. All the multilayer assembly was carried out at room temperature using Zeiss HMS series programmable slide stainer. The treated and dried substrates were first immersed in the BPEI-Cu^{2+} complex solution for 10 min followed by three separate DI water rinse baths. Then, the substrates are exposed to PAA solution for 10 min and then again to three DI water rinse baths. This cycle was repeated until the needed bilayer number was reached. The multilayer films are dried at room temperature for 24 hours before any tests or peeling off of the polystyrene substrates.

All films used for release studies were assembled on glass slides with 30 bilayers of BPEI-Cu^{2+}/PAA (pH 9.5/pH 4.5) with a copper concentration of 3 mmol/L in the BPEI-Cu^{2+} complex. They were then cut into pieces 2 cm×1 cm in dimension. In order to study the effect of pH, the DI water was adjusted to the desired pH using 1 mol/L NaOH and HCl. In studying the effect of salt strengths, different salt solutions were prepared over a concentration range of 0.1 mol/L to 1 mol/L. In the effect of surfactant study, the surfactant solutions were prepared over the concentration varying from 5 mmol/L to 100 mmol/L. The pH value of all the salt and surfactant solutions was not adjusted further after they were added to the DI water. A PEM sample of defined dimension and 5 ml of solution were placed in a centrifuge tube under continuous shaking for 1 hour. The release of Cu^{2+} in solution was tracked by UV-Vis spectrometer. Measurements were made immediately following the procedure to limit the possibility that released material would have time

to settle out of solution or adhere to the container walls. The PEMs were then rinsed with water and dried in a vacuum oven. The thickness of the PEMs was measured with stylus profilometer and an average was taken from measurements on 5 places on each sample and at least two different samples for each data point. All the normalized thickness (%) is measured by (dried film thickness after treatment×100%)/dried film thickness before treatment.

5.3. Results and discussion

5.3.1. The formation of BPEI-Cu^{2+} complex

The molecular geometry of oligomeric and low molecular weight amine-containing macromolecules has a large influence on their ability to form coordination complexes with metal ions and the stability of the resulting complexes. The association constant for Cu^{2+} and amines (K_f of $[Cu(NH_3)_4]^{2+}$ as 1.1×10^{13}) is higher than for amines with most other metal ions (i.e. K_f of $[Co(NH_3)_6]^{2+}$, $[Ag(NH_3)_2]^{+}$, and $[Zn(NH_3)_4]^{2+}$ as 5.0×10^{4}, 1.6×10^{7}, and 7.8×10^{8}, respectively), meaning that is it very easy for this complex to form.[171] BPEI has a branched structure, which contains primary, secondary and tertiary amine groups in the ratio of 25%, 50%, and 25%, respectively.[86] Concentrations of amine groups in BPEI solutions are calculated based on this ratio. This makes the BPEI-Cu^{2+} system an ideal model system for transition metal ion complexes within polyelectrolyte multilayers. Due to its highly branched and dense structure, BPEI does not change conformation in aqueous solution very easily[86] and will therefore form complexes with Cu^{2+} in a square planar geometric arrangement.[87]

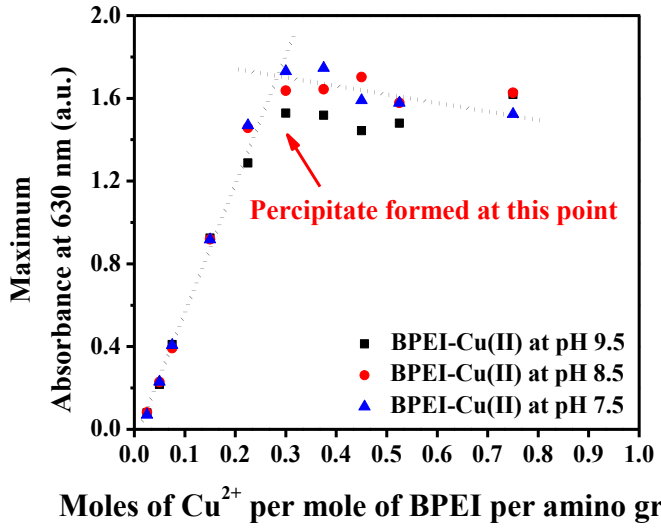

Figure 5.1. Analysis of the stability of BPEI-Cu^{2+} complex monitored by UV-Vis absorbance at λ_{max}=630 nm for solution pH of 7.5, 8.5 and 9.5. BPEI concentration was fixed at 40 mmol/L with respect to the repeat group. The complex becomes unstable and precipitate forms at a ratio of 0.3 moles of Cu^{2+}/moles of amine group in BPEI. Below that ratio, the complex can be stable over one week at all pH values.

The structure of the BPEI-Cu^{2+} complex will depend on the stoichiometric ratios between the two components as well as pH and ionic strength of the solution. To evaluate the chelation of BPEI with Cu^{2+} during multilayer assembly with varying pH value, a series of solutions of fixed BPEI concentration (40 mmol/L of amine group) and increasing copper nitrate concentration were prepared at different pH values (7.5, 8.5 and 9.5) to look for the window of parameters over which the complexes will form and be stable. UV-Vis absorbance intensity at 630 nm was chosen as a quantitative measure for the formation and stability of the complex.[86, 172] As can be seen in figure 5.1, the BPEI-Cu^{2+} complex is not stable beyond a ratio of approximately 0.3 moles of Cu^{2+}/moles of amine group of BPEI. At Cu^{2+} concentrations below this critical ratio, the excess positive charge keeps the complex stable in solution for over one week. TEM images show no that Cu nanoparticles (NPs) are formed over the course of a week (shown in figure 5.2(A, B)), even though

a large amount of Cu^{2+} has been incorporated into the complex solution. The images after $NaBH_4$ reduction (figure 5.2(C, D)) show the Cu^{2+} was reduced to be Cu nanoparticles (NPs) with diameter ~20 nm. We infer from this that the ions remain stable in the complex over this time period. Further increasing the Cu^{2+} concentration will cause precipitate to form as a result of not enough excess charge, destabilizing the complex.

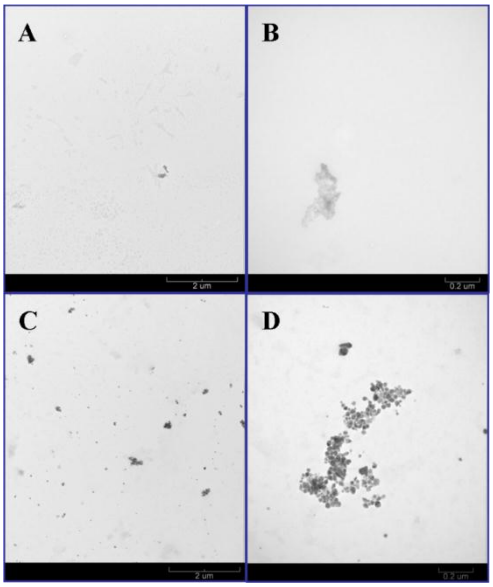

Figure 5.2. TEM images of BPEI-Cu^{2+} complex after prepared for one week. The low magnification (A) and the high magnification (B) images of the complex of BPEI and Cu^{2+}; The low magnification (C) and the high magnification (D) images of the complex with same composition reduced by $NaBH_4$. The concentrations of BPEI and PAA were fixed as 40 mmol/L and 20 mmol/L in repeat functional group, while the concentration of Cu^{2+} as 3 mmol/L. pH of complex was fixed as 9.5. The molar ratio of Cu^{2+} to amino groups of BPEI is 0.075.

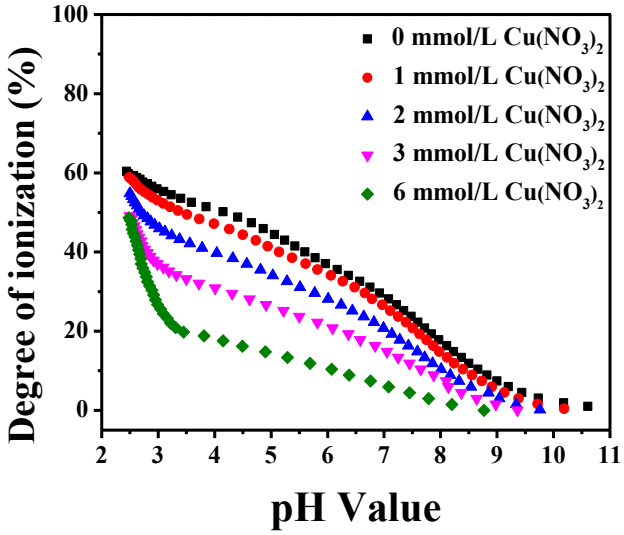

Figure 5.3. Degree of Ionization of BPEI and BPEI-Cu^{2+} complex as a function of pH. BPEI concentration was fixed at 40 mmol/L of polymer amine functional groups. Increasing the amount of Cu^{2+} in the complex will decrease the amount of charge groups available for ionic crosslink formation in the polyelectrolyte multilayers.

Multilayer assembly is an sequential dipping process, relying on the electrostatic interaction between opposite charges to hold together sequential polymer layers.[22] During the assembly process, the charge density of the BPEI-Cu^{2+} complex is not only important for determining the stability of the complex solution, but is also important for multilayer formation and final composition. As a weak polyelectrolyte, the charge density of BPEI can be modulated by solution pH value. Here, we investigate the charge density of BPEI and stable complex through the degree of ionization[38] following calculations in references 19 and 24, assuming that amine groups have the same ionization constant and each of amine group was cheated as the individual one. Figure 5.3 shows the degree of ionization of BPEI and BPEI-Cu^{2+} complex in the same compositions used in the assembly solutions. The BPEI concentration was fixed at 40 mmol/L of polymer amine groups for the assembly solution. As the concentration of Cu^{2+} in the complex is increased, the charge density of the complex becomes lower at the same pH value. As more amine

groups of the BPEI chains are used to form complex with Cu^{2+} it becomes less easy to alter the protonation of the groups and therefore leaves fewer groups that are able to bind with PAA during PEM formation.[174] Here, three Cu^{2+}concentration (as well as BPEI with no copper) have been chosen for assembly. These values are 0, 1, 3 and 6 mmol/L to form complex with 40 mmol/L of BPEI amine groups. These solutions are then assembled with 20 mmol/L PAA (with respect to repeat unit) in order to form films that are strongly blue in color when they contain copper, indicating that the metal-ligand coordination complexes remain intact in the solid state due to crystal field splitting.

5.3.2. Construction of BPEI-Cu^{2+}/PAA films under different assembly pH

For the films assembled in this work, the BPEI-Cu^{2+} complex, a stable complex with an excess of positive charge, is used as the polycation. Figure 5.4 schematically shows the internal structure of PEMs made by the multilayer assembly process. Film assembly is based on electrostatic interactions. Starting with a negatively charged surface first the positive charged BPEI-Cu^{2+} complex is deposited, then the oppositely charged PAA, followed by rinsing with water to remove physisorbed material. The Cu^{2+} are able to interact with carboxylic acid groups as well as amine groups, and therefore during the assembly process there should be some reorganization in the film, allowing for the formation of Cu^{2+}-carboxylic acid bonds. In this case, Cu^{2+} will behave as an ionic crosslinker once they form linkages with both the amine and carboxylic groups of BPEI and PAA.

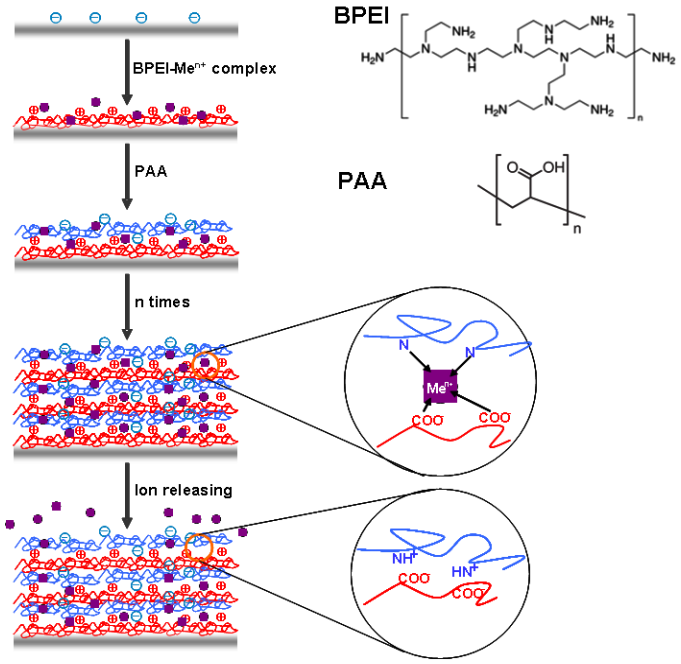

Figure 5.4. Schematic representation of multilayer assembly process, internal structures of BPEI-Me^{n+}/PAA, and Me^{n+} release process. Me^{n+} represents the metal ion, which can be Cu^{2+}, and performs as an ionic crosslinkers between functional groups of both BPEI and PAA. The film would be more realistic to show the interpenetrating networks structures, which is not shown here.

Figure 5.3 shows that the charge density of the BPEI-Cu^{2+} complex can be manipulated through both pH and Cu^{2+} concentration in the complex. The charge density of PAA can also be modulated by pH.[23] BPEI/PAA PEMs have been reported to follow exponential deposition during the initial 15 bilayers and then a rapid linear growth afterwards to quickly form thick films in the micrometer range.[54] Here, we investigate the variation in multilayer thickness with both the ratio of Cu^{2+} in the complex and pH value in the two assembly solutions. Figure 5.5 shows the thickness of 30 bilayer BPEI-Cu^{2+}/PAA PEM films as a function of assembled pH. These thickness values are measured on dry films.

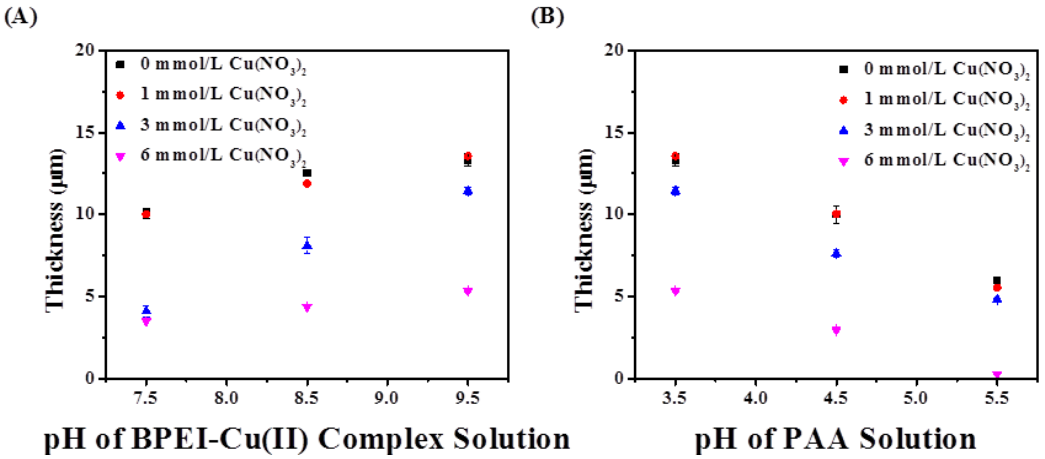

Figure 5.5. Dependence of film thickness of (BPEI-Cu^{2+}/PAA)$_{30}$ PEMs on pH of BPEI-Cu^{2+} complex and/or PAA solution. (A) pH of PAA is fixed as 3.5 and pH of the complex varies; (B) pH of BPEI-Cu^{2+} complex is fixed as 9.5 and pH of PAA varies. The concentration of BPEI and PAA are fixed at 40 mmol/L and 20 mmol/L with respect to the functional group (either carboxylic acid or amine group). The polyelectrolyte charge densities and their conformations influence the overall film thickness.

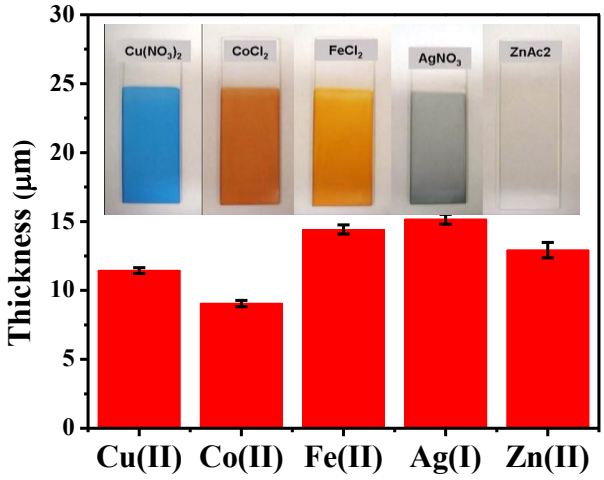

Figure 5.6. Film thickness values and images of (BPEI-Metal ion/PAA)^{30} PEMs deposited on glass slides under assembly conditions of pH 9.5 and 3.5 for the BPEI-metal ion complex and the PAA solution. The concentrations of BPEI and PAA were fixed as 40 mmol/L and 20 mmol/L in repeat functional group and the concentration of metal ions (Cu^{2+}, Co^{2+}, Fe^{2+}, Ag^{+}, and Zn^{2+}) as 3 mmol/L. Metal ions can be assembled into PEMs through chelation with BPEI and some of these complexes result in strongly absorbing colorful films.

All of the PEMs are in the micrometer thickness range, these thick films can easily be peeled off of and a hydrophobic substrate such as polystyrene or Teflon to make freestanding films. For the data in figure 5.5(A), pH of PAA is fixed as pH 3.5 and the PEM thickness is measured as a function of variation of the Cu^{2+} ratio and pH of the BPEI-Cu^{2+} complex. The charge density of the BPEI-Cu^{2+} complex with different ratios of Cu^{2+} can be found in figure 5.3. At a pH of 7.5, 8.5 or 9.5, increasing the amount of Cu^{2+} will decrease the charge density of complex and result in decreasing the PEM thickness. However, using the same Cu^{2+} ratio and increasing pH value, the PEM thickness increases with the corresponding decrease in charge densities. This is due to the more coiled conformation that polyelectrolytes take on at lower charge density leading to thicker deposition.

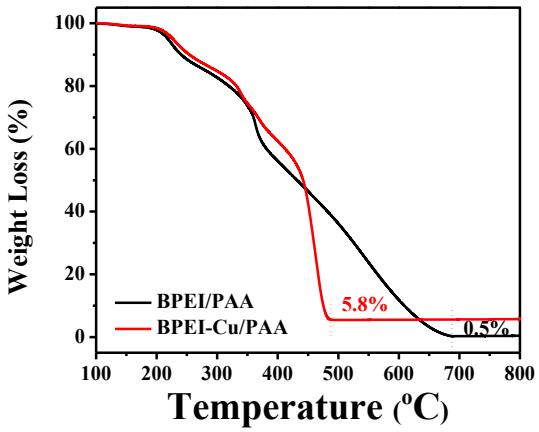

Figure 5.7. TGA graphs of $(BPEI/PAA)_{30}$ and $(BPEI\text{-}Cu^{2+}/PAA)_{30}$ PEMs as pH 9.5 for BPEI or BPEI-Cu^{2+} complex and pH 4.5 for PAA assembly solution. The concentrations of BPEI and PAA are fixed as 40 mmol/L and 20 mmol/L in repeat functional group, while the concentration of Cu^{2+} fixed as 3 mmol/L. The free-standing film was built on the polystyrene substrate and release from the substrate once it was dried.

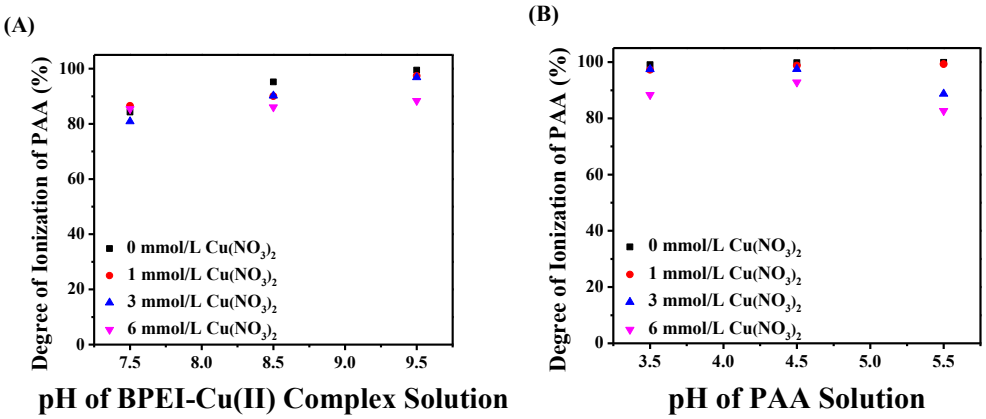

Figure 5.8. Degree of ionization of PAA in (BPEI-Cu^{2+}/PAA)$_{30}$ PEMs assembled under varying pH values of the of BPEI-Cu^{2+} complex and PAA solutions. (A) pH of PAA is fixed as 3.5 and pH of the BPEI-Cu^{2+} complex varies; (B) pH of BPEI-Cu^{2+} complex is fixed as 9.5 and pH of PAA varies. All the concentration of BPEI and PAA are fixed as 40 mmol/L and 20 mmol/L with respect to the functional group. The majority of the carboxylic acid groups in the PEMs are ionized, consistent with PAA being a minority component in the PEMs.

Figure 5.5(B) shows the PEM film thickness with a fixed BPEI-Cu^{2+} complex pH as 9.5. Similarly, a decrease in the ratio of Cu^{2+} in the BPEI-Cu^{2+} complex decreases the PEM thickness due to the lower charge density of the complex. The thickness of the PEMs can be increased by decreasing the pH value of the PAA solutions below 5.5, again corresponding to a lower polyelectrolyte charge density.[38] The pKa of PAA is roughly 5.5–6.5,[38] so lowering the pH value below the pKa corresponds to a decrease in overall charge density.

The thicker PEM layers, in this case, are due to the coiled conformation taken on by PAA. Both the charge densities due to the ratio of Cu^{2+} and polyelectrolyte conformations as determined by the pH values impact the overall PEM thickness. Varying these parameters will also impact the PEM composition and degree of ionization of functional group in the PEMs in as well as the overall layer thickness. The strong blue color of the BPEI-Cu^{2+}/PAA PEM as shown in Figure 5.6 demonstrates the presence of Cu^{2+} in the film, but the Cu content in the BPEI/PAA film was also measured by TGA (figure 5.7). The difference in mass after heating between BPEI/PAA films and

films containing the Cu^{2+} is ~5.3 wt%, and is indicative of the amount of Cu^{2+} in the films. Although it is possible that there are some minor differences in char formation due to the complexation with Cu^{2+}, ~5 wt% is a reasonable estimate for metal ion content.

The degree of ionization of PAA in these PEMs, shown in figure 5.8, was very high (>80%) which is consistent with a lower content of PAA in the PEMs as compared to the BPEI-Cu^{2+} complex (as LbL films are generally charge matched, and higher charge density of PAA compared to BPEI corresponds to less PAA in the film). The extent of carboxylic acid ionization was calculated from the ratio of the peak intensity at 1543 cm^{-1} ($-COO^-$ asymmetric stretching) to the sum of the peak intensity at 1543 and 1710 cm^{-1} (-COOH asymmetric stretching) and shown in the percentage range. Here, we assume the coefficient of extinction is the same for the protonated carboxyl at 1710 cm^{-1} and the deprotonated carboxyl at 1543 cm^{-1}.[38, 176,177] Most of carboxylic acid groups (>80%) in the PEM were ionized due to interactions with the amine groups of BPEI and Cu^{2+}. Carboxylic acid is a labile functional group and it is strongly influenced by its immediate environment. The p*Ka* value of PAA can much lower than that in solution.[38]

5.3.3. Construction of BPEI-Metal ion/PAA film

The highly branched BPEI chains are able to chelate many metal ions and still form a stable complex. Here, we have chosen different metal ions (Cu^{2+}, Co^{2+}, Fe^{2+}, Ag^+, and Zn^{2+}) which are able to form strong metal-ligand bonds with amine groups and hydroxyl groups as demonstrated by large complex formation constant values.[171] Figure 5.6 shows the thickness and images of 30 bilayers BPEI-metal ion/PAA PEMs deposited on the transparent glass slides. All of the various metal ion combinations adsorb as thick layers (~10 μm in thickness for 30 bilayer films). Also, PEMs with Cu^{2+}, Co^{2+}, Fe^{2+} form very colorful (royal blue, brick red, and bright yellow, respectively) films due to the crystal field splitting that occurs upon formation of the metal-ligand coordination bonds. Generally speaking, transition metal containing complexes are

colorful, whereas other complexes (Ag^{+}, Zn^{2+}) are not colored, or only weakly so. For the transition metal containing films, the intensity of the color in the films is much higher than the color intensity of the metal ion solutions at assembly concentration (3 mmol/L of metal ion). The strong color is actually formed when BPEI is added to the metal ion solution, indicating the formation of the metal-ligand complex in solution. Of note, when multilayer films are formed with the BPEI-metal ion complexes and poly(4-styrenesulfonic acid) (as opposed to PAA) the strong colors are not present. We hypothesize that either the sulfonate-amine bonds are strong enough to displace the metal-ligand coordination complexes or that coordination between the acrylic acid and metal ions also contributes to the strong colors in the thin films.

In addition to creating these strong colors, adding metal ions to the polyelectrolytes increases both the Young's modulus and hardness of these films, as shown in figure 5.9. Young's modulus of the BPEI/PAA films without Cu^{2+} is 8 GPa, which is in rough agreement with other values for multilayer films.[28] Different measurement techniques reported in the literature create some variations, but electrostatically assembled LbL systems tend to have Young's modulus values from several hundred MPa to low GPa.[177-179] Increasing Cu^{2+} content in the BPEI solution increases the resulting Young's modulus to about 11 GPa. Hardness values follow a similar trend. This seems to indicate that the metal ions are acting as crosslinkers in the films, and interacting with not only the BPEI but the PAA as well.

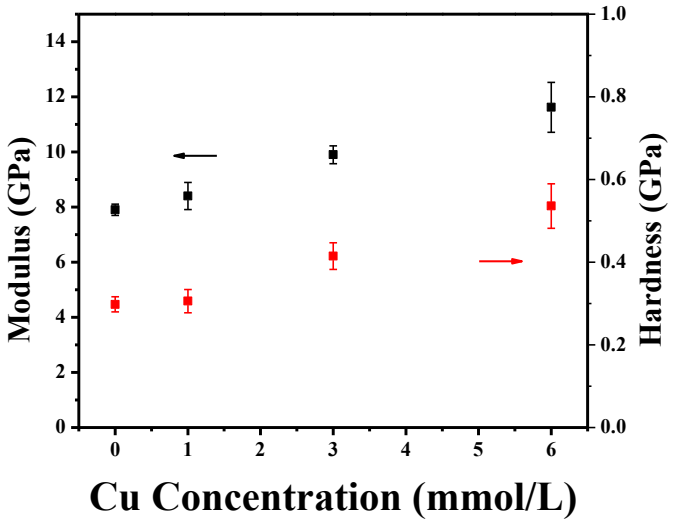

Figure 5.9. Modulus (black data points) and hardness (red data points) values of (BPEI-Cu^{2+}/PAA)$_{30}$ PEMs with varying Cu^{2+} concentrations in the BPEI-Cu^{2+} complex solution. The pH values for BPEI-Cu^{2+} complex solution and PAA solution were 9.5 and 4.5, respectively. Both modulus and hardness increase with increasing the Cu^{2+} concentration in the assembly complex solution. The measurement was done at ambient condition with temperature ~25°C and relative humidity ~50%.

5.3.4. Controllable disassembly and Cu^{2+} release

Copper is an element with some biological functions, such as a cofactor for the enzymes cytochrome c oxidase and Cu/Zn superoxide dismutase.[180] At the same time, however, Cu^{2+} is toxic, to most organisms at elevated concentrations, through enzyme inhibition,[181] the oxidation of membrane component (which might be related to the ability of copper to generate toxic hydroxyl radicals[182-185]), and membrane damage, resulting in the rapid leakage of ions and other low molecular weight compounds [36] through the cellular membrane. This is why copper is used in some fungicides. Therefore, controlled release of copper ion may be of interest for certain applications. Polyelectrolyte multilayers are a good candidate for loading and release of various cargos (here, Cu^{2+}) because the interactions within the multilayer can bind the cargo, but also be modulated with various external stimuli in order to release the cargo. This release can be achieved

through various types of film disassembly,[1,39,61,96, 98, 186-190] triggered by external stimuli such as pH,[39] ionic strength,[190] and surfactant,[61] because the ionization of weak polyelectrolytes is very sensitive to the local environment. Many multilayer films with different compositions, such as PAH/PAA[39,190] and LEPI/PAA[191,192] held together through electrostatic interactions and hydrogen-bonded films of PAA or carboxyl-terminated dentrimer with poly(4-vinylpyrinde),[193-195] have been reported to be disassembled and form porous (both microporous and nanoporous) films by exposure to these different types of environment.

BPEI-Cu^{2+}/PAA PEM films were found to release Cu^{2+} in a controllable way by disassembling the PEMs to form porous structures through exposure to different conditions of pH, salt strength, and surfactant. Figure 5.10(A) shows the release of Cu^{2+} by varying the pH value. The amount of Cu^{2+} was monitored through the maximum absorbance intensity at 630 nm.[173] By varying the pH value from 2 to 13, within an hour three regions were shown with different release behavior. Cu^{2+} releases from the film in low and high pH values, while the films are stable at an intermediate range from pH 4 to pH 10. The transition values in pH for which the Cu^{2+} containing films change from stable to unstable correspond to the formation of porous structures of weak polyelectrolyte film as reported.[190,193] The thickness, degree of ionization of PAA, and the morphology of film are also investigated and shown in figure 5.10(B-D) respectively. In the acidic (<pH 4) and basic (>pH 10) regions, the PEM films begin to decompose as demonstrated by decreases in thickness and the creation of a porous structure.

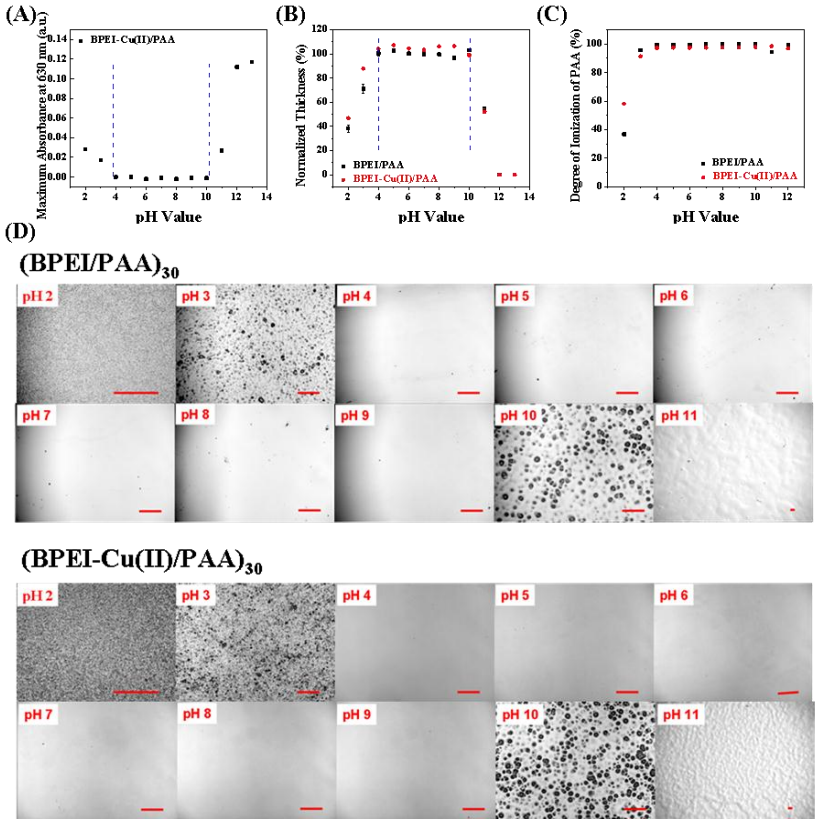

Figure 5.10. (A) Cu^{2+} release from (BPEI-Cu^{2+}/PAA)$_{30}$ PEM in aqueous environment of varying pH. (B) Normalized PEM thickness and (C) degree of ionization of PAA in dried (BPEI/PAA)$_{30}$ and (BPEI-Cu^{2+}/PAA)$_{30}$ PEM from FTIR spectra after immersion in different pH solutions. (D) Porous structures of (BPEI/PAA)$_{30}$ and (BPEI-Cu^{2+}/PAA)$_{30}$ PEM immersed in solutions with different pH value for 1 hr. Scale bar is 200 μm. The PEM as deposited on the glass substrate in the assembly pH of 9.5 and 4.5 for BPEI-Cu^{2+} complex and PAA solution. The concentrations of BPEI and PAA were fixed as 40 mmol/L and 20 mmol/L in repeat functional group and the concentration of Cu^{2+} as 3 mmol/L.

Both BPEI/PAA and BPEI-Cu^{2+}/PAA complex films show the same transitions for acidic and basic pH values. The decomposition of the films and creation of pores is caused by the changing charge density of the amine groups of BPEI and carboxylic acid groups of PAA, and breaking/redistributing the ionic crosslinks through electrostatic interactions. The degree of ionization of PAA in the PEM was calculated as discussed above. The degree of ionization of PAA in the PEM as prepared is ~97%. After exposure to different pH values, the degree of ionization

of PAA remains constant except for the cases of exposure to pH under 3. Under these exposure conditions, the PAA charge density decreases and pores are formed. A similar situation occurs to the charge density of BPEI also leading to the formation of pores in the basic regime. Unfortunately within the BPEI/PAA PEMs, quantifying the degree of ionization of BPEI is difficult because of the multiple types of amine groups and the overlap of their peaks with those of PAA.[192] The porous features formed in basic solution are also different from those formed in acidic solutions. These differences control the degree of decomposition of the film as well as the composition of what is dissolved from the film into solution and impacts the degree of released Cu^{2+}. Over the basic regime, the films are decomposed faster than those exposed to acidic solutions as evidenced by thinner remaining film thicknesses and faster release of Cu^{2+} as tracked by UV-Vis spectrometer. The porous features in the basic case are larger than in the acidic case until the films become completely dissolved.

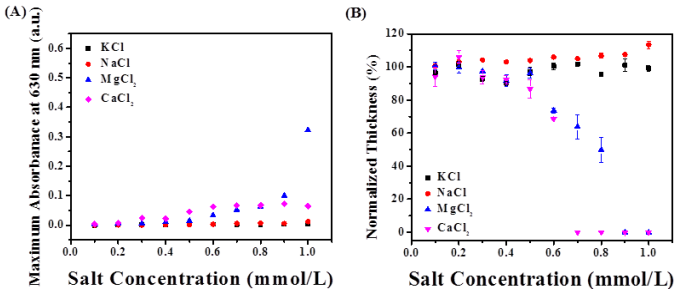

Figure 5.11. (A) Cu^{2+} release from (BPEI-Cu^{2+}/PAA)$_{30}$ PEM in aqueous environment of varying salt type and concentration and (B) normalized film thickness values. The PEM used here is BPEI-Cu^{2+}/PAA assembled under pH 9.5/4.5. The concentrations of BPEI and PAA were fixed as 40 mmol/L and 20 mmol/L with respect to functional group and the concentration of Cu^{2+} as 3 mmol/L. The amount of Cu^{2+} was monitored through the maximum absorbance intensity at 630 nm.

In summary, BPEI-Cu^{2+}/PAA is a pH-sensitive film. Similar to most weak polyelectrolyte PEMs, this system can form porous morphologies after exposure to both acidic and basic solutions.

The porous transformation that occurs through redistribution of ionic crosslinks is accompanied by mass loss and a decrease in thickness. The degree of film decomposition and Cu^{2+} release are different in acid and base region, corresponding to differences in pore formation. The degree of released Cu^{2+} can be controlled by pH and time interval.

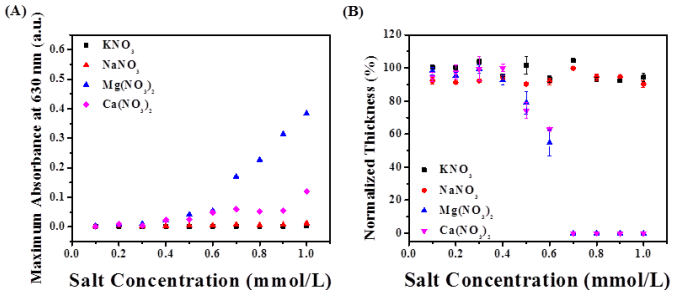

Figure 5.12. (A) Cu^{2+} release from $(BPEI\text{-}Cu^{2+}/PAA)_{30}$ PEM in aqueous environment of varying salt and salt concentration and (B) relative normalized thickness. The PEM as deposited on the glass substrate in the assembly pH of 9.5 and 4.5 for BPEI-Cu^{2+} complex and PAA solution. The concentrations of BPEI and PAA were fixed as 40 mmol/L and 20 mmol/L in repeat functional group and the concentration of Cu^{2+} as 3 mmol/L. The amount of Cu^{2+} was monitored through the maximum absorbance intensity at 630 nm.

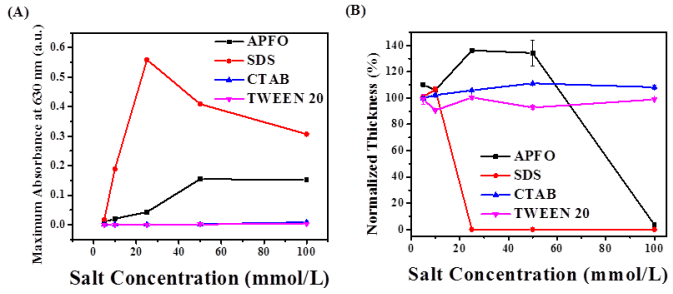

Figure 5.13. (A) Cu^{2+} release from $(BPEI\text{-}Cu^{2+}/PAA)_{30}$ PEMs in aqueous environment of varying surfactant and surfactant concentration and (B) related normalized thickness. The PEM was deposited on a glass substrate under assembly conditions of pH 9.5 and 4.5 for BPEI-Cu^{2+} complex and PAA solution. The concentrations of BPEI and PAA were fixed at 40 mmol/L and 20 mmol/L with respect to the functional group and the concentration of Cu^{2+} at 3 mmol/L. The amount of Cu^{2+} was monitored through the maximum absorbance intensity at 630 nm.

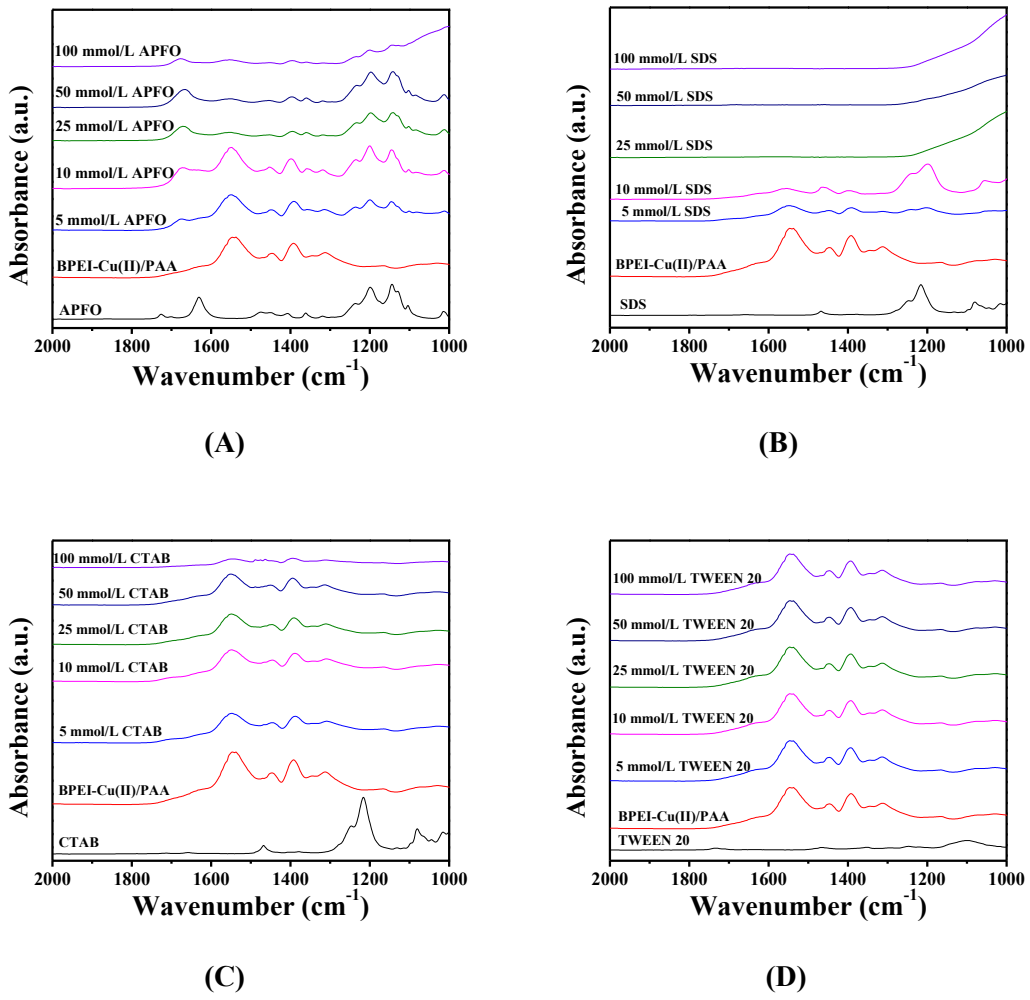

Figure 5.14. FTIR spectra showing (BPEI-Cu^{2+}/PAA)$_{30}$ PEM interdiffused with different surfactants (A) APFO, (B) SDS, (C) CTAB, (D) TWEEN 20. APFO and SDS exchanged with the components of PEMs in a fast rate, while CTAB and TWEEN® 20 exchanged with the components of PEMs in a slow rate.

Immersion in salt solution is also known to disassemble and rearrange PEM films in a controllable way by the loss by the charge screening of the ionic crosslinks.[190, 197] Figure 5.11 shows thickness decrease and release of Cu^{2+} with exposure to increasingly strong salt concentration for 1 hr. Both salts with monovalent (KCl and NaCl) and divalent ($MgCl_2$ and $CaCl_2$) cations were chosen as candidates to look for differences in Cu^{2+} release. The pH values of all the

salt concentrations were within the values corresponding to film stability. BPEI-Cu^{2+}/PAA PEMs are largely stable in the monovalent cation salt, which is similar to the PAH/PAA system as reported.[196] However, divalent cations decompose the film and release Cu^{2+} much more quickly. The degree of film decomposition and released Cu^{2+} can be also manipulated through concentration and time. Notably, there are few literature reports of the use of divalent cations to disassemble PEM films. Looking back to the Hofmeister Series, ions that are more hydrophobic (such as Mg^{2+} and Ca^{2+}) will more rapidly cause the dissociation of PEMs.[198-200] Also, nitrate salts with the same metal ions show similar results as their corresponding chloride salts (figure 5.12).

In addition to controllable release by pH and salt, we have demonstrated that organic small molecules, such as chelators and surfactants, are a third option to destabilize the film and release Cu^{2+} ions. Ethylenediaminetetraacetic acid (EDTA), a hexadentate chelating agent, can extract Cu^{2+} from films due to the larger association constant of Cu with EDTA ($[Cu(EDTA)]^{2-}$ as 6.3×10^{18}) compared to that with amine group ($[Cu(NH_3)_4]^{2+}$ as 1.1×10^{13}).[171] Disassembly with surfactants however, works in a similar way to disassembly by salt, by screening the electrostatic interactions within the multilayer. Recently, studies on the ion exchange of PEM with surfactant have shown the possibility for control of degree of decomposition by surfactant type, time and concentration.[199,200] Figure 5.13 tracks the Cu^{2+} release and the film thickness after exposure to different types of surfactants. Over the pH range that corresponds to film stability in the other cases, the PEMs are stable in the presence of surfactant. Similar to the case for PAH/PAA PEMs,[62] positively-charged CTAB and nonionic TWEEN® 20 do not disassemble the BPEI-Cu^{2+}/PAA PEMs. No release of Cu^{2+} can be detected and the thickness stays constant. However, for both the negatively-charged surfactants (APFO and SDS) chosen, the film is quickly decomposed and Cu^{2+} are released. One point of interest is the large increase in film thickness to ~140% of its original value for the APFO surfactant at the concentration of 25 mmol/L and 50 mmol/L. The

hydrophobic, fluorinated tails of APFO interact with the hydrophobic polymer backbones to create a more coiled conformation and increasing the film thickness. In addition to this, surfactant molecules may displace polymer chains within the PEM as shown in figure 5.14.[69] A small decrease in the characteristic absorbance of Cu^{2+} for the 100 mmol/L APFO release condition is due to the complex formed by Cu^{2+}, surfactant, and polyelectrolytes precipitate down during the UV-Vis measurement. Similar case happens for SDS release conditions when concentrations over 25 mmol/L.

5.4. Summary

We have demonstrated the formation of PEMs containing various metal-ligand complexes, forming different brightly colored materials. These strong colors are due to the crystal field splitting that occurs when the metal ions bind with the amine groups of BPEI, and also from the interplay between PAA, BPEI, and the metal ions. Both the hardness and Young's modulus of these films increase with increasing copper content, leading us to conclude that the Cu^{2+} interact with both BPEI and PAA and act as a crosslinking agent in the films. Choosing Cu^{2+} containing films as a model system, the disassembly of Cu containing PEMs was demonstrated under a range of conditions showing that pH, salt concentration, and surfactant are all external stimuli capable of triggering this disassembly, which could be used for antifungal application.

CHAPTER VI

GELATION-ENHANCED FLUORESCENCE EMISSION CHARACTERISTICS OF POLYELECTROLYTE-ION COMPLEX MULTILAYERS

6.1. Introduction

Coordinative assembly allows organic-inorganic coordination polymer,[1] metal ion,[53,167] and metallopolymers[98] to build up as the supramolecular functional assemblies. In most cases, organic fluorophores are conjugated polymers that exhibit a color change or emission of light when met with metal ion.[1,99,100] The conjugated polyelectrolyte, made by conjugated polymer with ionic moieties such as caboxylates,[201] sulfonates[202] and quaternary ammonium salts[203] quenches in luminescence when met with metal ion. This can be simply explained by self-quenching and intermolecular energy transfer caused by the aggregation of chromophores in the aqueous solution, called aggregation-caused quenching (ACQ).[99,100,204] Non-conjugated polymer in most of case can not emitting light because it is very hard to rigidified the backbone to activate the emission of light.[99]

In contrast, it is possible that aggregation will induce and enhance luminescence emission, called the aggregation-induced emission (AIE), which is first reported by Tang's group in 2001.[204] AIE compounds are non-fluorescent or weakly fluorescent in solution, but strongly emissive when aggregated due to restriction of the intramolecular torsional/rotational motions as opposed to conventional chromophores.[204]

Gelation is a type of aggregation accompanied with supramolecular self-assembly of gelators.[205-207] The designed organogelators perform enhanced emissions when aggregated as a gel state, called gelation-enhanced emission, which extends the concept of AIE.[207] One example will be organogels coordinated with metal ions, especial silver ion. However, only few reports have

described fluorescent silver-ion complexes and the silver ion complexation induced formation of fluorescent supramolecular gels.[14] Moreover, photoluminescence quenching occurs, even through the unbond ligand shows a strong fluorescence before chelating with Ag^+.[107] Therefore, the turn-on type fluorescent probe for Ag^+ still remains a significant challenge. Park *et al*[205] present a "turn-on" fluorescent supramolecular gel triggered by coordination of silver ion. It is non-fluorescent for ligand itself in solution but becomes highly fluorescent when self-assembled with Ag^+ to form supramolecular fibers.[205] Zhang *et al*[208,209] reported another "turn-on" fluorescent gel based on the tetraphenylthylene derivatives, which shows very weak fluorescence in solution. Once aggregated induced by Ag^+, a strong emission will be formed.

Here, we reported a (BPEI/PAA)-Ag^+ complex system that shows a similar fluorescence "turn-on" phenomena. The complex film was prepared via LbL assembly by sequential dipping in the basin of polycation and polyanion solutions till the desired number of layers was achieved. Ag^+ was introduced by forming the stable complex with either BPEI or PAA solution during assembly. During assembly, each deposition step captures Ag^+ into multilayer through both chelation with the amine groups of BPEI and carboxylic acid groups of PAA. The multilayer film without Ag^+ was non-fluorescent. Once Ag^+ was included in the assembly process—no matter if that was in polycation or polyanion solution, the orange emission color would be generated from the multilayer film. This interesting phenomenon can be explained as Ag^+ forming a complex with both BPEI and PAA to form a supramolecular structure and consequent splitting of highest occupied molecular orbital (HOMO) and lowest unoccupied molecular orbital (LUMO) with an energy difference that matches the photoluminescence emission. However, this will be more complicated when it happens to the metal ion-polycation-polyanion system compared with metal ion-gelators.

6.2. Materials and methods

Poly(acrylic acid) (PAA, MW=50,000 g/mol, 25 wt% in H_2O) was purchased from Polysciences Inc. Poly(acrylic acid) (PAA, MW=100,000 g/mol, 35 wt% in H_2O) and branched polyethylenimine (BPEI, MW=25,000 g/mol) were obtained from Sigma-Aldrich. Silver nitrate was purchased from Alfa Aesar. Pure water was obtained from Milli-Q system and used for all the experiment. All materials were used of at least analytical reagent grade and used as received without further purification.

The thickness of the (BPEI/PAA)-Ag^+ complex film was measured using profilometer (KLA Tencor Instruments P6), and values reported represent an average of 5 different positions of the film. Fluorescence spectra of (BPEI/PAA)-Ag^+ complex film and fluorescence quenching studies after exposure to formaldehyde vapor were measured by spectrofluorometer (PTI QuantaMaster Series, Photon Technology International, Inc, NJ). The slit width was 3 nm for both the excitation and emission mode using 30° solid sample holder. The amount of Ag^+ in the films were analyzed by inductively coupled plasma mass spectroscopy (ICP-MS) (NexIon 300 D, PerkinElmer Inc., USA).The (BPEI/PAA)-Ag^+ complex film and the films after formaldehyde treatment were measured by UV-2250 system (Shimadzu Corp., Japan). And FTIR spectra were obtained using an IR Prestige 21 system (Shimadzu Corp., Japan) and analyzed by IRsolution V.1.40 software.

PEMs were assembled onto glass slides, quartz glass and silicon wafers. Before use, they were treated in a freshly prepared piranha solution (mixture of H_2SO_4 (98%) and H_2O_2 (30%) with the volume ration v/v=7/3) at room temperature for 4 h and rinsed with water to neutral. All the substrates were dried by nitrogen steam before the layer-by-layer assembly. The (BPEI/PAA)-Ag^+ complex film were assembled by polycation (BPEI solution, 40 mmol/L with respect to the amine

groups) and polyanion (PAA solution, 20 mmol/L with respect to the carboxylic acid groups). The $AgNO_3$ can be mixed with either BPEI or PAA to form the stable complexes for assembly solution. The pH of these solutions was adjusted with 1 mol/L NaOH or 1 mol/L HNO_3 solution to 9.5 for BPEI or BPEI-Ag^+ complex solution and 4.5 for PAA or PAA-Ag^+ complex solution. All the multilayer assembly was carried out at room temperature using a StratoSeqiemce VI dipper (NanoStrata Inc.). The cleaned and dried substrates were first exposed to polycation solution for 10 min followed by three separate DI water rinse baths. Then, the substrates are exposed to polyanion solution for 10 min and then again to three DI water rinse baths. This cycle was repeated until desired bilayers were reached. The multilayer films were dried in dark environment (temperature ~25^{o}C and relative humidity at ~55%) for 24 h before any testing.

All films used for formaldehyde detection were assembled using 30 bilayers BPEI-Ag^+/PAA PEM with Ag^+ concentration of 3 mmol/L in the assembly complex solution. Formaldehyde gas detection was carried out by vaporizing formaldehyde solution (100 μL, 37 % in H_2O) in a close-capped 30 mL bottle. The formaldehyde vapor concentration in the closed-capped bottle was 0.13%. The formaldehyde in aqueous solution was vaporized to gas and reduces Ag^+ in the PEM to Ag particle. PEMs were kept in this formaldehyde gas environment and dark environment as well for different time and the fluorescent intensity of each specimen was detected by the spectrofluorometer and UV-Vis spectrometer.

10 bilayer BPEI-Ag^+/PAA film loaded with different Ag^+ concentrations (1 mmol/L, 3 mmol/L, and 6 mmol/L as the Ag^+ concentrations in assembly solution) were reduced via heating at 200^{o}C for 1 hour with Ar flow (flow rate set as 1 L/min (LPM)). Ag nanocluster was formed in the film and detected by the spectrofluorometer and UV-Vis spectrometer.

6.3. Results and discussions

6.3.1. Fluorescent (BPEI/PAA)-Ag^+ complex film

Branched polyethylenimine (BPEI) is especially attractive due to its primary, secondary, and tertiary amine groups and branched structures, which allow the formation of stable complexes with a wide variety of transition metal ion.[52,210] The system, BPEI-metal ion/PAA, has the ability to capture different kinds of transition metal ions into the polyelectrolyte multilayers through both chelation with the amine groups of BPEI and the carboxylic acid groups of PAA.[52] This universal method also works for monovalent ions, such as Ag^+. As shown in figure 6.1(B), the deposition of complexes into films begins with a stable BPEI-Ag^+ complex with excess of positive charges, which absorb negatively charged PAA through electrostatic interaction for the incoming deposition. The immobilized Ag^+ would be able to interact with both amine groups and carboxylic acid groups of BPEI and PAA in the film with a certain reorganization of polyelectrolyte chains. Unlike the royal blue color seen in the BPEI-Cu^{2+}/PAA film,[2] the film with Ag^+ looks nearly colorless under visible light, while it emits intense orange color under UV radiation.

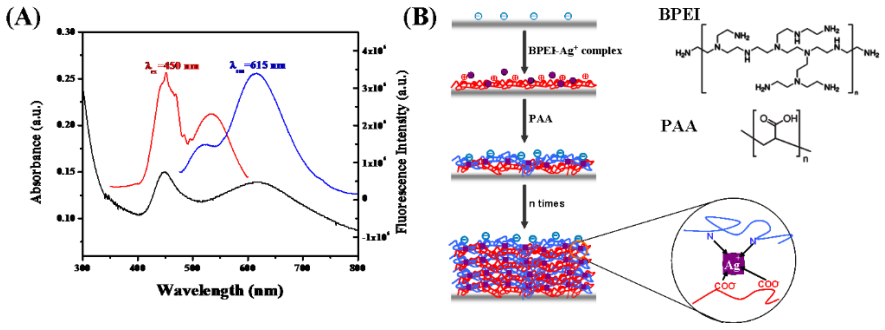

Figure 6.1. (A) UV-Vis and fluorescence spectra of 30 bilayer BPEI-Ag^+/ PAA films. Black color spectrum was the UV-Vis spectrum. Red and blue color spectra were the excitation (with fixed emission wavelength of 615 nm) and emission spectrum (with fixed excitation wavelength of 450 nm), respectively. Concentration of BPEI and PAA were 40 mmol/L and 20 mmol/L with respect to the repeating group. Concentration of Ag^+ in the BPEI-Ag^+ complex solution was fixed as 3 mmol/L.

UV-Vis spectrum (black line) in figure 6.1(A) shows the weakly absorbance of BPEI-Ag^+/PAA film in the visible range at 450 nm and 615 nm, which matches with the maximum fluorescence excitation (red color spectrum) at 450 nm and emission (blue color spectrum) at 615 nm.

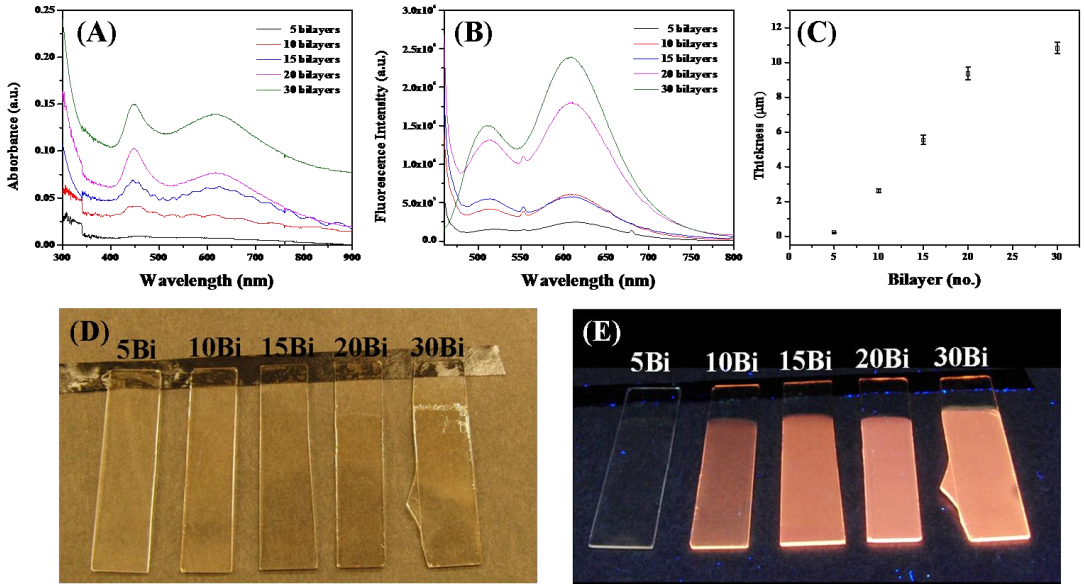

Figure 6.2. The growth of BPEI-Ag^+/PAA film. UV-Vis (A), fluorescence spectra (B) and thickness (C) of BPEI-Ag^+/PAA film with different bilayer number. The fluorescence spectra with different bilayers were obtained with excitation wavelength of 450 nm. The photographs of BPEI-Ag^+/PAA film with different bilayer number under visible light (D) and 302 nm UV radiation (E). Films show colorless under visible light, while those under 302 nm UV radiation shows orange emission color and the intensity increase with increasing the bilayer number. Concentration of BPEI and PAA were 40 mmol/L and 20 mmol/L with respect to the repeating group. Concentration of Ag^+ in the BPEI-Ag^+ complex solution was 3 mmol/L.

Interestingly, the fluorescence emission comes from the (BPEI/PAA)-Ag^+ complex containing film, not from reduced Ag cluster. It has been observed that Ag clusters as part of a polyelectrolyte complex containing film can also generate the fluorescence emission due to discontinuous band structures.[101-104] Photochemical reduction of the complex film (from Ag^+ to

Ag nanocluster), however, gives the quenching in fluorescence, which is not shown here. This indicates the emission comes from (BPEI/PAA)-Ag^+ complex film instead of Ag nanocluster.

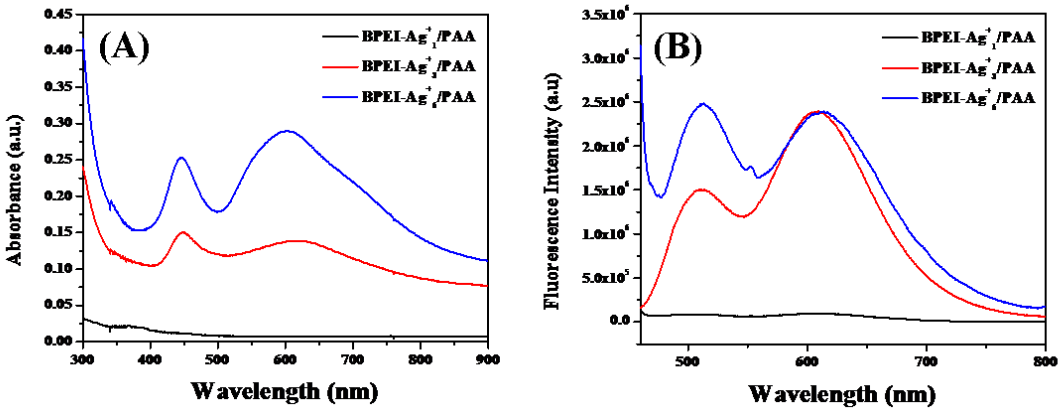

Figure 6.3. UV-Vis (A) and fluorescence spectra (B) of 30 bilayer BPEI-Ag^+/PAA film with different Ag^+ concentration in BPEI-Ag^+ assembly complex solution. The emission spectra were obtained with 450 nm excitation wavelength and the relative intensities increase with Ag^+ concentration from 1 mmol/L to 6 mmol/L. The concentration of BPEI and PAA were 40 mmol/L and 20 mmol/L with respect to the repeating group. The concentration of Ag^+ in the BPEI-Ag^+ complex solution was 1 mmol/L, 3 mmol/L and 6 mmol/L in the BPEI-Ag^+ complex solution for LbL assembly.

Different from single emission band of Ag nanocluster either in solution[1,102,202,211] or in the film,[212-214] two overlapped emission bands at 515 nm and 615 nm have been observed for BPEI-Ag^+/PAA film with excitation at 450 nm. There may be multiple types of bonding with the Ag^+ resulting in the two overlapped emission band.

Similar to the growth of BPEI/PAA film,[54,215] BPEI-Ag^+/PAA film grows exponentially (figure 6.2(C)). Both UV-Vis absorbance (figure 6.2(A)) and fluorescent intensity (figure 6.2(B)) increase with the increase in bilayer number. However, peaks of UV-Vis and fluorescence spectra do not shift in wavelength. The relative intensities of two peaks in the fluorescence spectra keep the similar ratio with film grown thicker. This means the chelation mode in the film does not

change distinguishably due to this exponential growth. Although this increase in absorbance in the visible range has been detected via UV-Vis spectra, the film shows nearly colorless under visible light (figure 6.2(D)). Once they were exposure in the UV irradiation, orange emission color shows spontaneously (figure 6.2(E)). The emission intensities increase with the increase in bilayer number of BPEI-Ag^+/PAA film (figure 6.2(B)).

Table 6.1. Amount of Ag^+ was assembled in 30 bilayer BPEI-Ag^+/PAA film with different Ag^+ concentration in BPEI-Ag^+ assembly complex solution with The concentration of BPEI and PAA were 40 mmol/L and 20 mmol/L with respect to the repeating group. The concentration of Ag^+ in the BPEI-Ag^+ complex solution was 1 mmol/L, 3 mmol/L and 6 mmol/L in the BPEI-Ag^+ complex solution for LbL assembly.

Polyelectrolyte-ion complex multilayer	Amount of Ag^+ ($x10^{-4}$, mmol/mm^3)
BPEI-Ag^+_1/PAA	3.8256
BPEI-Ag^+_3/PAA	8.6617
BPEI-Ag^+_6/PAA	14.2431

The UV-Vis absorbance and fluorescent intensity also varied via manipulating Ag^+ concentration in the BPEI-Ag^+ complex solution (figure 6.3). Although the Ag^+ in the BPEI-Ag^+ complex solution for LbL assembly would not be all assembled into the film (table 6.1), the increase in Ag^+ concentration in the complex solution would changes the chelation behavior with BPEI before assembled into the film and charge density of the complex for the incoming PAA interaction during the film assembly.[52] Ag^+ concentrations (chosen as 1 mmol/L, 3 mmol/L and 6 mmol/L) allow forming the stable complex with BPEI for weeks. When assembled into the film with PAA, both UV-Vis absorbance and fluorescent intensity of the films increase with the increase in Ag^+ concentration in BPEI-Ag^+ complex solution. Moreover, the ratio in relative intensity of emission at 515 nm to 615 nm increases when the Ag^+ concentration was 6 mmol/L in complex solution. The emission intensity at 615 nm kept close to BPEI-Ag^+/PAA film with Ag^+

concentration of 3 mmol/L, while the emission intensity at 515 nm continue increasing. UV-Vis spectrum was also observed at the increase in band at 600 nm when the Ag^+ concentration increases to 6 mmol/L. In this case, the dominate chelation mode in the BPEI-Ag^+/PAA film might change from one to another.

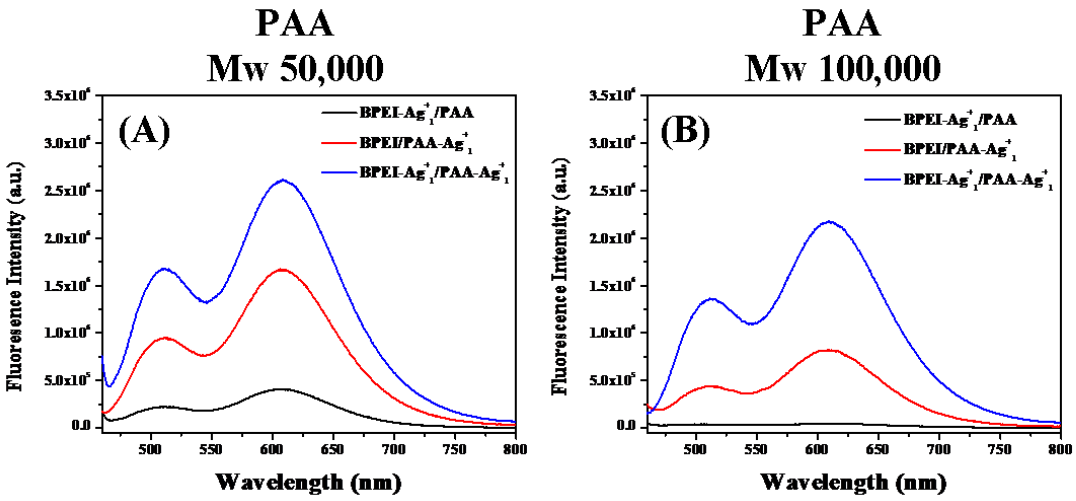

Figure 6.4. Fluorescence spectra of 30 bilayer (BPEI/PAA)-Ag^+ complex films—BPEI-Ag^+/PAA, BPEI/PAA-Ag^+, and BPEI-Ag^+/PAA-Ag^+ PEM with different molecular weight PAA as assemble solution. The emission spectra were obtained by excited at 450 nm. The concentration of BPEI and PAA were 40 mmol/L and 20 mmol/L with respect to the repeating group. The concentrations of Ag^+ in the BPEI-Ag^+ complex solution or PAA-Ag^+ complex solution were fixed as 1 mmol/L. The fluorescence intensity varies when change Ag^+ in BPEI and PAA solution and also varies with PAA in different molecular weight.

Fluorescence emission occurs not only when Ag^+ in the BPEI-Ag^+ complex and form the film assembled with PAA—BPEI-Ag^+/PAA film, but also when Ag^+ forms complex with PAA, such as BPEI-Ag^+/PAA, BPEI/PAA-Ag^+, and BPEI-Ag^+/PAA-Ag^+ films. Figure 6.4 shows the fluorescence spectra of (BPEI/PAA)-Ag^+ complex film. Here, Ag^+ in the complex solution was fixed as 1 mmol/L. The two emission bands in the fluorescence spectra kept the same when excited at 410 nm. However, the complexes (either BPEI-Ag^+ or PAA-Ag^+) results in the difference of the

amount of Ag^+ captured in the film (table 6.2) and the fluorescent intensity when performed as the assemble solution. Compared with ICP-MS results (table 6.2), we find out that the higher the amount of Ag^+ captured in the film, the higher the fluorescent intensity will be.

The amount of Ag^+ captured in the film was affected by the charge densities of the complex and the polyelectrolyte/complex pairs, the binding force with functional groups of polyelectrolytes when assembled as the film, the structures of complex. First, PAA has less capability to form complex with Ag^+ with higher concentration. The complex start precipitates at the early stage, like (Ag^+:carboxylic acid group of PAA=1 mmol: 20 mmol, at pH 4.5). However, BPEI can stay the stability longer to form complex with Ag^+. It can be stable at the stage (Ag^+: amine group of BPEI=3 mmol: 20 mmol, at pH 9.5). Even when the Ag^+ in the complex (with BPEI or PAA) is fixed as 1 mmol/L, the charge density, affinity to Ag^+ and complex structure will have the distinguishable difference for the Ag^+ chelated with BPEI and PAA. The existence of PAA-Ag^+ complex captures more Ag+ into the film and performs higher fluorescent intensity than BPEI-Ag^+ complex.

Table 6.2. Amount of Ag^+ was assembled in 30 bilayer (BPEI/PAA)-Ag^+ complex films—BPEI-Ag^+/PAA, BPEI/PAA-Ag^+, and BPEI-Ag^+/PAA-Ag^+ PEM with different molecular weight PAA as assemble solution. The concentration of BPEI and PAA were 40 mmol/L and 20 mmol/L with respect to the repeating group. The concentrations of Ag^+ in the BPEI-Ag^+ complex solution or PAA-Ag^+ complex solution were fixed as 1 mmol/L.

Polyelectrolyte-ion complex multilayer	Amount of Ag^+ ($x10^{-4}$, mmol/mm^3)
BPEI-Ag^+_1/PAA	3.8256
BPEI/PAA-Ag^+_1	6.4534
BPEI-Ag^+_1/PAA-Ag^+_1	13.2038
BPEI-Ag^+_1/PAA	1.8852
BPEI/PAA-Ag^+_1	5.7982
BPEI-Ag^+_1/PAA-Ag^+_1	6.9069

Moreover, the increase in molecular weight of PAA chain would also decrease the capture of Ag^+ into the film. Both the structure of PAA-Ag^+ complex changes in this case and causes this obvious decrease in both the fluorescent intensity and the amount of Ag^+ captured. Moreover, even Ag^+ only existed in BPEI-Ag^+ complex solution, BPEI-Ag^+/PAA film still shows the decrease in both the fluorescent intensity and the amount of Ag^+ captured. Here, PAA might wash off some of the Ag^+ from BPEI-Ag^+ complex in the next dipping sequence due to slightly difference of the way PAA chelated with Ag^+ and complex formation through molecular weight various.

6.3.2. Formaldehyde detection via Ag^+ reduction

Formaldehyde is widely used in the manufacture of many resins and construction materials.[28] However, formaldehyde is a toxic and allergenic chemical, and accumulates widely over cities. It has caused an increasing serious problem on human health and in 2004 the International Agency for Research on Cancer reclassified formaldehyde as a human carcinogen.[217] And the World Health Organization (WHO) has set a safe exposure limit of 0.08 ppm averaged over 30 min[218] and the established limit by Chinese Environmental Protection Agency (EPA) is 0.06 ppm (1h in average).[219] OSHA has set the permissible exposure limit (PEL) at 750 ppb and the immediately dangerous to life or health (IDLH) limit at 20 ppm.[220]

While there are numerous methods for detecting and measuring gaseous formaldehyde, there remains a need for an inexpensive, sensitive, and rapid analytical technology. Here, fluorescent (BPEI/PAA)-Ag^+ complex film can be an easy way for formaldehyde detection. Formaldehyde was known as the weak reducer for Ag^+ as the Tollen's reagent.[221,222] It can reduce Ag^+ to Ag nanoparticles with the existence of water.[34] The 30 bilayer BPEI-Ag^+/PAA film, which has the orange emission color (figure 6.2(E)) via UV irradiation and nearly transparent (figure 6.2(D)) under white light. Once met with vaporized formaldehyde from formaldehyde solution, the fluorescence of the film starts quenching (figure 6.5(B) and (D)) and show the brownish color

of the film (figure 6.5(A)), showing the formation of nanoparticles. The Ag nanoparticles were formed gradually with elongating the exposure time to formaldehyde vapor. Moreover, the formation of Ag nanoparticles did not increase the film thickness. In the same time, the formaldehyde reduction did not form the very small size particle, silver nanocluster, which shows the increase in the fluorescence in a certain wavelength.

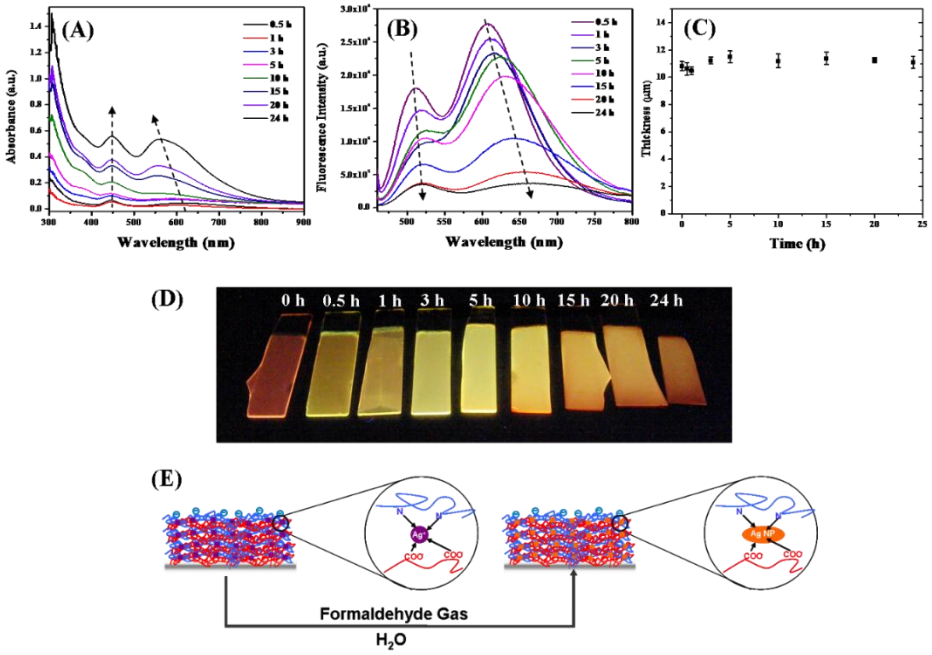

Figure 6.5. UV-Vis (A), fluorescence spectra (B) and thickness of 30 bilayer BPEI-Ag^{+}/PAA film with exposure to formaldehyde gas for different time. The excitation spectra were obtained with 450 nm. The concentration of BPEI and PAA were 40 mmol/L and 20 mmol/L with respect to the repeating group. The concentration of Ag^{+} in the BPEI-Ag^{+} complex solution was fixed as 3 mmol/L. The fluorescence intensity quenches with elongating the formaldehyde exposure time and the visible absorbance from 400 nm to 700 nm increase in the same time. These changes do not at the cost of the decrease in thickness. (D) Pictures show fluorescence emission color of PEM exposure to formaldehyde from 0 h (left) to 24 h (right) excited by 302 nm UV radiation. (E) The illustration shows the way formaldehyde gas interact with Ag^{+} in the PEM and reduce them to Ag nanoparticles (NP) in the existence of moisture.

6.3.3. Formation of Ag nanocluster via thermal reduction

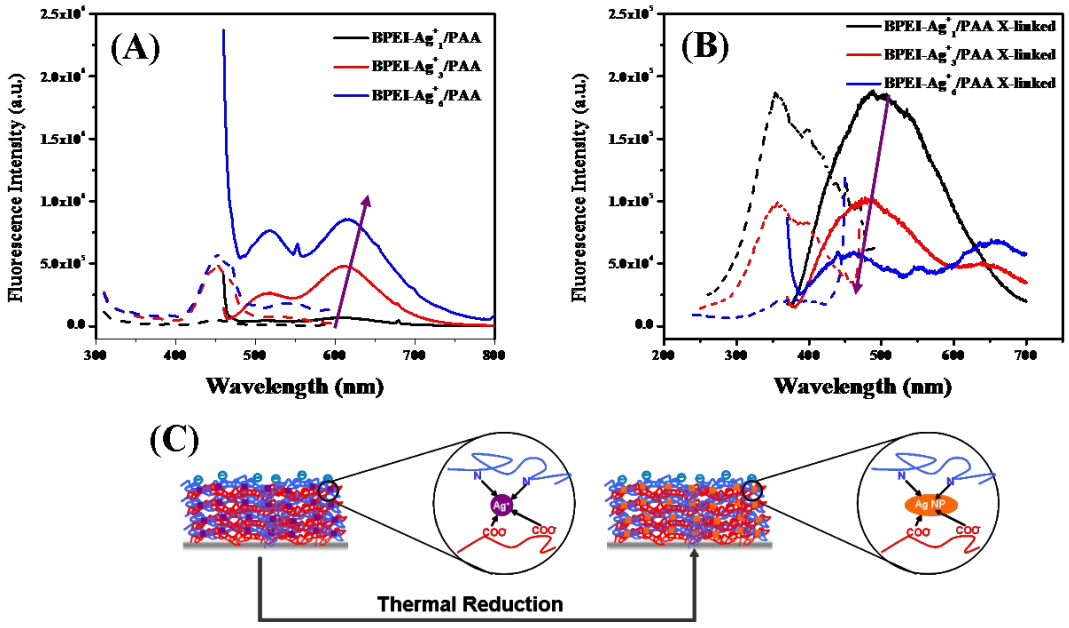

Figure 6.6. Fluorescence spectra of 10 bilayer BPEI-Ag^+/PAA PEM before (A) and after (B) heating at 200°C for 1 h. The dash line was the excitation spectra with fixed emission peak wavelength and solid line was the emission spectra with fixed excitation peak wavelength, respectively. The fluorescence intensity quenches after thermal treatment but emitting fluorescence at different wavelength. (C) The illustration shows the thermal reduction of Ag^+ to Ag nanoparticle in the film. The concentration of BPEI and PAA were 40 mmol/L and 20 mmol/L with respect to the repeating group. The concentration of Ag^+ in the BPEI-Ag^+ complex solution was fixed as 1 mmol/L, 3 mmol/L and 6 mmol/L.

Silver nanoclusters have been reported as a fluorescent probe for biological application to introduce luminescence.[101,223-225] Luo *et al*[102,103] have reported that Ag nanocluster capped by BPEI, which responds rapidly to pH fluctuations by both the color and fluorescence intensity. They also can be used to selective recognize halide ions (i.e. Cl^-, Br^-, and I^-) due to a strong fluorescence quenching. Ag nanocluster has also been reported in the polymer gels, such as poly(N-isopropylacrylamide-acrylic acid-2-hydroxyethyl acrylate) (poly(NIPAM-AA-HEA).[213] The

silver nanocluster was introduced through ion exchanged with Ag+ and photoreduction.[213] Zhu *et al*[212] reported the in-situ photoreduction of Ag nanocluster in the polyelectrolyte multilayer film. Here, LbL technique provides a simple way to distribute ion well dispersed in the matrix Based on nanoreactor chemistry, the Ag^+ can be capture into the PVPON/PAA film with a simple immersion.

In section 6.3.2, the formaldehyde was used as reducer to reduce the Ag^+ in the BPEI-Ag^+/PAA complex film to Ag nanoparticles. However, the size of Ag nanoparticles achieved in that way was not small enough to the size of nanocluster and increase in the fluorescent in a certain wavelength. Here, thermal reduction[115,173] was used to get another trial to obtain Ag nanoclusters. Compared with other reduction appoaches, thermal reduction gives the extra stability for the film. During the thermal reduction at 200^{o}C, polyelectrolyte-metal ion complex film was also crosslinked at the same time. The formation of Ag nanoparticles was visually observed from the change in color of film from transparent (before reduction) to the yellow-brownish (after reduction). The fluorescent emission, as shown in figure 6.6 was change from ~610 nm (before reduction) to ~470 nm (after reduction). Before thermal reduction, the fluorescence comes from the supramolecular interaction of Ag^+ and polyelectrolyte pairs. The higher the amount of Ag^+ in the film gives the higher fluorescent intensity (figure 6.6(A)). After thermal reduction, the fluorescent emission comes from Ag nanocluster. In this case, the higher the amount of Ag^+ in the film will not help to increase the fluorescent intensity at all. On the other hand, it decreases in the fluorescent intensity, as shown in figure 6.6(B). The Ag^+ might immigrate together to form larger particles during thermal reduction when the amount of Ag^+ was high enough to let Ag^+ close to each other in the film.

6.4. Summary

We have reported a (BPEI/PAA)-Ag^+ complex system with shows the fluorescence “turn-

on" phenomena. The complex film was prepared via LbL assembly by sequential dipping in the basin of polycation and polyanion complex solutions with Ag^+. The strong orange emission color was generated from the film with Ag^+, while the (BPEI/PAA) does not show any fluorescence. This fluorescent intensity can be tuned by Ag^+ concentration, molecular weight of polyelectrolyte, and LbL assembly sequence. Fluorescent film can be used as formaldehyde vapor detection via Ag^+ reduction. The fluorescent Ag nanocluster can also be obtained via simple thermal reduction of this fluorescent film.

CHAPTER VII

SILVER NANOPARTICLE AIDED SELF-HEALING OF POLYELECTROLYTE MULTILAYERS*

7.1. Introduction

The layer-by-layer (LbL) method for directing the complexation of oppositely charged polyelectrolytes has proven to be a powerful and versatile tool for creating thin films and coatings (called polyelectrolyte multilayers or PEMs) composed of a range of components including but not limited to polymers (such as nanoparticles, oligomers, surfactants, and various biomaterials).[12,13,56,226,227] These coatings have been proposed in use for a range of applications, but one of the remaining challenges for these materials when considering moving them from the laboratory to the real world is mechanical robustness.[13] This includes not only strength as represented by a high Young's modulus, but other factors as well such as toughness, cracking, adhesion to the underlying substrate, and resistance to wear.[13,228-231] A related property that deals with materials' use and lifespan is the ability to self-heal, or to somehow mitigate physical damage.[232]

A common way to improve the mechanical properties of polymer thin films is the inclusion of metal or inorganic nanoparticles.[227] Due to their small size, metal nanoparticles often have properties that are different from those of bulk metals. These novel properties may find application in areas such as photoelectronics, catalysis, magnetism, and sensing in addition to their mechanical benefits.[227] As well as metal nanoparticle containing films showing increased

*Part of the data reported in this chapter is reprinted with permission from "Silver nanoparticle aided self-healing of polyelectrolyte multilayers" by Xiayun Huang, Matthew J. Bolen, and Nicole S. Zacharia, 2014, *Physical Chemistry Chemical Physics*, 16, 10267-10273, http://pubs.rsc.org/en/content/articlehtml/2014/cp/c4cp00349g, Copyright 2014 by Royal Society of Chemistry.

mechanical behavior, PEMs containing metal ions have been shown to possess improved mechanical properties.[52] The addition of Cu^{2+} to BPEI/PAA PEMs has been shown to increase both the modulus and hardness and these changes in mechanical properties can be tuned with Cu^{2+} concentration, which in turn can be controlled by the specific assembly procedure.[52]

The work presented here looks at the self-healing ability of PEMs containing metal nanoparticles and ions. A range of self-healing strategies has been demonstrated including encapsulated healing agent (generally monomer) that bursts open upon mechanical damage or the use of various reversible bonding schemes.[55,232,233] In the case of incorporating healing agent there are some difficulties regarding the embedding of the agent (which sometimes must include catalyst) and keeping it from reacting before physical damage occurs, and then providing for sustained release once the damage does happen.[55,232,233] On the other hand reversible bonding schemes generally have some limitations and often need an external stimulus to operate such as light or heat.[55,233] To date, there are a few literature reports of self-healing within PEM systems, and generally the presence of water or high amounts of humidity is required for self-healing to occur. These reports of self-healing PEMs usually rely on the so-called exponentially growing PEM systems wherein the polymer chains are very mobile and some degree of unbound polyelectrolyte chains remain in the film.[54] In these systems the unbound material is able to laterally diffuse to the site of a scratch or other kind of damage and heal the film. Specifically, the branched polyethylenimine (BPEI)/poly(acrylic acid) (PAA) PEM system has been reported by Sun *et al* to have self–healing properties when submerged in water.[54] Shchukin *et al* report anti-corrosion coatings incorporating BPEI with other polyelectrolytes (PAA as well as sulfonated polystyrene) and found that one of the beneficial aspects of PEMs for anti-corrosion coatings is their ability to laterally diffuse and heal over cracks that might come to be formed in the coating.[234]

Here, we report on the influence of the addition of silver ions and particles of various sizes to the self-healing ability of BPEI/PAA. Thanks to the branched structure of BPEI, which contains primary, secondary and tertiary amino groups in a ratio of 1:2:1,[86] the polymer has the ability to form a complex with Ag^+ (or other metal) ions.[52] Water allows the PEMs to soften and flow, and we demonstrate that the presence of silver nanoparticles somehow enhances this effect.

7.2. Materials and methods

Branched polyethylenimine (BPEI, MW=25,000 g/mol) was obtained from Sigma-Aldrich and poly(acrylic acid) (PAA, MW=50,000 g/mol, 25 wt% solution) was purchased from Polysciences Inc. Sodium borohydride ($NaBH_4$) and silver nitrate ($AgNO_3$) were purchased from EMD and formaldehyde (35 wt% solution) were from Alfa Aesar. 4-(2-hydroxyethyl)-1-poperazineethanesulfonic acid (HEPES) was purchased from Amresco. De-ionized (DI) water with 18.2 MΩ • cm resistivity from a Milli-Q filtration system was used for all experiments. All materials were used as received without further purification.

Film thickness was measured using a stylus profilometer (KLA Tencor Instruments P6), and values reported represent an average of 5 different position of the film. Static water contact angle values were measured using a VCA Optima system (AST products Inc.) equipped with a video camera at room temperature with DI water (18.2 MΩ·cm) as a probe fluid (1.5 μL). PEM were stored in an environment with relative humidity of ~55% for over 24 h before the test. Each contact angle reported was the average value of 5 independent measurements in each case. An optical microscope (VHX-600, Keyence Co.) was used for *in-situ* observation of the films' self-healing properties with a long working distance and wide depth of field lens (VH-Z100). The 30 bilayer thick films grown on glass slides were cut into 1 cm×2.5 cm pieces and then scratched with a razor blade. The film was then submerged into 10 mL of DI water. The in-situ observation started from the time of immersion. Time lapse images of the films underneath water were also taken

every 10 min till the film healed or continued for as long as 60 min if healing was not complete. After the healing test the films were allowed to dry in the same 55% relative humidity atmosphere in which they had originally been stored for 5 hours and then photographed again. Transmission electron microscopy (TEM) images were taken using a FEI Tecnai G2 F20 microscope operated at 200 kV and the JEOL 1200 EX microscope operated at 100 kV. The free-standing films were dissolved in 1 mmol/L HNO_3 solution and cast drop onto 200 mesh carbon film supported copper grids (TED PELLA, Inc). After having completely dried, the specimens were stored in the desiccator for a few hours before observation and the TEM images were always taken within a few hours. FTIR spectra were obtained using an IR Prestige 21 system (Shimadzu Corp., Japan) and analyzed by IRsolution V.1.40 software. Films coated on silicon wafer were measured via attenuated total reflection (ATR) mode. To study the water uptake of the various films, each film was assembled on a glass slide and immersed in 140 mL of DI water for various times. Mass uptake was measured using an Excellence XS analytical balance (Mettler Toledo, Switzerland). The film was then immersed into 1 mol/L HCl for 30 min in order to decompose the film. The mass of water uptake of each of the polyelectrolyte films were calculated by subtracting out the mass of glass slide. The surface Young's modulus of the film was measured by Atomic Force Microscopy (Bruker Dimension Icon AFM, Germany) through Peak Force Quantitative Nanomechanical Property Mapping mode using silicone probe with a spring constant of 5 N/m. The modulus was obtained by fitting the force-displacement curve with the Hertzian model using data that was collected from ~10 different positions. All measurements were done at room temperature with the relative humidity of ~30%.

PEM were assembled on glass slides, silicon wafers, and polystyrene substrates. Before use, the glass slides and silicon wafers were treated in a freshly prepared piranha solution (mixture of H_2SO_4 (98%) and H_2O_2 (30%) with a volume ratio of v/v=7/3) at room temperature for 4 h and

then rinsed with DI water until neutralized. The polystyrene substrates were rinsed with ethanol and then DI water. All the substrates were dried by nitrogen steam before being used for layer-by-layer assembly. BPEI/PAA multilayer films were assembled using concentrations of 80 mmol/L BPEI and 60 mmol/L PAA with respect to the functional group (either amine groups or carboxylic acid groups). The pH of these solutions was adjusted with 1 mol/L NaOH or 1 mol/L HNO_3 solution to pH 9.5 for the BPEI solution and pH 4.5 for the PAA solution. All multilayer assembly was carried out at room temperature using a StratoSequence VI dipper (NanoStrata Inc.). The cleaned and dried substrates were first exposed to BPEI solution for 10 min followed by three separate DI water rinse baths. Then, the substrates are exposed to PAA solution for 10 min again followed by three DI water rinse baths. This cycle was repeated until desired bilayers were reached. The multilayer films were dried at room temperature (~25°C and relative humidity at ~55%) for 24 h before any testing. BPEI-Ag^+/PAA multilayer films were prepared using a stable complex of the polycation BPEI (concentration 80 mmol/L with respect to the functional group) and silver nitrate (concentration 1 mmol/L) and the negative polyanion PAA (60 mmol/L with respect to the repeating unit). The assembly pH and procedure were the same as for the BPEI/PAA multilayer films. BPEI-Ag NP/PAA multilayer films were fabricated by reducing the Ag^+ ions in the BPEI-Ag^+/PAA multilayer film using a 10 mmol/L $NaBH_4$ solution. BPEI-Ag^+/PAA multilayer films were immersed in $NaBH_4$ solutions for 30 min then followed by 1 min of water rinsing. The wet film was dried for 24 h before any tests. BPEI-Ag NC/PAA multilayer films were then prepared using silver nanoclusters (Ag NC) dispersion in BPEI solution (80 mmol/L with respect to the functional group) with the same concentration of negative polyanion PAA. The Ag NC was synthesized following the literature.[17] Typically, silver ions were sequestered in BPEI solution and reduced by formaldehyde. BPEI (0.094 g/mL, 100 μL) and HEPES (1 mmol/L, 50 μL) were first dissolved in DI water (95 μL) by stirring for 2 min. Then, $AgNO_3$ (100 mmol/L,

250 μL) was added and homogenized by stirring for another 2 min. Finally, formaldehyde (5 μL) was added under vigorous stirring. The resultant solution was heated at 70°C for 10 min, cooled at room temperature, and stored at 4°C for over 48 h before use. The assembly pH and procedure were the same as BPEI/PAA multilayer films.

7.3. Results and discussions

Polyelectrolyte multilayer films of BPEI and PAA as well as those containing Ag^+ ions, Ag nanoparticles (Ag NP), or Ag nanoclusters (Ag NC) were fabricated using typical layer-by-layer deposition procedures. Figure 7.1 shows the film thickness versus the number of deposition bilayers as well as images of the films showing different colors formed by the incorporation of different types of silver. The film thicknesses increase exponentially during the first 15 bilayers, following the "in and out" diffusion mechanism.[236] For films of this type one (or both) of the polyelectrolytes are able to not only to add on to the surface of the LbL film but to diffuse into the bulk of the film. Then during subsequent deposition steps this 'extra' polymer diffuses back out and complexes with material at the film's surface. In a manner consistent with the reported growth of BPEI/PAA PEMs,[54] the thickness values then switch to a linear growth regime forming films as thick as ~25 μm within 25 or 30 bilayers.

Thanks to its branched structure and the ratio of primary, secondary, and tertiary amine groups present,[86,237] BPEI can form a stable complex with most of the transition metal ions, such as Ag^+ and Cu^{2+},[52] over a wide range of ion concentrations. These stable complexes can then be used in polyelectrolyte assembly with negatively charged PAA.[52] The growth of BPEI-ion complex/PAA follows the trend of BPEI/PAA with exponential growth during the first 15 bilayers[238] and a very thickly depositing linear growth thereafter. The thickness of BPEI-Ag^+/PAA is slightly less than that of BPEI/PAA above 20 bilayers due to the increased crosslink density introduced by the silver ions and their interactions with both carboxylic acids and amine groups.

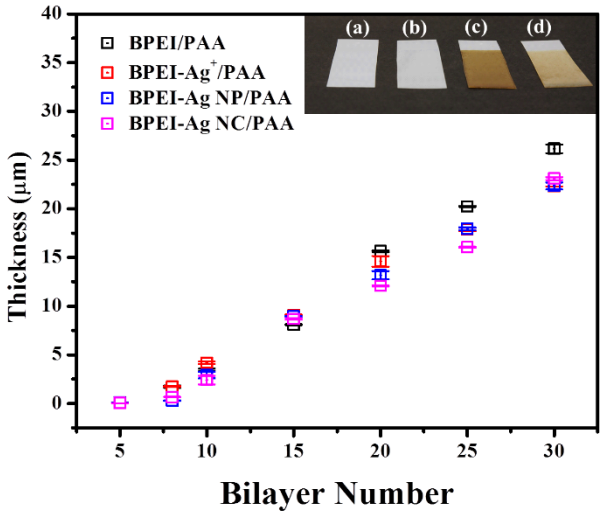

Figure 7.1. The growth curves of polyelectrolyte multilayer films. (a) BPEI/PAA, (b) BPEI-Ag^+/PAA, (c) BPEI-Ag NP/PAA and (d) BPEI-Ag NC/PAA. All PEMs follow the exponential growth initially and rapid linear growth afterwards. Insert pictures show the 30 bilayer PEMs deposited on the white polystyrene films.

Although the concentration of Ag^+ in the BPEI assembly solution is as low as 1 mmol/L, silver ion is incorporated into the BPEI-Ag^+/PAA films, which are transparent (figure 7.1). When the BPEI-Ag^+/PAA film was exposed to a reducing environment to form silver particles in situ by using a 10 mmol/L $NaBH_4$ aqueous solution, the transparent film will change to dark brown gradually over the course of 30 minutes due to the formation of Ag nanoparticles from the Ag^+ already embedded in the film.[237] The size of the Ag nanoparticles formed in the PEM though in situ reduction are around 55 nm, shown in figure 7.2. The creation of these Ag nanoparticles does not make any appreciable changes in film thickness.

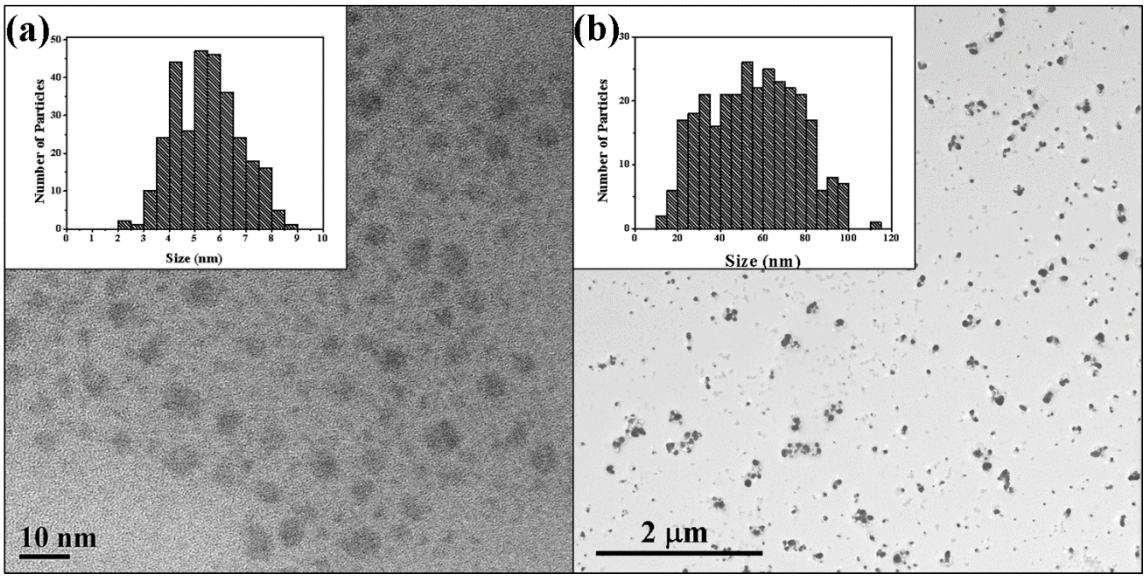

Figure 7.2. TEM images of (a) Ag nanoclusters and (b) Ag nanoparticles embedded in the PEMs. Insert images were the respective histogram of 300 silver particles measured in different area. The size of nanocluster was 5.5±1.3 nm, while that of nanoparticles was 54.8±21.1 nm.

In order to test the influence of particle size, in addition to the BPEI/PAA films with in situ reduced particles, another kind of particle containing PEM was fabricated. Ag nanoclusters approximately 5 nm in size (figure 7.2) and BPEI were mixed together and used as the positively charged polyelectrolyte for the multilayer assembly. The branched structure of BPEI allows for silver particles (5.4 mg/mL) to be partitioned into its structure,[235] forming a stable solution for weeks. Film assembly using the particle dispersion follows the same growth trend observed in the previously discussed cases and a film 20 μm in thickness is formed with 30 bilayers. Due to the small size of the silver clusters, the color of the Ag NC containing film was much lighter than the PEM with the in situ reduced particles.

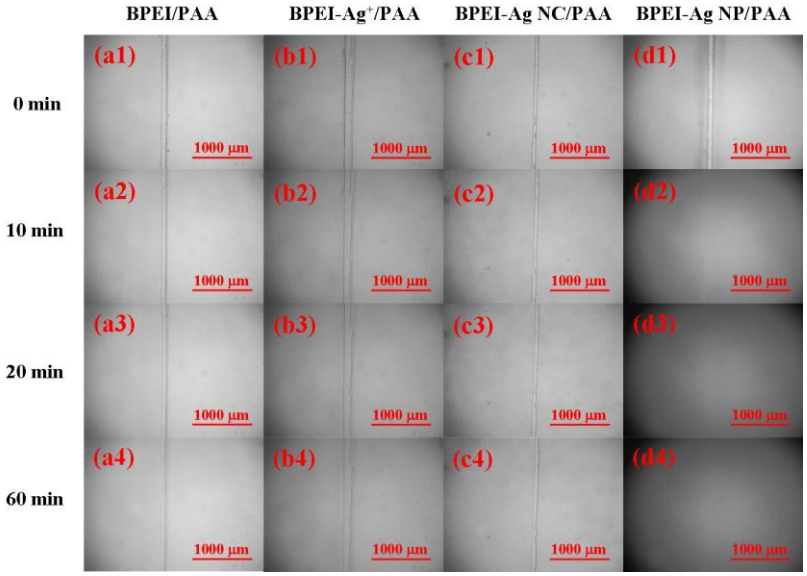

Figure 7.3. Time lapse optical micrographs of scratched films immersed in water for as long as 60 min. (a1-a4) 30 bilayers film of BPEI/PAA with a 89 µm scratch (b1-b4) BPEI-Ag^{+}/PAA film, scratch width 135 µm (c1-c4) BPEI-Ag NC/PAA film, scratch width 60 µm, and (d1-d4) BPEI-Ag NP/PAA film with a 76 µm wide scratch underneath water for 0 min, 10 min, 20 min and 60 min, respectively. The BPEI-Ag NP/PAA film can be completely healed after 10 min, however other films can not be healed even till 60 min immersed in the water.

The self-healing ability of the four different types of 30 bilayer films immersed in water was tested. Scratches were made by razor blade on dried films, completely scratching through the film to the substrate. For the samples depicted in figure 7.3, the scratch widths are 89 µm for the BPEI/PAA film, 135 µm for the BPEI-Ag^{+}/PAA film, 60 µm for the BPEI-Ag NC/PAA film, and 76 µm for the BPEI-Ag NP/PAA film. Figure 7.3 shows images of the scratch under water as time passes. The scratch on a BPEI-Ag NP/PAA film can be healed within 10 min, while none of the other films can be healed after even 60 min water immersion. However, in the cases when complete healing is not achieved the size of the scratch is slightly reduced over the course of 60 minutes. Figure 7.4 shows a set of scratched films before immersion in water (a1, b1, c1, d1) and after immersion for 10 minutes and then immediately being dried to capture the morphology present at that time (a2, b2, c2, d2). The scratches on these samples were made in the same way as for the

samples in figure 7.3. One can again see that the BPEI-Ag NP/PAA film was re-healed much faster than the other films. The scratch on the BPEI/PAA film is also noticeably smaller after 10 min of water immersion, but the same cannot be said for the other films. Elsewhere in the literature BPEI/PAA without any additives has been reported to have better self-healing properties than we report here, but these films were assembled with different pH conditions and using a higher molecular weight of BPEI. We believe that the assembly conditions are the dominant factor in determining self-healing as this dictates the amount of 'excess' polyelectrolyte present within the film, but the rheological properties of the system may also be influenced by molecular weight.

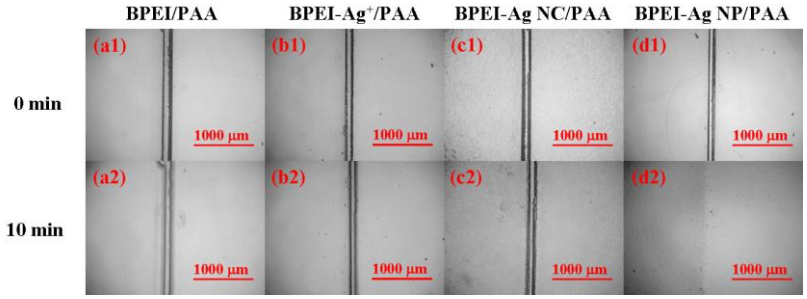

Figure 7.4. Optical microscope images of self-healed properties dried film before water immersion and after water immersion of 10 min. (a1-a2) 30 bilayers of dried BPEI/PAA film (b1-b2) BPEI-Ag^{+}/PAA film, (c1-c2) BPEI-Ag NC/PAA film, and (d1-d2) BPEI-Ag NP/PAA and dried film after 10 min water immersion, respectively.

This self-healing property under water seems to be related to the ability the PEM network to flow and perhaps its affinity to water. That is, perhaps systems that take up more water more quickly are also able to self-heal more quickly. For this reason, the relative hydrophobicity of these different systems was investigated.

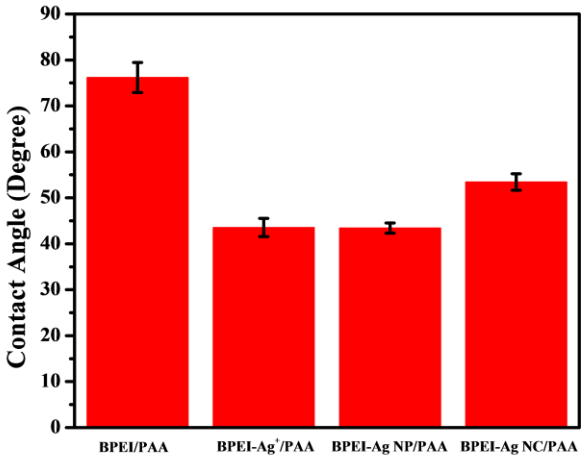

Figure 7.5. Static water contact angle of polyelectrolyte multilayer films. (a) BPEI/PAA, (b) BPEI-Ag^{+}/PAA, (c) BPEI-Ag NP/PAA and (d) BPEI-Ag NC/PAA. Water contact angle decreases from ~75° to ~45° from the introduction of Ag+ ion or Ag particles to the PEMs.

The water contact angle of the BPEI/PAA PEM (figure 7.5) without Ag ion or Ag particles is ~75°, which is higher than either reports of multilayer contact angles with either BPEI or PAA as the outermost layer[239-241] and also is higher than measured contact angles for monolayers and implies that the film surface is composed of more C-H polymer backbone than amine or carboxyl groups as compared to the monolayer case. This could be because the motion of these charged groups is hindered when they form the complex. The partition of polymer backbone to the surface results in a slightly higher water contact angle. However, the addition of silver decreases the contact angle sharply to about ~45°. The presence of Ag^{+} ion near the film surface increases affinity to water and the same low contact angle value is observed for PEMs with Ag nanoparticles and clusters, as shown in figure 7.5.

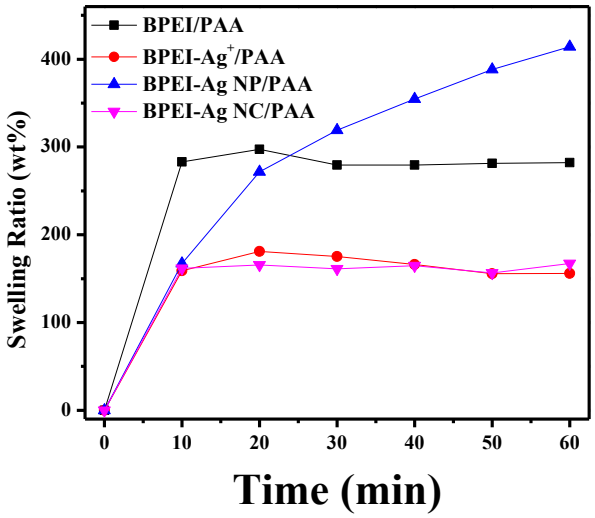

Figure 7.6. The swelling ratio of 30 bilayers polyelectrolyte multilayer films immersed in the water for different time periods. The water uptake behaviors of BPEI-Ag^+/PAA and BPEI-Ag NC/PAA were similar. However, these behaviors of BPEI/PAA and BPEI-Ag NP/PAA were quite different.

Water uptake for these systems was also measured. The results of this measurement follow a now familiar trend. All of these films do swell once immersed in the water, but they have quite different swelling ratios. Here the swelling ratio is defined as the fractional increase in the weight of the film due to water absorption. As shown in figure 7.6, both BPEI-Ag^+/PAA and BPEI-Ag NC/PAA films swell ~150 wt%. The swelling happens in the first 10 min and the water uptake reaches a plateau after this time. In comparison, the swelling ratio for BPEI/PAA film is ~300% which is the twice of both BPEI-Ag^+/PAA and BPEI-Ag NC/PAA films. This process is also saturated very quickly, during the first 10 min of exposure to water. Interestingly, the BPEI-Ag NP/PAA film took up water continuously to ~400%, a process that did not saturate within 60 min of water immersion. This large difference in water uptake behavior may point to the reason why the BPEI-Ag NP/PAA film was able to heal in the presence of water much faster than all other films. The BPEI/PAA film also swells much more than BPEI-Ag^+/PAA and BPEI-Ag NC/PAA

films and has the second greatest ability to self-heal after 10 min of water immersion shown in figure 7.3(a2).

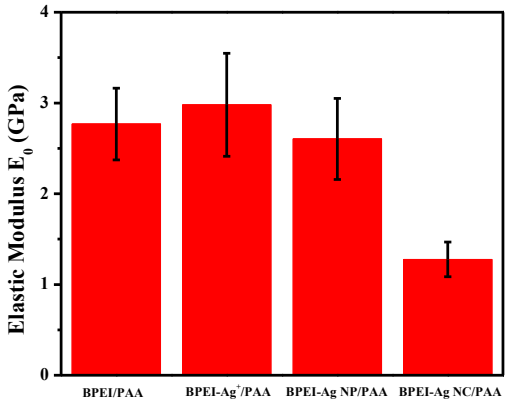

Figure 7.7. Surface Young's modulus E_0 determined by the AFM nanoindentation technique for 30 bilayers polyelectrolyte multilayer thin film (a) BPEI/PAA, (b) BPEI-Ag^+/PAA, (c) BPEI-Ag NP/PAA and (d) BPEI-Ag NC/PAA. The thicknesses of these films were ~25 μm.

Elastic modulus of this series of films was measured using AFM. The results can be seen in figure 7.7. Although Cu^{2+} ions have been shown to increase PEM modulus,[52] in the case of the addition of silver the modulus of BPEI/PAA, BPEI-Ag^+/PAA, and BPEI-Ag NP/PAA were all approximately the same (close to 3 GPa) within the error of the measurement. Interestingly, the BPEI-Ag NC/PAA film is somewhat softer at a little over 1 GPa. Multivalent ions have been shown to enhance mechanical properties because of their ability to act as crosslinkers. The monovalent silver does not act in this capacity.

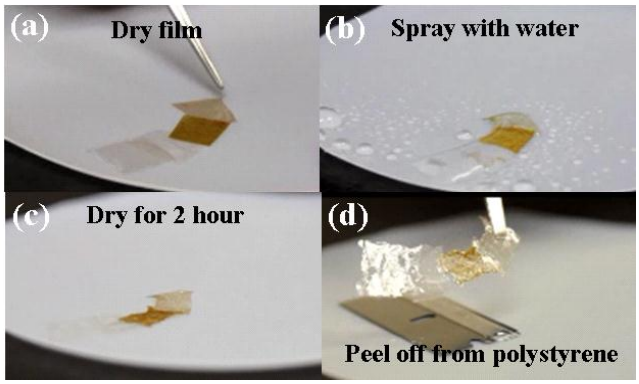

Figure 7.8. Illustration of self-healing properties of free standing polyelectrolyte film segments. (a) Dried films of BPEI/PAA, BPEI-Ag^{+}/PAA, BPEI-Ag NP/PAA and BPEI-Ag NC/PAA (from left to right) were placed on a polystyrene surface slightly overlapping. (b) The dried films were then sprayed with water. (c) The films become tacky and are able to reconfigure into one piece over the course of 2h while the water evaporates. (d) The resultant "healed" film which contains all of the original PEM segments is peeled off from the polystyrene substrate.

Although scratch healing was chosen as the demonstration of self-healing property of the polyelectrolyte thin film, this demonstration also depends on factors such as the thickness of the film, the width of scratches, and adhesion to the substrate. Adhesion to the substrate might in particular slow the lateral diffusion of polyelectrolyte chains, especially in very thin films. Inspired by demonstrations of self-healing hydrogels, four types of free-standing polyelectrolyte thin films were made with the same assembly procedure as previously and deposited on a polystyrene substrate instead of glass slide or silicon wafer. The films were cut into 1 cm × 1 cm pieces before being fully dried. In this way, once fully dried they can be easily peeled off from the polystyrene substrate due to the weak hydrophobic interactions between the film and the substrate. Due to the hydrophilicity of all of these films, they become tacky and hydrogel-like once they are rehydrated with water (here from a spray bottle). As in the case of healable hydrogels,[242] water acts as a plasticizer within the polyelectrolyte multilayers. This also allows for the interdiffusion of BPEI and PAA chains at the various film interfaces. Moreover, using water of neutral pH ensures some extent of degree of ionization of both amino and carboxyl groups of the BPEI and PAA and the

formation of new ionic bonds, ensuring a strong interface. Weakness at healed interfaces is often an issue in self-healed materials, and the ability to locally reform bonds may be an advantage of PEM systems.

7.4. Summary

We have demonstrated that polyelectrolyte multilayer systems made from BPEI/PAA have enhanced ability to self-heal in water with the addition of silver nanoparticles. Addition of silver ions alone or silver nanoclusters does not give this enhancement in property. We have also found that the assembly condition, that is the pH of the assembly solutions, seems to create differences in self-healing ability when comparing our work to literature reports. These differences in the pH create different charge densities along the polyelectrolyte backbones which then lead to different amounts of polymer diffusing in and out of the film. A film with more "reservoir" of polyelectrolyte or just more chain mobility will then have a greater ability to heal over a scratch.

The enhanced healing ability of the nanoparticle containing film does not seem to have to do with changes in mechanical properties as those films have about the same modulus as the multilayers with no additional silver. Instead, it seems that hydrophilicity and water uptake are more important factors in the film's ability to self-repair. These finds should enable us to better sign next generation polyelectrolyte based self-healing materials.

CHAPTER VIII

CONCLUSIONS AND FUTURE WORK

8.1. Thesis summary

In this thesis, layer-by-layer (LbL) assembly was utilized as a versatile bottom-up approach to build up functional thin film coatings. Functionalities of the film can be introduced by incorporating the film with surfactant, lubricant, transition metal ions, or nanoparticles, etc. The following is a brief summary of the research that has been presented in this thesis and the suggestions for the future work related to these researches.

In chapter III and IV, film wettability was focused on. We attempt to create a robust, scalable, and low-cost surface with a controllable wettability property. Chapter III introduced fluorinated surfactants into polyelectrolyte coatings via ion exchange or co-assembly to simply tune a greater range of wettability surface—from hydrophilicity to hydrophobicity. Generally, polyelectrolyte films made out of commercial water soluble polyelectrolytes are hydrophilic, which limit the range of application. Doping the film with surfactant at low concentration (i.e. 1mmol/L) can successfully achieve this wide range of surface wettability. Chapter IV introduced omniphobic and slippery coatings from lubricant-infused porous LbL film. It has been shown to have superior properties as a slippery material, with low contact angle hysteresis and low sliding angles. This can be easily achieved by imbibing a superhydrophobic coating with lubricant (in our case, a perfluorinated oligomer) and the porosity of the film not only textures the surface but also serves as the locker for lubricant onto the surface.

In Chapter V, VI and VII, a new type of film, polyelectrolyte-metal ion complex film, was presented. LbL assembly of stable complex solutions was the typical strategy to build this type of film, which works for various transition metal ions. The polyelectrolyte pair, branched

polyethylenimine and poly(acrylic acid), works the best when compared with other water soluble commercial polyelectrolytes. Chapter V chose Cu^{2+} as a model system to fundamentally study the assembly and disassembly of this blue color Cu^{2+}-containing polyelectrolyte film. It can be decomposed in response to various stimuli, such as pH, salt, and surfactant. In Chapter VI, Ag^{+} was chosen to assemble as the transparent film, which emitted strong orange color under UV irradiation. This fluorescent Ag^{+}-polyelectrolytes complex film could be used as formaldehyde vapor detector with fluorescence quenching. The reduced Ag^{+}-polyelectrolytes complex film introduces other properties, such as fluorescence due to the formation of nanoclusters, catalytic properties due to the size effect of noble metal, and mechanical properties due to embedding the metal nanoparticles into the thin film. Then, in Chapter VII, the mechanical properties, especially the self-healing property, were studied based on these different types of film—film without silver ion, film with silver ions, and film with silver nanoparticles of different sizes.

8.2. Suggestions for future research

One of the ultimate goals in the field of thin film coating is to create a robust, scalable, and low-cost coating, which at the same time has the multifunctionalities described earlier. However, in most cases, these characteristics can not be achieved easily in a single type of coating. Here, we propose looking at a wider range of functionalities besides the ones already extensively researched in the functional thin films as well as simplifying the coating application process.

LbL assembly is a simple way to build up coatings. However, commercial viability of the coatings are still limited by size and time frame when scaled up using the traditional dipping method, especially when modulating wettability and adding omniphobic slippery surfaces. ‘How can we make the procedure simple and fast?’ is always an important question for the researcher. The spray-assisted assembly will be a substitute way instead of traditional dipping. Moreover, it will save a lot of time and expense if the coating only needs to be sprayed one or a small amount

of times instead of multiple sequences. Janus particles, with hydrophilicity at one end and hydrophobicity at the other end, will be a good candidate for this spray coating. With the particle size being well controlled of the particles size, it is possible to build up a transparent coating. The particles themselves introduce the texture to the coating. At the same time, similar to the role of surfactant, hydrophilic/hydrophobic functionalized Janus particles allow them alignment via hydrophobic interaction when forming the thin film coating, with the hydrophobic side extended out when coated on the hydrophilic substrates. It will be interesting to extend the concept of 'surfactant' to this hydrophilic/hydrophobic functionalized Janus particle and to study the wettability modulation by different particle size, different shape of particle (tetrahedron, cubic, nanorod), different length and graft density of funcionalized molecules on Janus particles, etc.

For the omniphobic slippery coating, simplifying the process is also a big challenge for us. Ideally, we want a surface that can repel any fluid, self-heal upon damage, allow for smart/switchable control of wettability, and operate under a wide range of environmental conditions, such as extreme temperatures, high pressures, and harsh chemicals. At the same time, the procedure was expected to be simple, scalable, and low-cost. However, many of the surfaces face severe limitations to their practical applications: they show limited oleophobicity with high contact angle hysteresis; fail under severe conditions (high pressure, low/high temperature) and when physically damaged (cannot completely self-heal). Recently, we will focus on the study (not shown in this thesis) of the robustness of our omniphobic slippery coatings over low (anti-icing) and high temperature (steam resistance). Moreover, continuing with previous Janus particle idea, the hydrophilic/hydrophobic functionalized Janus particles will also a good substitute. For this case, a porous particle or porous shell hollow particles will be chosen to lock the lubricant infusion after spraying on the surface. Metal/semiconductor particles will be considered as another interesting candidate. For most of the application, the existence of metal/semiconductor particle

will helps the heating transfer from the substrate to throughout the coating which fastens the response time at a certain condition. More importantly, the existence of metal/semiconductor particle will help the directional assembly of Janus particles through electrical and magnetic field and in the same time bring in the extra functionalities, such as electrical, optical, catalytic, magnetic and mechanical properties. At this point, this project can be related to the fundamental studies of transition metal ion/polyelectrolytes complex and their correlated properties.

The existence of transition metal ion in the transition metal ion/polyelectrolytes complex film introduces a variety of functionalities to the film, such as electrical, optical catalytic, magnetic and mechanical properties. Fundamentally, the interaction between transition metal ions and polyelectrolytes is not well studied when they are aggregated. Only for a few polyelectrolyte systems, transition metal ions are stabilized when forming a complex and continue to be stable when built as a film. There is a special case with (BPEI/PAA)-Ag^+ complex film due to an orange emission color appearing when the complex film was formed. However, for other Ag^+-polyelectrolytes systems we have studied so far, none of these have fluorescent emission even though Ag^+ has been assembled into the film. It will be worthwhile to investigate the mechanism of this aggregation-induced emission compared with other Ag^+-polyelectrolytes systems.

Once Ag^+ in polyelectrolyte complex film was reduced to become Ag particles, it introduces into the coating or free-standing film of various optical, catalytic, and electrical properties. The ions can be reduced to nanoclusters via thermal reduction, which will have special optical (i.e. surface-enhanced raman spectroscopy, SERS), catalytic and electrical properties. Moreover, bimetallic particles (i.e. Ag-Au bimetallic particles) can be formed in the film based on combining the procedure of ion exchanging with other metal ions and reduction of the ion-embedded polyelectrolyte film. These bimetallic particles will provide a variety of possibilities to obtain interesting optical, catalytic and electrical properties.

Additional work will include polyelectrolyte complex film with other transition metal ions. Here, we aim at Fe^{2+}, Fe^{3+}, Ti^{4+} and Zn^{2+}. When oxidized, complex films with Fe^{2+} and Fe^{3+} are expected to gain an interesting magnetic property, while complex film with Ti^{4+} and Zn^{2+} are expect to obtain good optical and catalytic properties.

REFERENCES

(1) Decher, G.; Schlenoff, J. B. *Multilayer thin film: sequential assembly of nanocomposte materials*, 2nd Eds. Wiley-VCH: Weinheim, Germany, **2012**.

(2) Quinn, J. F.; Johnston, A. P. R.; Such, G. K.; Zelikin, A. N.; Caruso, F. "Next generation, sequentially assembled ultrathin films: beyond electrostatics". *Chem. Soc. Rev.* **2007**, *36*, 707-718.

(3) Kozlovskaya, V.; Kharlampieva, E.; Erel, I.; Sukhishvili, S. A. "Multilayer-derived, ultrathin, stimuli-responsive hydrogels". *Soft Matter* **2009**, *5*, 4077-4087.

(4) Kotov, N. A. "Layer-by-layer self-assembly: the contribution of hydrophobic interaction". *Nanostruct. Mater.* **1999**, *12*, 789-796.

(5) Mentbayeva, A.; Ospanova, A.; Tashmuhambetova, Z.; Sokolova, V.; Sukhishvili, S. "Polymer-metal complexes in polyelectrolyte multilayer films as catalysts for oxidation of toluene". *Langmuir* **2012**, *28*, 11948−11955.

(6) Ariga, K.; Hill, J. P.; Ji, Q. "Layer-by-layer assembly as a versatile bottom-up nanofabrication technique for exploratory research and realistic application". *Phys. Chem. Chem. Phys.* **2007**, *9*, 2319-2340.

(7) Farhat, T.; Yassin, G.; Dubas, S. T.; Schlenoff, J. B. "Water and ion pairing in polyelectrolyte multilayers". *Langmuir* **1999**, *15*, 6621-6623.

(8) Pergushov, D. V.; Muller, A. H. E.; Schacher, F. H. "Micellar interpolyelectrolyte complexes". *Chem. Soc. Rev.* **2012**, *41*, 6888-6901

(9) Wohl, B. M.; Engbersen, J. F. J. "Responsive layer-by-layer materials for drug delivery". *Journal of Controlled Release* **2012**, *158*, 2-14.

(10) Decher, G.; Hong, J. D.; Schmitt. J. "Buildup of ultrathin multilayer films by a self-assembly process: III. Consecutively alternating adsorption of anionic and cationic polyelectrolytes on charged surfaces". *Thin Solid Films* **1992**, *210-211*, 831-835.

(11) Sato, K.; Yoshida, K.; Takahashi, S.; Anzai, J. "pH- and sugar-sensitive layer-by-layer films and microcapsules for drug delivery". *Advanced Drug Delivery Reviews* **2011**, *63*, 809-821.

(12) Hammond, P. T. "Form and function in multilayer assembly: new applications at the nanoscale". *Adv. Mater.* **2004**, *16*, 1271-1293.

(13) Li, Y.; Wang, X.; Sun, J. "Layer-by-layer assembly for rapid fabrication of thick polymeric films". *Chem. Soc. Rev.* **2012**, *41*, 5998-6009.

(14) De Cock, L. J.; De Koker, S.; De Geest, B. G.; Grooten, J.; Vervaet, C.; Remon, J. P.; Sukhorukov, G. B.; Antipina, M. N. "Polymeric Multilayer Capsules in Drug Delivery". *Angewandte Chemie-International Edition* **2010**, *49*, 6954-6973.

(15) Schlenoff, J. B.; Dubas, S. T. "Mechanism of polyelectrolyte multilayer growth: charge overcompensation and distribution". *Macromolecules* **2001**, *34*, 592-598.

(16) Schlenoff, J. B.; Ly, H.; Li, M. "Charge and mass balance in polyelectrolyte multilayer". *J. Am. Chem. Soc.* **1998**, *120*, 7626-7634.

(17) Joanny, J. F. "Polyelectrolyte adsorption and charge inversion". *Eur. Phys. J. B* **1999**, *9*, 117-122.

(18) Netz, R. R.; Joanny, J. F. "Adsorption of semiflexible polyelectrolytes on charged planar surface: charge compensation, charge reversal, and multilayer formation". *Macromolecules* **1999**, 32, 9013-9025.

(19) Decher, G. "Fuzzy nanoassemblies: toward Layered Polymeric multicomposites". *Science* **1997**, *277*, 1232-1237.

(20) Kroschwitz, J. I. *Encyclopedia of polymer science and engineering, vol. 11: peroxy compounds to polyesters*, 2nd Eds, Wiley-Interscience, Germany, **1988**.

(21) Zelikin, A. N.; Davydova, O. V.; Akritskaya, N. I.; Kargov, S. I.; Izumrudov, V. A. J. "Conformation of polyelectrolyte chains in dilute aqueous solutions investigated by conductometry. 4. Influence of molecular mass and charge density of the chains on conformation of symmetrical aliphatic ionene bromides". *J. Phys. Chem. B* **2004**, *108*, 490-495.

(22) Davydova, O. V.; Zelikin, A. N.; Kargov, S. I.; Izumrudov, V. A. "Influence of charge density on the conformation of partly alkylated poly(N-ethyl-4-vinylpyridinium) cations and ionenes". *Macromol. Chem. Phys.* **2002**, *203*, 837-844.

(23) Limbach, H. J.; Holm, C. "End effects of strongly charged polyelectrolyte: a molecular dynamics study". *J. Chem. Phys*. **2001**, *114*, 9674-9682.

(24) Shew, C. Y.; Yethiraj, A. "The effect of acid-base equilibria on the fractional charge and conformational properties of polyelectrolyte solutions". *J. Chem. Phys.* **2001**, *114*, 2830-2838.

(25) Fleer, G. J.; Stuart, M. A. C.; Scheutjens, J. M. H. M.; Cosgrove, T.; Vincent, B. *Polymers at interfaces*, Wiley-VCH: New York, Germany, **1993**.

(26) Farhat, T. R.; Schlenoff, J. B. "Ion transport and equilibria in polyelectrolyte multilayers". *Langmuir* **2001**, *17*, 1184-1192.

(27) Dubas, S. T.; Schlenoff, J. B. "Swelling and smoothing of polyelectrolyte multilayers by salt". *Langmuir* **2001**, *17*, 7725-7727.

(28) Ecaterina S. D. *New trends in ionic copolymer and hybrids*, Nova Science Publisher, Inc., New York, **2007**.

(29) Krasemann, L.; Tieke, B. "Composite membranes with ultrathin separation layer prepared by self-assembly of polyelectrolytes". *Mat. Sci. Eng. C* **1999**, *8-9*, 513-518.

(30) Krasemann, L.; Tieke, B. "Selective ion transport across self-assembled alternating multilayers of cationic and anionic polyelectrolytes". *Langmuir* **2000**, *16*, 287-290.

(31) Toutianoush, A.; Tieke, B. "Selective transport and incorporation of highly charged metal and metal complex ions in self-assembled polyelectrolyte multilayer membranes". *Mat. Sci. Eng. C* **2002**, *22*, 135-139.

(32) Balachandra, A. M.; Dai, J. H.; Bruening, M. L. "Enhancing the anion-transport selectivity of multilayer polyelectrolyte membranes by templating with Cu^{2+}". *Macromolecules* **2002**, *35*, 3171-3178.

(33) Toutianoush, A.; Schnepf, J.; El Hashani, A.; Tieke, B. "Selective ion transport and complexation in layer-by-layer assemblies of *p*-sulfonato-calix[*n*]arenes and cationic polyelectrolytes". *Adv. Funct. Mater.* **2005**, *15*, 700-708.

(34) Tieke, B.; Toutianoush, A.; Jin, W. "Selective transport of ions and molecules across layer-by-layer assembled membranes of polyelectrolytes, *p*-sulfonato-calix[*n*]arenes and Prussian blue-type complex salts". *Adv. Colloid Interface Sci*. **2005**, *116*, 121-131.

(35) Yoo, D.; Shiratori, S. S.; Rubner, M. F. "Controlling bilayer composition and surface wettability of sequentially adsorbed multilayers of weak polyelectrolytes". *Macromolecules* **1998**, *31*, 4309-4318.

(36) Shiratori, S. S.; Rubner, M. F. "pH-dependent thickness behavior of sequentially adsorbed layers of weak polyelectrolytes". *Macromolecules* **2000**, *33*, 4213-4219.

(37) Chen, W.; McCarthy, T. J. "Layer-by-layer deposition: a tool for polymer surface modification". *Macromolecules* **1997**, *30*, 78-86.

(38) Choi, J.; Rubner, M. F. "Influence of the degree of ionization on weak polyelectrolyte multilayer assembly". *Macromolecules* **2005**, *38*, 116-124.

(39) Mendelsohn, J. D.; Barrett, C. J.; Chan, V. V.; Pal, A. J.; Mayes, A. M.; Rubner, M. F. "Fabrication of microporous thin films from polyelectrolyte multilayers". *Langmuir* **2000**, *16*, 5017-5023.

(40) Zhai, L.; Cebeci, F. C.; Cohen, R. E.; Rubner, M. F. "Stable superhydrophobic coatings from polyelectrolyte multilayers". *Nano Lett.* **2004**, *4*, 1349-1353.

(41) Lowman, G. M.; Tokuhisa, H.; Lutkenhaus, J. L.; Hammond. P. T. "Novel solid-sate polymer electrolyte consisting of a porous layer-by-layer polyelectrolyte thin film and oligoethylene glycol". *Langmuir* **2004**, *20*, 9791-9795.

(42) Huang, X.; Chrisman, J. D.; Zacharia, N. S. "Omniphobic slippery coatings based on lubricant infused porous polyelectrolyte multilayers". *ACS Macro Letters* **2013**, *2*, 826-829.

(43) Hiller, J.; Mendelsohn, J. D.; Rubner, M. F. "Reversible erasable nanoporous anti-reflection coatings from polyelectrolyte multilayers". *Nature Materials* **2002**, *1*, 59-63.

(44) Zhai, L.; Nolte, A. J.; Cohen, R. E.; Rubner, M. F. "pH-gated porosity transitions of polyelectrolyte multilayers in confined geometries and their application as tunable bragg reflectors". *Macromolecules* **2004**, *37*, 6113-6123.

(45) Hiller, J.; Rubner, M. F. "Reversible molecular memory and pH-switchable swelling transitions in polyelectrolyte multilayers". *Macromolecules* **2003**, *36*, 4078-4283.

(46) Sui, Z.; Schlenoff, J. B. "Phase separations in pH-responsive polyelectrolyte multilayers: charge extrusion versus charge expulsion". *Langmuir* **2004**, *20*, 6026-6031.

(47) Sui, Z.; Salloum, D.; Schlenoff, J. B. "Effect of molecular weight on the construction of polyelectrolyte multilayers: stripping versus sticking". *Langmuir* **2003**, *19*, 2491-2495.

(48) Lee, H.; Mensire, R.; Cohen, R. E.; Rubner, M. F. "Strategies for hydrogen bonding based layer-by-layer assembly of poly(vinyl alcohol) with weak polyacids". *Macromolecules* **2012**, *45*, 347-355.

(49) Lutkenhaus, J. L.; Hammond, P. T. “Electrochemically enabled polyelectrolyte multilayer devices: from fuel cells to sensors”. *Soft Matter* **2007**, *3*, 804-816.

(50) Wang, Y.; Angelatos, A. S.; Caruso, F. “Template synthesis of nanostructured materials via layer-by-layer assembly”. *Chem. Mater.* **2008**, *20*, 8480-858.

(51) Ariga, K.; Yamauchi, Y.; Rydzek, G.; Ji, Q.; Yonamine, Y.; Wu, K. C. W.; Hill, J. P. “Layer-by-layer nanoarchitectionics: invention, innovation, and evolution”. *Chem. Lett.* **2014**, *43*, 36-68.

(52) Huang, X.; Schubert, A. B.; Chrisman, J. D.; Zacharia, N. S. “Tunable disassembly of polyelectrolyte-Cu^{2+} layer-by-layer complex film”. *Langmuir* **2013**, *29*, 12959-12968.

(53) Dvoracek, C. M.; Sukhonosova, G.; Benedik, M. J.; Grunlan, J. C. “Antimicrobial behavior of polyelectrolyte-surfactant thin film assemblies”. *Langmuir* **2009**, *25*, 10322-10328.

(54) Wang, X.; Liu, F.; Zheng, X.; Sun, J. “Water-enabled self-healing of polyelectrolyte multilayer coatings”. *Angew. Chem. Int. Ed.* **2011**, *50*, 11378-11381.

(55) Shchukin, D. G.; Mohwald, H. “Self-repairing coatings containing active nanoreservoirs”. *Small* **2007**, 3, 926-943.

(56) Johal, M. S.; Chiarelli, P. A. “Polymer-surfactant complexation in polyelectrolyte multilayer assemblies”. *Soft Matter* **2007**, *3*, 34-46.

(57) Swarup, S.; Schoff, C. K. “A survey of surfactants in coating technology”. *Progress in Organic Coatings* **1993**, *23*, 1-22.

(58) Chiappisi, L.; Hoffmann, I.; Gradzielski, M. “Complexes of oppositely charged polyelectrolytes and surfactants-recent developments in the field of biologically derived polyelectrolytes”. *Soft Matter* **2013**, *9*, 3896-3909.

(59) Ober, C. K.; Wegner, G. “Polyelectrolyte-surfactant complexes in the solid state: facile building blocks for self-organizing materials”. *Adv. Mater.* **1997**, *9*, 17-31.

(60) Iturri Ramos, J. J.; Llarena, I.; Fernandez, L.; Moya, S. E.; Donath, E. "Controlled stripping of polyelectrolyte multilayers by quaternary ammonium surfactants". *Macromolecular Rapid Communications* **2009**, *30*, 1756-1761.

(61) Iturri Ramos, J. J.; Llarena, I.; Moya, S. E. "Selective removal of hybrid di-block polyelectrolyte multilayers by means of quaternary ammonium surfactants". *J. Mater. Sci.* **2010**, *45*, 4970-4976.

(62) Rahim, A.; Choi, W. S.; Lee, H. J.; Jeon, I. C. "Ionic surfactant-triggered renewal of the structures and properties of polyelectrolyte multilayer films". *Langmuir* **2010**, *26*, 4680-4686.

(63) Wang, Y.; Han, P.; Wu, G.; Xu, H.; Wang, Z.; Zhang, X. "Selectively erasable multilayer thin film by photoinduced disassembly". *Langmuir* **2010**, *26*, 9736-9741.

(64) Rahim, A.; Choi, W. S.; Lee, H. J.; Park, J. B.; Jeon, I. C. "Unusual growth of polyelectrolyte multilayers by introduction of a rugged multilayer template and their unique adsorption behaviors". *Polymer* **2011**, *52*, 3112-3117.

(65) Chen, W.; McCarthy, T. J. "Layer-by-layer deposition: A tool for polymer surface modification". *Macromolecules* **1997**, *30*, 78-86.

(66) El-Khouri R. J.; Johal, M. S. "Fine tuning the wetting behavior of polyelectrolyte films with sodium dodecyl sulfate". *Langmuir* **2003**, *19*, 4880-4883.

(67) Wang, L.; Lin, Y.; Su, Z. "Counterion exchange at the surface of polyelectrolyte multilayer film for wettability modulation". *Soft Matter* **2009**, *5*, 2072-2078.

(68) Wang, L.; Peng, B.; Su, Z. "Tunable wettability and rewritable wettability gradient from superhydrophilicity to super hydrophobicity". *Langmuir* **2010**, *26*, 12203-12208.

(69) Huang, X.; Zacharia, N. S. "Surfactant co-assembly and ion exchange to modulate polyelectrolyte multilayer wettability". *Soft Matter* **2013**, *9*, 7735-7742.

(70) Wong T. S.; Sun, T.; Feng, L.; Aizenberg, J. “Interfacial materials with special wettability”. *MRS Bulletin* **2013**, *30*, 366-371.

(71) Kota, A. K.; Choi, W.; Tuteja, A. “Superomniphobic surface: design and durability”. *MRS Bulletin* **2013**, *38*, 383-390.

(72) Daniel, D.; Mankin, M. N.; Belisle, R. A.; Wong, T. S.; Aizenberg, J. “Lubricant-infused micro/nano-structured surfaces with tunable dynamic omniphobicity at high temperature”. *Appl. Phys. Lett.* **2013**, *102*, 231603/4.

(73) Liu, M.; Wang, S.; Jiang, L. “Bioinspired multiscale surfaces with special wettability”. *MRS Bulletin* **2013**, *38*, 375-382.

(74) Liu, Y.; Chen, X.; Xin, J. H. “Can superhydrophobic surfaces repel hot water?” *J. Mater, Chem.* **2009**, *19*, 5602-5611.

(75) Feng, X.; Jiang, L. “Design and creation of superwetting/antiwetting surfaces”. *Adv. Mater.* **2006**, *18*, 3063-3078.

(76) Tuteja, A.; Choi, W.; Ma, M.; Mabry, J. M.; Mazzella, S. A.; Rutledge, G. C.; Mckinley, G. H.; Cohen, R. E. “Designing superoleophobic surfaces”. *Science* **2007**, *318*, 1618-1622.

(77) Wong, T. S.; Kang, S. H.; Tang, S. K. Y.; Smythe, E. J.; Hatton, B. D.; Crinthal, A.; Aizenberg, J. “Bioinspired self-repairing slippery surfaces with pressure-stable omniphobicity”. *Nature* **2011**, *477*, 443-447.

(78) Nosonovsky, M. “Slippery when wetted”. *Nature* **2011**, *477*, 412-413.

(79) Epstein, A. K.; Wong, T. S.; Belisle, R. A.; Boggs, E. M.; Aizenberg, J. “Liquid-infused structured surfaces with exceptional anti-biofouling performance”. *PNAS* **2012**, *109*, 13182-13187.

(80) Kim, P.; Wong, T. S.; Alvarenga, J.; Kreder, M. J.; Adorno-Martinez, W. E.; Aizenberg, J. "Liquid-infused nanostructured surfaces with extreme anti-ice and anti-frost performance". *ACS Nano* **2012**, *6*, 6569-6577.

(81) Anand, S.; Paxson, A. T.; Dhiman, R.; Smith, J. D.; Varanasi, K. K. "Enhanced condensation on lubricant-impregnated nanotextured surfaces". *ACS Nano* **2012**, *6*, 10122-10129.

(82) Yao, X.; Hu, Y.; Grinthal, A.; Wong, T. S.; Mahadevan, L.; Aizenberg, J. "Adaptive fluid-infused porous films with tunable tranparency and wettability". *Nature Materials* **2013**, *12*, 529-534.

(83) Wang, T. C.; Rubner, M. F.; Cohen, R. E. "Polyelectrolyte multilayer nanoreactors for preparing silver nanoparticle composites: controlling metal concentration and nanoparticle size". *Langmuir* **2002**, *18*, 3370-3375.

(84) Furia, T. E. *Chapter 6-Sequestrant in foods in CRC handbook of food additives*, 2nd Eds. CRC Press, **1972**.

(85) Shi, X.; Shen, M.; Mohwald, H. "Polyelectrolyte multilayer nanoreactors toward the synthesis of diverse nanostructured materials". *Prog. Polym. Sci*. **2004**, *29*, 987-1019.

(86) Shiro, K.; Kazuhisa, H.; Masazumi, T.; Takeo, S. "Chelating properties of linear and branched poly(ethylenimines)". *Macromolecules* **1987**, *20*, 1496-1500.

(87) Rivas, B. L.; Seguel, G. V.; Geckeler, K. E. "Synthesis and properties of transition metal complexes with branched poly(ethyleneimine)". *Die Angewandte Makromolekulare Chernie* **1996**, *238*, 1-10.

(88) Kurth, D. G.; Pitarch Lopez J.; Dong, W. F. "A new Co(II)-metalloviologen-based electrochromic material integrated in thin multilayer films". *Chem. Commum*. **2005**, *16*, 2119-2130.

(89) Xiong, H.; Cheng, M.; Zhou, Z.; Zhang, X.; Shen, J. "A new approach to the fabrication of a self-organizing film of heterostructured polymer/Cu_2S nanoparticles". *Adv. Mater.* **1998**, *10*, 529-532.

(90) Zhang, G.; Ruan, Z.; Ji, S.; Liu, Z. "Construction of metal-ligand coordination multilayers and their selective separation behavior". *Langmuir* **2010**, *26*, 4782-4791.

(91) Krass, H.; Papastavrou, G.; Kurth, D. G. "A polyelectrolyte bearing metal ion receptors and electrostatic functionality for layer-by-layer self-assembly". *Macromol. Symp.* **2004**, *210*, 311-319.

(92) Toutianoush A.; El-Hashani, A.; Schnepf, J.; Tieke, B. "Multilayer membranes of *p*-sulfonato-calix[8]arene and polyvinylamine and their use for selective enrichment of are earth metal ion". *Applied Surface Science* **2005**, *246*, 430-436.

(93) El-Hashani, A.; Toutianoush, A.; Tieke, B. "Layer-by-layer assembled membranes of protonated 18-azacrown-6 and polyvinylsulfate and their application for highly efficient anion separation". *J. Phys. Chem. B* **2007**, *111*, 8582-8590.

(94) El-Hashani, A.; Toutianoush, A.; Tieke, B. "Use of layer-by-layer assembled ultrathin membranes of dicopper-[18]azacrown-*N6* complex and polyvinylsulfate for water desalination under nanofiltration conditions". *Journal of Membrane Science* **2008**, *318*, 65-70.

(95) Shuetz, P.; Caruso, F. "Copper-assisted weak polyelectrolyte multilayer formation on microspheres and subsequent film crosslinking". *Adv. Funct. Mater.* **2003**, *13*, 929-937.

(96) Krogman, K. C.; Lyon, K. F., Hammond, P. T. "Metal ion reactive thin films using spray electrostatic LbL assembly". *J. Phys. Chem. B* **2008**, *112*, 14453-14460.

(97) Cao, M.; Wang, J.; Wang, Y. "Surface patterns induced by Cu^{2+} ions on BPEI/PAA layer-by-layer assembly". *Langmuir* **2007**, *23*, 3142-3149.

(98) Han, F. S.; Hiuchi, M.; Kurth, D. G. "Metallosupramolecular polyelectrolytes self-assembled from various pyridine ring-substituted bisterpyridines and metal ions: photophysical, electrochemical, and eletrochormic properties". *JACS* **2008**, *130*, 2073-2081.

(99) Ahn, H.; Kin, S. Y.; Kin, O.; Choi, I.; Lee, C. H.; Shim, J. H.; Park, M. J. "Blue-emitting self-assembled polymer electrolytes for fast, sensitive, label-free detection of Cu(II) ions in aqueous media". *ACS Nano* **2013**, *7*, 6162-6169.

(100) Cheng, Y. J.; Yang, S. H.; Hsu, C. S. "Synthesis of conjugated polymers for organic solar cell applications". *Chem. Rev.* **2009**, *109*, 5868-5923.

(101) Diez, I.; Ras, R. H. A. "Fluorescent silver nanocluster". *Nanoscale* **2011**, *3*, 1963-1970.

(102) Qu, F.; Li, N. B.; Luo, H. Q. "Highly sensitive fluorescent and colorimetric pH sensor based on polyethylenimine-capped silver nanoclusters". *Langmuir* **2013**, *29*, 1199-1205.

(103) Qu, F.; Li, N. B.; Luo, H. Q. "Transition from nanoparticles to nanocluster: microscopic and spectroscopic investigation of size-dependent physicochemical properties of polyamine-functionalized silver nanoclusters". *J. Phys. Chem. C* **2013**, *117*, 3548-3555.

(104) Qu, F.; Li, N. B.; Luo, H. Q. "Polyethyleneimine-templated Ag nanoclusters: a new fluorescent and colorimetric platform for sensitive and selective sensing halide ions and high disturbance-tolerant recognitions of iodide and bromide in coexistence with chloride under condition of high ionic strength". *Anal. Chem.* **2012**, *84*, 10373-10379.

(105) Huang, X.; Bolen, M. J.; Zacharia, N. S. "Silver nanoparticle aided self-healing of polyelectrolyte multilayers". *PCCP* **2014**, *under review*.

(106) Zhang, W.; Song, J.; Liao, W.; Guan, Y.; Zhang, Y.; Zhu, X. X. "*In situ* generation of fluorescent silver nanoclusters in layer-by-layer assembled films". *J. Mater. Chem. C* **2013**, *1*, 2036-2043.

(107) Zhang, J. F.; Zhou, Y.; Yoon, J.; Kim, J. S. "Recent progress in fluorescent and colorimetric chemisensors for detection of precious metal ion (silver, gold and platinum ions)". *Chem. Soc. Rev.* **2011**, *40*, 3416-3429.

(108) Dai, J.; Bruening, M. L. "Catalytic nanoparticles formed by reduction of metal ions in multilayered polyelectrolyte films". *Nano Lett.*, **2002**, *2*, 497-501.

(109) Bhattacharjee, S.; Dotzauer, D. M.; Bruening, M. L. "Selectivity as a function of nanoparticles size in the catalytic hydrogenation of unsaturated alcohols". *JACS* **2009**, *131*, 3601-3610.

(110) Kidambi, S.; Dai, J.; Bruening, M. L. "Selective hydrogenation by Pd nanoparticles embedded in polyelectrolyte multilayers". *JACS* **2004**, *126*, 2658-2659.

(111) Kidambi, S.; Bruening, M. L. "Multilayer polyelectrolyte films containing palladium nanoparticles: Synthesis, characterization and application in selective hydrogenation". *Chem. Mater.* **2005**, *17*, 301-307.

(112) Dotzauer, D. M.; Dai, J.; Sun, L.; Bruening, M. L. "Catalytic membranes prepared using layer-by-layer adsorption of polyelectrolyte/metal nanoparticles films in porous supports". *Nano Lett.*, **2006**, *6*, 2268-2272.

(113) Zhang, X.; Zan, X.; Su, Z. "Polyelectrolyte multilayer supported Pt nanoparticles as catalysts for methanol oxidation". *J. Mater. Chem*. **2011**, *21*, 17783-17789.

(114) Shang, L.; Jin, L. H.; Guo, S. J.; Zhai, J. F.; Dong, S. J. "A facile and controllable strategy to synthesize Au-Ag alloy nanoparticles within polyelectrolyte multilayer nanoreactors upon thermal reduction". *Langmuir* **2010**, *26*, 6713-6719.

(115) Rahim, M. A.; Nam, B.; Choi, W. S.; Lee, H. J.; Jeon, I. C. "Polyelectrolyte complex particle-based multifunctional freestanding films containing highly loaded bimetallic particles". *J. Mater. Chem.* **2011**, *21*, 11831-11837.

(116) Li, S. K.; Zhang, L.; Huang, F. Z.; Yu, X. R.; Xie, A. J.; Shen, Y. H.; Wang, Y. "$AuCl_4^-$ ions-assisted fabrication of bimetallic {poly(ethylenimine)-Ag/Au} multilayer polyelectrolyte film and application in electrocatalysis". *Thin Solid Films* **2011**, *519*, 5609-5615.

(117) Zhang, X.; Wang, H.; Su, Z. "Fabrication of Au@Ag core-shell nanoparticles using polyelectrolyte multilayers as nanoreactors". *Langmuir* **2012**, *28*, 15705-15712.

(118) Zhang, X.; Su, Z. "Polyelectrolyte-multilayer-supported Au@Ag core-shell nanoparticles with high catalytic activity". *Adv. Mater*. **2012**, *24*, 4574-4577.

(119) Jiang, H. L.; Xu, Q. "Recent progress in synergistic catalysis over heterometallic nanoparticles". *J. Mater. Chem*. **2011**, *21*, 13705-13725.

(120) Zhang, X.; Zhang, G.; Zhang, B.; Su, Z. "Synthesis of hollow Ag-Au bimetallic nanoparticles in polyelectrolyte multilayers". *Langmuir* **2013**, *29*, 6722-6727.

(121) Joly, S.; Kane, R.; Radzilowski, L.; Wang, T.; Wu, A.; Cohen, R. E.; Thomas, E. L.; Rubner, M. F. "Multilayer nanoreactors for metallic and semiconducting particles". *Langmuir*, **2000**, *16*, 1354-1359.

(122) Yang, S. Y.; Rubner, M. F. "Micropatterning of polymer thin films with pH-sensitive and cross-linkable hydrogen-bonded polyelectrolyte multilayers". *J. Am. Chem. Soc*. **2002**, *124*, 2100-2101.

(123) Harris, J. J.; DeRose, P. M.; Bruening, M. L. "Synthesis of passivating, nylon-like coatings through cross-linking of ultrathin polyelectrolyte films". *J. Am. Chem. Soc*. **1999**, *121*, 1978-1979.

(124) Kurita, K. "Controlled functionalization of the polysaccharide chitin". *Prog. Polym. Sci*. **2001**, *26*, 1921-1971.

(125) Podsiadlo, P.; Kaushik, A. K.; Arruda, E. M.; Waas, A. M.; Shim, B. S.; Xu, J.; Nandivada, H.; Pumplin, B. D.; Lahann, J.; Ramamoorthy, A.; Kotov, N. A. "Ultrastrong and stiff layered polymer nanocomposites". *Science* **2007**, *318*, 80-83.

(126) Tong, W.; Cao, C.; Mohwald, H. "Manipulating the properties of polyelectrolyte microcapsules by glutaraldehyde cross-linking". *Chem. Mater.* **2005**, *17*, 4610-4616.

(127) Niu, J.; Shi, F.; Liu, Z.; Wang, Z.; Zhang, X. "Reversible disulfide cross-linking in layer-by-layer films: preassembly enhanced loading and pH/reductant dually controllable release". *Langmuir*, **2007**, *23*, 6377-6384.

(128) Pergushov, D. V.; Muller, A. H. E.; Schacher, F. H. "Micellar interpolyelectrolyte complexes". *Chem. Soc. Rev.* **2012**, *41*, 6888-6901.

(129) Stuart, M. A. C.; Huck, W. T. S.; Genzer, J.; Muller, M.; Ober, C.; Stamm, M.; Sukhorukov, G. B.; Szleifer, I.; Tsukruk, V. V.; Urban, M.; Winnik, F.; Zauscher, S.; Luzinov, I.; Minko, S. "Emerging applications of stimuli-responsive polymer materials". *Nat. Mater.* **2010**, *9*, 101-113.

(130) Tuteja, A.; Choi, W.; Mckinley, G. H.; Cohen, R. E.; Rubner, M. F. "Design parameters for superhydrophobicity and superoleophobicity". *MRS Bulletin* **2008**, *33*, 752-758.

(131) Zhai, L.; Berg, M. C.; Cebeci, F. C.; Kim, Y.; Milwid, K. M.; Rubner, M. F.; Cohen, R. E. "Patterned superhydrophobic surfaces: towards a synthetic mimic of the namib desert beetle". *Nano Lett*. **2006**, *6*, 1213-1217.

(132) Johal, M. S.; Ozer, B. H.; Casson, J. L.; John, A.; Robinson, J. M.; Wang, H. L. "Coadsorption of sodium dodecyl sulfate and a polyanion onto poly(ethylenimine) in multilayer thin films". *Langmuir* **2004**, *20*, 2792-2796.

(133) Treger, J. S.; Ma, V. Y.; Gao, Y.; Wang, C. C.; Jeon, S.; Robinson, J. M.; Wang, H. L.; Johal, M. S. "Controlling layer thickness and photostability of water-soluble cationic poly(*p*-phenylenevinylene) in multilayer thin films by surfactant complexation". *Langmuir* **2008**, *24*, 13127-13131.

(134) Liu, X. K.; Zhou, L.; Geng, W.; Sun, J. Q. "Layer-by-layer-assembled multilayer films of polyelectrolyte-stabilized surfactant micelles for the incorporation of noncharged organic dyes". *Langmuir* **2008**, *24*, 12986-12989.

(135) Nolte, A. J.; Takane, N.; Hindman, E.; Gaynor, W.; Rubner, M. F.; Cohen, R. E. "Thin film thickness gradients and spatial patterning via salt etching of polyelectrolyte multilayers". *Macromolecules,* **2007**, *40*, 5479-5486.

(136) Tettey, K. E.; Yee, M. Q.; Lee, D. "Layer-by-layer assembly of charged particles in nonpolar media". *Langmuir,* **2010**, *26*, 9974-9980.

(137) Giesche, H. "Synthesis of monodispersed silica powders I: particle properties and reaction kinetics". *J. Eur. Ceram. Soc*. **1994**, *14*, 189-204.

(138) Clark, S. L.; Montague, M. F.; Hammond, P. T. "Ionic effects of sodium chloride on the template deposition of polyelectrolytes using layer-by-layer ionic assembly". *Macromolecules* **1997**, *30*, 7237-7244.

(139) Jin, C.; Yan, P.; Wang, C.; Xiao, J. X. "Effect of counterions on fluorinated surfactants". *Acta Chimica Sinica* **2005**, *63*, 279-282.

(140) Cassie, A. B. D. "Contact angles". *Discuss Faraday Soc.* **1948**, *3*, 11-16.

(141) Jarn, M.; Xu, Q.; Linden, M. "Wetting studies of hydrophilic-hydrophobic TiO_2@SiO_2 nanopatterns prepared by photocatalytic decomposition". *Langmuir* **2010**, *26*, 11330-11336.

(142) Cho, C.; Valverde, L.; Ozin, G. A.; Zacharia, N. S. "Reactive wet stamping for patterning of polyelectrolyte multilayers". *Langmuir* **2010**, *26*, 13637-13643.

(143) Katagiri, K.; Matsuda A.; Caruso, F. "Effect of UV-irradiation on polyelectrolyte multilayered films and hollow capsules prepared by layer-by-layer assembly". *Macromolecules* **2006**, *39*, 8067-8074.

(144) Simons, W. W. *The Sadtler Handbooks of Infrared Spectra*, Sadtler Research Laboratories, Philadelphia, **2004**.

(145) Quinn, J. F.; Yeo, J. C. C.; Caruso, F. "Layer-by-layer assembly of nanoblended thin films: poly(allylamine hydrochloride) and a binary mixture of a synthetic and natural polyelectrolyte". *Macromolecules* **2004**, *37*, 6537-6543.

(146) Wenzel, R. N. "Resistance of solid surfaces to wetting by water". *Ind. Eng. Chem.* **1936**, *28*, 988-994.

(147) Lehaf, A. M.; Hariri, H. H.; Schlenoff, J. B. "Homogeneity, Modulus, and viscoelasticity of polyelectrolyte multilayers by nanoindentation: refining the buildup mechanism". *Langmuir* **2012**, *28*, 6348-6355.

(148) Willner, I.; Eichen, Y.; Frank, A. J.; Fox, M. A. "Photoinduced electron-transfer processes using organized redox-functionalized bipyridinium-polyethylenimine-titania colloids and particulate assemblies". *J. Phys. Chem.* **1993**, *97*, 7264-7271.

(149) Hiller, J.; Mendelsohn, J. D.; Rubner, M. F. "Reversibly erasable nanoporous anti-reflection coating from polyelectrolyte multilayers". *Nature Materials* **2002**, *11*, 59-63.

(150) Zhai, L.; Cebeci, F. C.; Cohen, R. E.; Rubner, R. F. "Stable superhydrophobic coatings from polyelectrolyte multilayers". *Nano Letters* **2004**, *4*, 1349-1353.

(151) Zhai, L.; Berg, M. C.; Cebeci, F. C.; Kim, Y.; Milwid, J. M.; Rubner, M. F.; Cohen, R. E. "Patterned superhydrophobic surfaces: Toward a synthetic mimic of the namib desert beetle". *Nano Letters* **2006**, *6*, 1213-1217.

(152) Bravo, J.; Zhai, L.; Wu, Z.; Cohen, R. E.; Rubner, M. F. "Transparent superhydrophobic films based on silica nanoparticles". *Langmuir* **2007**, *23*, 7293-7298.

(153) Li, Y.; Li, L.; Sun, J. "Bioinspired self-healing superhydrophobic coatings". *Angew. Chem. Int. Ed.* **2010**, *49*, 6129-6133.

(154) Ma, W.; Higaki, Y.; Otsuka, H.; Takahara, A. "Perfluoropolyether-infused nano-texture: a versatile approach to omniphobic coatings with low hysteresis and high transparency". *Chem. Commun*. **2013**, *49*, 597-599.

(155) Kim, P.; Kreder, M. J.; Alvarenga, J.; Aizenberg, J. "Hierarchical or not? Effect of the length scale and hierarchy of the surface roughness on omniphobicity of lubricant-infused substrates". *Nano Letters* **2013**, *13*, 1793-1799.

(156) Howard, A. S. "Ice-phobic surfaces that are wet". *ACS Nano* **2012**, *6*, 6536-6540.

(157) Nishimoto, S.; Bhushan, B. "Bioinspired self-cleaning surfaces with superhydrophobicity, superoleophobicity, and superhydrophilicity". *RSC Adv*. **2013**, *3*, 671-690.

(158) Wilson, P. W.; Lu, W.; Xu, H.; Kim, P.; Kreder, M. J.; Alvarenga, J.; Aizenberg, J. "Inhibition of ice nucleation by slippery liquid-infused porous surface (SLIPS)". *Phys. Chem. Chem. Phys*. **2013**, *15*, 581-585.

(159) Quéré, D. "Wetting and roughness". *Annu. Rew. Mater. Res.* **2008**, *38*, 71-99.

(160) Bocquet, L.; Lauga, E. "A smooth future?" *Nature Material* **2011**, *10*, 334-337.

(161) Smith, J. D.; Dhiman, R.; Anand, S.; Reza-Garduno, E.; Cohen, R. E.; McKinley, G. H.; Varanasi, K. K. "Droplet mobility on lubricant-impregnated surfaces". *Soft Matter* **2013**, *9*, 1772-1780.

(162) Daniel, D.; Mankin, M. N.; Belisle, R. A.; Wong, T. S.; Aizenberg, J. "Lubricant-infused micro/nano-structured surfaces with tunable dynamic omniphobicity at high temperatures". *Applied Physics Letters* **2013**, *102*, 231603-1-4.

(163) Liu, Y.; Chen, X.; Xin, J. H. "Can superhydrophobic surfaces repel hot water?" *J. Mater. Chem.* **2009**, *19*, 5602-5611.

(164) Wang, Y.; Angelatos, A. S.; Caruso, F. "Template synthesis of nanostructured materials via layer-by-layer assembly". *Chem. Mater*. **2008**, *20*, 848-858.

(165) Mentbayeva, A.; Ospanova, A.; Tashmuhambetova, Z.; Sokolova, V.; Sukhishvili, S. "Polymer-metal complexes in polyelectrolyte multilayer films as catalysts for oxidation of toluene". *Langmuir* **2012**, *28*, 11948-11955.

(166) Sun, J. Y.; Zhao, X.; Illeperuma, W. R. K.; Chaudhuri, O.; Oh, K. H.; Mooney, D. J.; Vlassak, J. J.; Suo, Z. "Highly stretchable and tough hydrogels". *Nature* **2012**, *489*, 133-136.

(167) Kurth, D. G.; Pitarch Lopez, J.; Dong, W. F. "A new Co(II)-metalloviologen-based electrochromic material integrated in thin multilayer films". *Chem. Commun*. **2005**, *16*, 2119-2130.

(168) Zhang, G.; Ruan, Z.; Ji, S.; Liu, Z. "Construction of metal-ligand coordination multilayers and their selective separation behavior". *Langmuir* **2010**, *26*, 4782-4791.

(169) El-Hashani, A.; Toutianoush, A.; Tieke, B. "Use of layer-by-layer assembled ultrathin membranes of dicopper-[18]azacrown-*N6* complex and polyvinylsulfate for water desalination under nanofiltration conditions". *Journal of Membrane Science* **2008**, *318*, 65-70.

(170) Krogman, K. C.; Lyon, K. F.; Hammond, P. T. "Metal ion reactive thin films using spray electrostatic LbL assembly". *J. Phys. Chem. B* **2008**, *112*, 14453−14460.

(171) Furia, T. E. *Chapter 6-Sequestrant in Foods in CRC Handbook of Food Additives*, *2nd ed*. CRC Press, **1972**.

(172) Ungaro, F.; De Rosa, G.; Miro, A.; Quaglia, F. "Spectrophotometric determination of polyethylenimine in the presence of an oligonucleotide for the characterization of controlled release formulations". *Journal of Pharmaceutical and Biomedical Analysis* **2003**, *31*, 143-149.

(173) Rahim, A.; Islam, S.; Bae, T. S.; Choi, W. S.; Noh, Y. Y.; Lee, H. J. "Metal ion-enriched polyelectrolyte complexes and their utilization in multilayer assembly and catalytic nanocomposite films". *Langmuir* **2012**, *28*, 8486-8495.

(174) Suh, J.; Paik, H. J.; Hwang, B. K. "Ionization of poly(ethylenimine) and poly(allylamine) at various pH's". *Bioorganic Chemistry* **1994**, *22*, 318-327.

(175) Zacharia, N. S.; DeLongchamp, D. M.; Modestino, M.; Hammond, P. T. "Controlling diffusion and exchange in layer-by-layer assemblies". *Macromolecules* **2007**, *40*, 1598-1603.

(176) Zacharia, N. S.; Modestino, M.; Hammond, P. T. "Factor influencing the interdiffusion of weak polycations in multilayers". *Macromolecules* **2007**, *40*, 9523-9528.

(177) Pavoor, P. V.; Bellare, A.; Strom, A.; Yang, D.; Cohen, R. E. "Mechanical characterization of polyelectrolyte multilayers using quasi-static nanoindentation". *Macromolecules* **2004**, *37*, 4865-4871.

(178) Nolte, A. J.; Rubner, M. F.; Cohen, R. E. "Determining the young's modulus of polyelectrolyte multilayer films via stress-induced mechanical buckling instabilities". *Macromolecules* **2005**, *38*, 5367-5370.

(179) Nolte, A. J.; Cohen, R. E.; Rubner, M. F. "A two plate buckling technique for thin film modulus measurement: applications to polyelectrolyte multilayers". *Macromolecules* **2006**, *39*, 4841-4847.

(180) Ito, H.; Inouhe, M.; Tohoyama, H.; Joho, M. "Characteristics of copper tolerance in *Yarrowia lipolytica*". *BioMetals* **2007**, *20*, 773-780.

(181) Smarrelli, J.; Campbell, W. H. "Heavy metal inactivation and chelators stimulation of higher plant nitrate reductase". *Biochim Biophys Acta* **1983**, *742*, 435-445.

(182) Shi, X.; Stoj, C.; Romeo, A.; Kosman, D. J.; Zhu, Z. "Fre1p Cu^{2+} reduction and Fet3p Cu^{1+} oxidation modulate copper toxicity in *Saccharomyces cerevisiae*". *J. Biol. Chem.* **2003**, *278*, 50309-50315.

(183) Melo, R. G.; Leitáo, A. C.; Pádula, M. "Role of OGG1 and NTG2 in the repair of oxidative DNA damage and mutagenesis induced by hydrogen peroxide in *Saccharomyces cerevisiae*: relationship with transition metals iron and copper". *Yeast* **2004**, *21*, 991-1003.

(184) Shanmuganathan, A.; Avery, S. V.; Willetts, S. A.; Houghton, J. E. "Copper-induced oxidative stress in *Saccharomyces cerevisiae* targets enzymes of the glycolytic pathway". *FEBS Lett*. **2004**, *556*, 253-262.

(185) Soares, E. V.; Hebbelinck, K.; Soares, H. M. "Toxic effect caused by heavy metals in the yeast *Saccharomyces cerevisiae*: a comparative study". *Can. J. Microbiol.* **2003**, *49*, 336-343.

(186) Lynn, D. M. "Peeling back the layers: controlled erosion and triggered disassembly of multilayered polyelectrolyte thin films". *Adv. Mater.* **2007**, *19*, 4118-4130.

(187) Johnston, A.P.R.; Cortez, C.; Angelatos, A. S.; Caruso, F. "Layer-by-layer engineered capsules and their applications". *Current Opinion in Colloid & Interface Science* **2006**, *11*, 203-209.

(188) de Villiers, M. M.; Otto, D. P.; Strydom, S. J.; Lvov, Y. M. "Introduction to nanocoatings produced by layer-by-layer (LbL) self-assembly". *Advanced Drug Delivery Reviews* **2011**, *63*, 701-715.

(189) Hammond, P. T. "Building biomedical materials layer-by-layer". *Materials today* **2012**, *15*, 196-206.

(190) Fery, A.; Schöler, B.; Cassagneau, T.; Caruso, F. "Nanoporous thin films formed by salt-induced structural changes in multilayers of poly(acrylic acid) and poly(allylamine)". *Langmuir* **2001**, *17*, 3779-3783.

(191) Lowman, G. M.; Tokuhisa, H.; Lutkenhaus, J. L.; Hammond, P. T. "Novel solid-state polymer electrolyte consisting of a porous layer-by-layer polyelectrolyte thin film and oligoethylene glycol". *Langmuir* **2004**, *20*, 9791-9796.

(192) Lutkenhaus, J. L.; McEnnis, K.; Hammond, P. T. "Nano- and microporous layer-by-layer assemblies containing linear poly(ethylenimine) and poly(acrylic acid)". *Macromolecules* **2008**, *41*, 6047-6054.

(193) Fu, Y.; Bai, S.; Cui, S.; Qiu, D., Wang, Z.; Zhang, X. "Hydrogen-bonding-directed layer-by-layer multilayer assembly: reconformation yielding microporous films". *Macromolecules* **2002**, *35*, 9451-9458.

(194) Zhang, H.; Fu, Y.; Wang, D.; Wang, L.; Wang, Z.; Zhang X. "Hydrogen-bonding-directed layer-by-layer assembly of dendrimer and poly(4-vinylpyridine) and micropore formation by post-base treatment". *Langmuir* **2003**, *19*, 8497-8502.

(195) Bai, S.; Wang, Z.; Zhang, X. "Hydrogen-bonding-directed layer-by-layer films: effect of electrostatic interaction on the microporous morphology variation". *Langmuir* **2004**, *20*, 11828-11832.

(196) Cho, C.; Zacharia, N. S. "Film stability during postassembly morphological changes in polyelectrolyte multilayers due to acid and base exposure". *Langmuir* **2012**, *28*, 841-848.

(197) Notle, A. J.; Takane, N.; Hindman, E.; Gaynor, W.; Rubner, M. F.; Cohen, R. E. "Thin film thickness gradients and spatial patterning via salt etching of polyelectrolyte multilayers". *Macromolecules* **2007**, *40*, 5479-5486.

(198) Dubas, S. T; Schlenoff, J. B. "Factors controlling the growth of polyelectrolyte multilayers". *Macromolecules* **1999**, *32*, 8153-8160.

(199) Dubas, S. T.; Schlenoff, J. B. "Polyelectrolyte multilayers containing a weak polyacid: construction and deconstruction". *Macromolecules* **2001**, 34, 3736-3740.

(200) Jenkins, H. D. B, Marcus, Y. "Viscosity *B*-coefficients of ions in solution". *Chem. Rev.* **1995**, *95*, 2695-2724.

(201) Andrew, S.; Swager, T. M. "Anthryl-doped conjugated polyelectrolytes as aggregation-based sensors for nonquenching multicationic analytes". *JACS* **2007**, *129*, 16020-16028.

(202) Lv, J.; Ouyang, C.; Yin, X.; Zheng, H.; Zuo, Z.; Xu, J.; Liu, H.; Li, Y. "Reversible and highly sensitive fluorescent sensor for mercury(II) based on a water-soluble poly(*para*-phenylene)s containing thymine and sulfonate boieties". *Macromol. Rapid Commun.* **2008**, *29*, 1588-1592.

(203) Jaeger, W.; Bohrisch, J.; Laschewsky, A. "Synthetic polymers with quaternary nitrogen atoms: synthesis and structure of the most used type of cationic polyelectrolytes". *Prog. Polym. Sci.* **2010**, *35*, 511-577.

(204) Hong, Y.; Lam, J. W. Y.; Tang B. Z. "Aggregation-induced emission". *Chem. Soc. Rev.* **2011**, *40*, 5361-5388.

(205) Seo, J.; Chung, J. W.; Cho, I.; Park, S. Y. "Concurrent supramolecular gelation and fluorescence turn-on triggered by coordination of silver ion". *Soft Matter* **2012**, *8*, 7617-7622.

(206) Li, H.; Zhu, Y.; Zhang, J.; Chi, Z.; Chen, L.; Su, C. Y. "Luminescent metal-organic gels with tetraphenylethylene moieties: porosity and aggregation-induced emission". *RSC Advances* **2013**, *3*, 16340-16344.

(207) Zhao, Z.; Lam, J. W. Y.; Tang, B. Z. "Self-assembly of organic luminophores with gelation-enhanced emission characteristics". *Soft Matter* **2013**, *9*, 4564-4679.

(208) Liu, L.; Zhang, G.; Xiang, J.; Zhang, D.; Zhu, D. "Fluorescence "turn on" chemosensors for Ag^{+} and Hg^{2+} based on tetraphenylethylene motif featuring adenine and thymine moieties". *Organic Letters* **2008**, *10*, 4581-4584.

(209) Liu, L.; Zhang, D.; Zhang, G.; Xiang, J.; Zhu, D. "Highly slective ratiometric fluorescence dtermination of Ag^{+} based on a molecular motif with one pyrene and two adenine moieties". *Organic Letters* **2008**, *10*, 2271-2274.

(210) Dai, J.; Bruening, M. L. "Catalytic nanoparticles formed by reduction of metal ions in multilayered polyelectrolyte films". *Nano Lett.* **2002**, *2*, 497-501.

(211) Shang, L.; Dong, S. "Facile preparation of water-soluble fluorescent silver nanoclusters using a polyelectrolyte template". *Chem. Commum.* **2008**, *9*, 1088-1090.

(212) Zhang, W.; Song, J.; Liao, W.; Guan, Y.; Zhang Y.; Zhu, X. X. "*In situ* generation of fluorescent silver nanoclusters in layer-by-layer assembled film". *J. Mater, Chem. C* **2013**, *1*, 2036-2043.

(213) Zhang, J. Xu, S. Kumacheva, E. "Photogeneration of Fluorescent silver nanocluster in polymer microgels". *Adv. Mater.* **2005**, *17*, 2336-2340.

(214) Shao, C.; Yuan, B.; Wang, H.; Zhou, Q.; Li, Y.; Guan, Y.; Deng, Z. "Eggshell membrane as a multimodal solid state platform for generating fluorescent metal nanoclusters". *J. Mater. Chem.* **2011**, *21*, 2863-2866.

(215) Huang, X.; Bolen, M. J.; Zacharia, N. S. "Silver nanoparticle aided self-healing of polyelelctrolyte multilayers". *Physical Chemistry Chemical Physics* **2014**, *16*, 10267-10273.

(216) Leikauf, G. D. *In environmental toxicants: human exposures and their health effects*, 3rd ed.; Lippmann, M., Ed.; Wiley: Hoboken, NJ, **2009**, 257-316.

(217) Achmann, S.; Hammerle, M.; Moos, R. "Amperometric enzyme-based biosensor for direct detection of formaldehyde in the gas phase: dependence on electrolyte composition". *Electroanalysis* **2008**, *20*, 410-417.

(218) *WHO air quality guidelines for Europe*, 2nd ed.; World Health Organization: Copenhagen, **2000**.

(219) GB/T 18883-2002 *Indoor air quality standard by Chinese environmental protection agency (EPA)*. **2002**.

(220) Armour, S. J. *International task force 40: toxic industrial chemicals (TICs)—operational and medical concerns*. U.S. Government Printing Office: Washington, DC. **2001**.

(221) Zhou, Y.; Li, M.; Su, B.; Lu, Q. "Superhydrophobic surface created by the silver mirror reaction and its drag-reduction effect on water". *J. Mater. Chem*. **2009**, *19*, 3301-3306.

(222) Chou, K. S.; Lu, Y. C.; Lee, H. H. "Effect of alkaline ion on the mechanism and kinetics of chemical reduction of silver". *Materials Chemistry and Physics* **2005**, *94*, 429-433.

(223) Vosch, T. Antoku, Y. Hsiang, J. C. Richards, C. I., Gonzalez, J. I., Dickson, R. M. "Strongly emissive individual DNA-encapsulated Ag nanoclusters as single-molecule fluorophores". *PNAS* **2007**, *104*, 12616-12621.

(224) de Souza, N. "All that glitters that does not blink". *Nature Methods* **2007**, *4*, 540.

(225) Lin, C. A. J.; Lee, C. H.; Hsieh, J. T.; Wang, H. H.; Li, J. K.; Shen, J. L.; Chan, W. H.; Yeh, H. I.; Chang, W. H. "Synthesis of fluorescent metallic nanoclusters toward biomedical application: recent progress and present challenges". *J. Med. Biol. Eng.* **2009**, *29*, 276-283.

(226) Lavalle, P.; Voegel, J. C.; Vautier, D.; Senger, B.; Schaaf, P.; Ball, V. "Dynamic aspects of films prepared by a sequential deposition of species: perspectives for smart and responsive materials". *Adv. Mater.* **2011**, *23*, 1191-1221.

(227) Srivastava, S.; Kotov, N. A. "Composite Layer-by-Layer (LbL) assembly with inorganic nanoparticles and nanowires". *Accounts of Chemical Research* **2008**, *41*, 1831-1841.

(228) Tang, Z.; Kotov, N. A.; Magonov, S.; Ozturk, B. "Novel approaches to polymer blends based on polymer nanoparticles". *Nature Materials* **2003**, *2*, 413-418.

(229) Podsiadlo, P.; Kaushik, A. K.; Arruda, E. M.; Waas, A. M.; Shim, B. S.; Xu, J.; Nandivada, H.; Pumplin, B. G.; Lahann, J.; Ramamoorthy, A.; Kotov, N. A. "Ultrastrong and stiff layered polymer nanocomposites". *Science* **2007**, *318*, 80-83.

(230) Podsiadlo, P.; Michel, M.; Lee, J.; Verploegen, E.; Kam, N. W. S.; Ball, V.; Lee, J.; Qi, Y.; Hart, A. J.; Hammond P. T.; Kotov, N. A. "Exponential growth of LBL films with incorporated inorganic sheets". *Nano Letters* **2008**, *8*, 1762-1770.

(231) Liu, X.; Zhou, L.; Liu, F.; Ji, M.; Tang, W.; Pang, M.; Sun, J. "Exponential growth of layer-by-layer assembled coatings with well-dispersed ultrafine nanofillers: a facile route to scratch-resistant and transparent hybrid coatings". *J. Mater. Chem.* **2010**, *20*, 7721-7727.

(232) Blaiszik, B.J.; Kramer, S. L. B.; Olugebefola, S. C.; Moore, J. S.; Sottos, N. R.; White, S. R. "Self-healing polymers and composites". *Annu. Rev. Mater. Res.* **2010**, *40*, 179-211.

(233) Shchukin, D. G. "Container-based multifunctional self-healing polymer coatings". *Polym. Chem.* **2013**, *4*, 4871-4877.

(234) Andreeva, D. V.; Skorb, E. V.; Shchukin, D. G. "Layer-by-layer polyelectrolyte/inhibitor nanostructures for metal corrosion protection". *ACS Applied Materials & Interfaces* **2010**, *2*, 1954-1962

(235) Qu, F.; Li, N. B.; Luo, H. Q. "Transition from nanoparticles to nanoclusters: microscopic and spectroscopic investigation of size-dependent physicochemical properties of polyamine-functionalized silver nanoclusters". *J. Phys. Chem. C* **2013**, *117*, 3548-3555.

(236) Fu, J.; Ji, J.; Shen, L.; Küller, A.; Rosenhahn, A.; Shen, J.; Grunze, M. "pH-amplified exponential growth multilayers: a facile method to develop hierarchical micro- and nanostructured surfaces". *Langmuir* **2009**, *25*, 672-675.

(237) Dai, J.; Bruening, M. L. "Catalytic nanoparticles formed by reduction of metal ions in multilayered polyelectrolyte films". *Nano Letters* **2002**, *2*, 497-501.

(238) Ji, J.; Fu, J.; Shen, J. "Fabrication of a superhydrophobic surface from the amplified exponential growth of a multilayer". *Adv. Mater.* **2006**, *18*, 1441-1444.

(239) Tan, Q.; Ji, J.; M. Barbosa, M. A.; Fonseca, C.; Shen, J. "Constructing thromboresistant surface on biomedical stainless steel via layer-by-layer deposition anticoagulant". *Biomaterials* **2003**, *24*, 4699-4705.

(240) Thierry, B.; Winnik, F. M.; Merhi, T.; Silver, J.; Tabrizian, M. "Bioactive coatings of endovascular stents based on polyelectrolyte multilayers". *Biomacromolecules* **2003**, *4*, 1564-1571.

(241) Boyes, S. G.; Akgun, B.; Brittain, W. J.; Foster, M. D. "Synthesis, characterization, and properties of polyelectrolyte block copolymer brushes prepared by atom transfer radical polymerization and their use in the synthesis of metal nanoparticles". *Macromolecules* **2003**, *36*, 9539-9548.

(242) Phadke, A.; Zhang, C.; Arman, B.; Hsu, C. C.; Mashelka, R. A.; Lele, A. K.; Tauber, M. J.; Arya, G.; Varghese, S. "Rapid self-healing hydrogels". *PNAS* **2012**, *109*, 4383-4388.

APPENDIX

LIST OF ABBREVIATIONS AND FULL NAME OF POLYELECTROLYTES

BPEI: branched polyethylenimine

PAA: poly(acrylic acid)

PAH: poly(allylamine hydrochloride)

PAN: poly(acrylonitrile)

PAO: poly(allylamine) containing a pyridine based osmium complex

PDAC: poly(diallyldimethyl ammonium chloride)

PMAA: poly(methacrylic acid)

PVA: poly(vinyl alcohol)

PVAm: poly(vinyl amine)

PVPON: poly(vinyl pyrrolidone)

PVS: poly(vinyl sulphate)

SPS: sodium poly(styrene sulfonate)